The Dissertation Committee for Everett Monroe Stone Certifies that this is the approved version of the following dissertation:

The Catalytic Mechanism of Dimethylarginine Dimethylaminohydrolase (DDAH) from *Pseudomonas aeruginosa*

Committee:

Walter Fast, Supervisor

Shawn Bratton

David Graham

David Hoffman

Christian Whitman

The Catalytic Mechanism of Dimethylarginine Dimethylaminohydrolase (DDAH) from *Pseudomonas aeruginosa*

by

Everett Monroe Stone, B.A.

Dissertation

Presented to the Faculty of the Graduate School of

The University of Texas at Austin

in Partial Fulfillment

of the Requirements

for the Degree of

Doctor of Philosophy

The University of Texas at Austin

August 2006

Dedication

To my wonderful children, Tristan and Kaya

May you always pursue your dreams and follow your heart

Let no one stand in your way

To your own self be true

Acknowledgements

I would like to thank my supervisor, Walt Fast, for his open–door policy and our numerous scientific conversations. Dr. Fast allowed me the freedom to experimentally explore many different avenues of thought, which I greatly appreciate. I have truly enjoyed doing science in the Fast lab. I also thank my parents for educating me at home, giving me unique perspectives I would not have obtained elsewhere. To my dearest friends, Michael, Retha, and Christiaan: Thank you for all the years of conversations, scientific and not so scientific. To Eva: Thank you for the "reformatting the hard drive" sessions. I also thank all the people, who over the years have touched my life in one way or another, you know who you are.

The Catalytic Mechanism of Dimethylarginine Dimethylaminohydrolase (DDAH) from *Pseudomonas aeruginosa*

Publication No._____

Everett Monroe Stone, Ph.D.

The University of Texas at Austin, 2006

Supervisor: Walter Fast

Dimethylarginine dimethylaminohydrolase (DDAH) catalyzes the hydrolysis of N^{ω}–methyl–L–arginine (NMMA) and N^{ω},N^{ω}–methyl–L–arginine (ADMA) to L-citrulline and methylamine or dimethylamine, respectively. ADMA and NMMA are endogenous inhibitors of nitric oxide synthase (NOS) in mammals. DDAH therefore partially regulates NOS activity, making it an attractive therapeutic target in disease states involving overproduction of nitric oxide. Understanding the mechanism of DDAH is important to inhibitor design and elucidating its physiological function.

DDAH is a member of the amidinotransferase superfamily, and has conserved active–site residues including cysteine, histidine, and glutamate/aspartate that are integral to catalysis. In DDAH from *Pseudomonas aeruginosa,* the active–site Cys249 is activated as a nucleophile upon binding substrate, and forms a covalent intermediate concomitant with loss of the alkylamine leaving group. The active–site His162 has a

dual role, first as a general acid in protonating the alkylamine leaving group and second as a general base in generating a hydroxide for attack on the covalent intermediate. The active–site Glu114 is essential for properly orienting and ionizing His162. The use of a substrate analog, *S*–methyl-L-thiocitrulline (SMTC), enabled development of a new method of continuously monitoring DDAH activity, allowing facile screening of inhibitors. Using this method, a haloacetamidine was identified as an active–site directed inactivator motif for DDAH, and other members of the amidinotransferase superfamily.

Table of Contents

List of Tables

List of Figures

List of Schemes

Chapter 1 Introduction

NITRIC OXIDE AN IMPORTANT BIOMOLECULE

Nitric oxide (NO) is an important molecule for normal physiological function in regulating blood pressure, immune cell function and neuronal signaling. NO is produced by the enzyme nitric oxide synthase (NOS), which catalyzes nitric oxide production through a five electron oxidation of arginine, resulting in NO and citrulline (*1*). Mammals have three NOS isozymes, neuronal NOS (nNOS) involved in neuronal signaling via synaptic potentiation, endothelial NOS (eNOS), distributed in vascular endothelium and important for smooth muscle relaxation and inducible NOS (iNOS) which is involved in macrophage mediated immune response. Although production of NO is important to normal physiology, overproduction of NO is involved in a number of disease states such as septic shock, rheumatoid arthritis, cerebral ischemic damage during stroke, Parkinson's, Huntington's and various other diseases (*2*). Regulation of NOS is an area of intense research.

NOS REGULATION BY ADMA AND NMMA

Although eNOS and nNOS are primarily regulated in a Ca^{2+}/calmodulin dependent manner, and iNOS is transcriptionally regulated, asymmetric *N*$^{\omega}$,*N*$^{\omega}$–dimethyl–L–arginine (ADMA) and *N*$^{\omega}$–methyl–L-arginine (NMMA) (Figure 1.1) have recently been found to act as endogenous competitive inhibitors of NOS in mammalian systems (*3*). ADMA and NMMA are thought to be derived from proteins that are post–translationally methylated on arginine residues by the protein arginine methyl transferases (PRMTs), using *S*–adenosylmethionine as a cofactor for methyl

transfer. These proteins are subsequently degraded, releasing free ADMA and NMMA. Symmetric N^{ω},N^{ω}–dimethyl–L–arginine (SDMA) is also produced but is not an inhibitor of NOS. Interestingly, elevated plasma ADMA concentrations have been recently recognized as a novel cardiovascular risk factor, as increased ADMA is associated with hypercholesterolemia, atherosclerosis, hypertension, chronic renal failure, and chronic heart failure (*4, 5*). High ADMA levels are also concomitant with reduced NOS activity as demonstrated with impaired endothelium-dependent vasodilation (*6*).

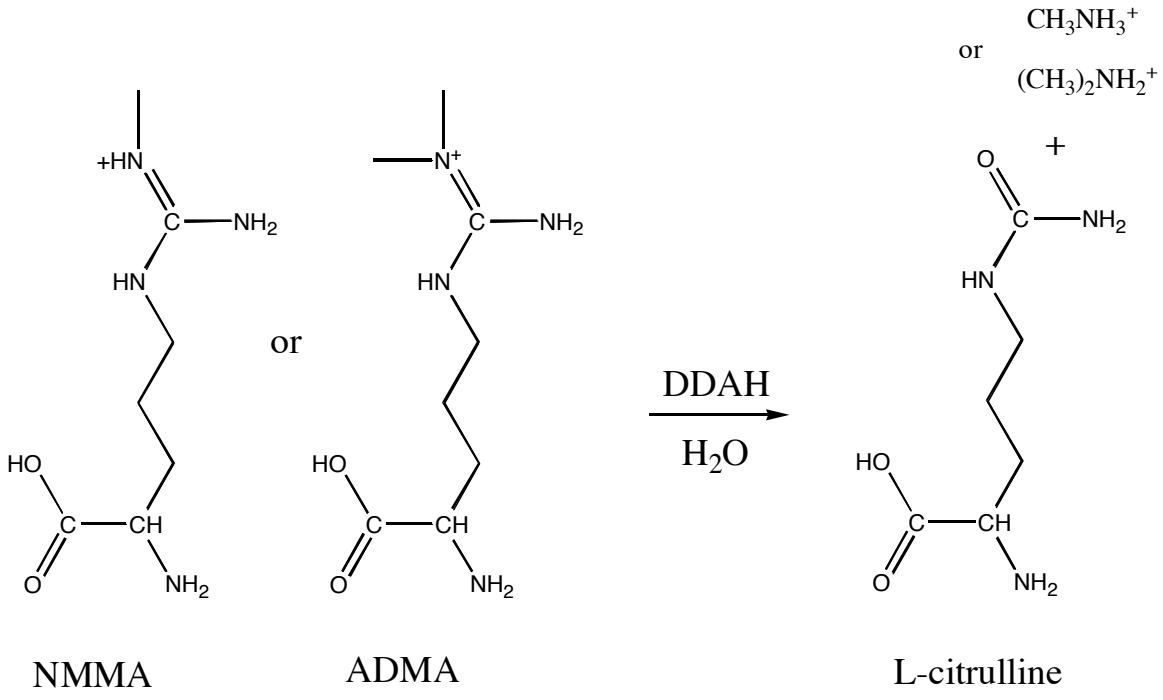

Figure 1.1 DDAH catalyzed hydrolysis of NMMA and ADMA

Although the exact intracellular concentrations of ADMA and NMMA are not known, one study of healthy adults revealed a plasma ADMA baseline of 0.4 ± 0.1 μM, while patients with chronic renal failure had elevated ADMA levels of 0.7 ± 0.1 μM (*7*). One estimate, based on mouse and rat kidney tissue, measures a cytosolic ADMA concentration of approximately 10 μM (*8*). Conversely, reduced ADMA levels

(approximately 2–fold below baseline) are found in the cerebrospinal fluid of Alzheimer's patients, while L-Arg levels remain normal, suggesting NOS is dysregulated in this disease (*9*). The treatment of certain hypotensive disorders with NMMA is also being explored (*10*). The discovery of ADMA and NMMA as endogenous inhibitors of NOS is an important advance and deserves further research to investigate the interplay between N^{ω}–methylated arginines and NOS dysregulation.

REGULATION OF ADMA AND NMMA

In mammals, ADMA and NMMA concentrations are regulated by two isozymes of dimethylarginine dimethylaminohydrolase (DDAH) (EC 3.5.318). DDAH–1 is found highly co–expressed with nNOS in neural tissue, and DDAH–2 is found highly co–expressed with eNOS in heart and placenta, and both isoforms are highly expressed in the kidney and liver (*11*). DDAH thus partially regulates NOS activity by hydrolysis of ADMA and NMMA, relieving basal inhibition of NOS (*12*), and making DDAH an attractive drug target for diseases involving NO overproduction. (DDAH does not hydrolyze SDMA, which will not be discussed further here.) Inhibition of DDAH could either allow endogenous ADMA and NMMA to accumulate or allow lower doses of administered NMMA to effectively regulate NOS. Conversely, therapeutic treatment with DDAH might help to lower elevated ADMA levels in hypertensive patients.

Ogawa et al. first identified that mono– and di–asymmetrically N^{ω}-methylated arginines were metabolites in rats, and subsequently purified DDAH to homogeneity from rat kidney (*13, 14*). DDAH was found to catalyze the hydrolysis of NMMA and ADMA to L-citrulline and methylamine or dimethylamine, respectively (Figure 1.1) (*14*). Soon thereafter, Leiper et al. demonstrated that certain microbes also had DDAH

encoding genes in what appear to be arginine handling operons (*15*), which is somewhat surprising because bacteria are not known to produce methylated arginines. While the biological relevance of prokaryotic DDAHs is not yet known, it is interesting to note that many of the bacteria harboring DDAH genes are also lung pathogens, including *Pseudomonas areuginosa, Legionella pneumophila, and Mycobacterium tuberculosis*. However, gene knockout experiments that test whether DDAH is a virulence factor in these organisms have not yet been reported.

Shirai et al. used sequence alignments, structural alignments and similar reaction chemistry, to define a superfamily of enzymes that includes arginine deiminase (ADI), amidinotransferase (AT), and peptidyl arginine deiminase (PAD)(*16*). Murray–Rust et al. obtained the first structure of a DDAH from *Pa areuginosa* (PDB 1H70), showing an overall fold of a barrel comprised of five modules with a □□□□ structural motif. The DDAH fold showed strong structural homology to ADI, AT and PAD, indicating that DDAH is a structural member of the same guanidine modifying superfamily (*17*). The amino acid sequence of *Pa* DDAH compared to the mammalian isozymes DDAH–1 and DDAH–2 is only about 23–29% identical but a recent structure of bovine DDAH–1 has shown the overall fold to be nearly identical (*18*). Murray–Rust et al. also proposed a putative catalytic triad of active–site residues for *Pa* DDAH consisting of Cys249, His162 and Glu114, similar to active–site residues found in other superfamily members (*17*). However, only a few studies to characterize this putative active–site triad have been reported.

REGULATION OF DDAH

There have been some reports regarding the physiological regulation of DDAH isozymes. The presence of a reactive cysteine in the active–site of DDAH led Leiper et al. to explore the possibility that DDAH might be regulated through *S*–nitrosylation. *Pa* DDAH and mammalian DDAH are reversibly inhibited by NO donors in vitro and DDAH–2 is *S*–nitrosylated after cytokine induced expression of iNOS in vivo (*19*). Through the use of site–directed mutagenesis, Leiper et al. demonstrated that wild–type *Pa* DDAH, but not an inactive C249S variant, could be nitrosylated, indicating the active–site cysteine was modified (*19*). Knipp et al. also found that bovine DDAH-1 was specifically nitrosylated on two cysteine residues, one of which is the active–site nucleophile (*20*). In addition to *S*–nitrosylation, bovine DDAH–1 can also be regulated by Zn(II) ion binding. One tightly bound inhibitory Zn(II) ion ($K_d \sim 4$ nM) is found at the active–site, which, upon release, activates DDAH (*21*). This tightly bound Zn(II) ion was also found to protect against cysteine modification by NO donors (*20*). In mammalian systems DDAH acts to partially regulate NOS by controlling ADMA and NMMA levels (*22*), and it appears that feedback inhibiton by NO is also a possible form of regulation (Figure 1.2). However, the mechanism of Cys activation has not been well characterized.

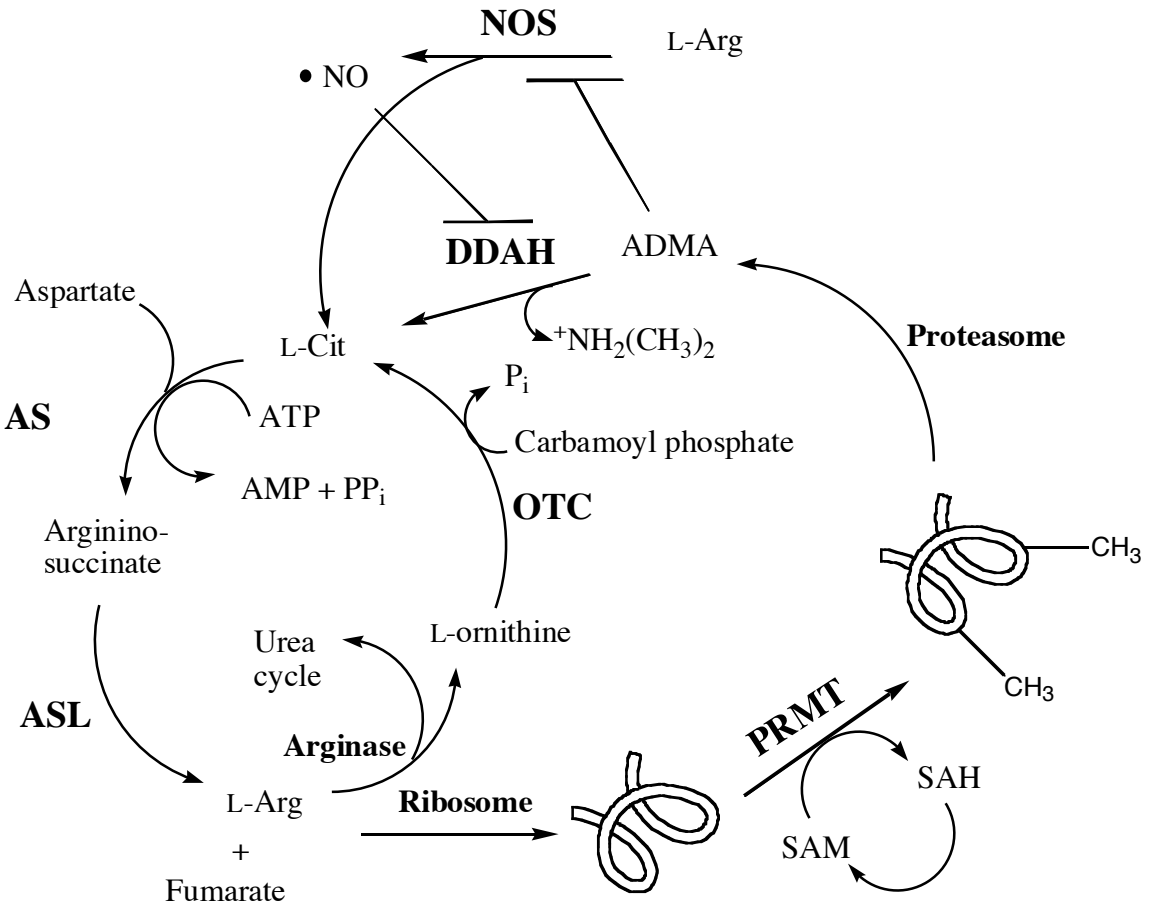

Figure 1.2 Methyl–arginine cycle

Mono– and di– methylated arginines arise through post–translational methylation of proteins by PRMTs. Subsequent proteolysis releases free *N*□-methylarginines. NOS activity is partly regulated by ADMA and NMMA, concentrations of which are controlled by DDAH. DDAH in turn can be nitrosylated, indicating possible regulation by •NO. DDAH–catalyzed hydrolysis of ADMA yields L–Cit, which can be returned to the urea cycle. AS = argininosuccinate synthetase, ASL = argininosuccinate lyase, OTC = ornithine transcarbamoylase, SAM = *S*–adenosylmethionine, SAH = *S*–adenosylhomocysteine, L–Cit = L–Citrulline.

DDAH MECHANISM, ASSAYS, AND INHIBITION

At the onset of this research project, the physiological relevance of DDAH as modulator of NOS activity was becoming clear. The structure of *Pa* DDAH was also an important advance, indicating that DDAH is a structural member of the amidinotransferase family, and suggesting a catalytic triad of Cys249, His162, and Glu114 residues. However, only limited mutagenesis studies had been reported, and the reaction mechanism was unclear. There were also only a few reported inhibitors for DDAH (*22, 23*), and a facile method for screening for new inhibitors was not available.

The research reported here has been able to address several of the gaps that existed at the beginning of this research. Using the DDAH from *Pa aeruginosa* as a model system, we have provided evidence supporting a substrate–assisted reaction mechanism, and determined the role of the active–site residues Cys249, His162, and Glu114 during catalysis. We have also built on these discoveries and identified a covalent inactivator, as well as a simple continuous method for detecting DDAH activity and screening potential inhibitors.

Chapter 2 Characterization of *Pa* DDAH, substrate specificity, and covalent intermediate in the reaction mechanism

Introduction

DDAH catalyzes the hydrolysis of NMMA, and ADMA to citrulline and either methylamine or dimethylamine respectively and belongs to a superfamily of guanidine modifying enzymes that includes arginine deiminase, amidinotransferase, and peptidyl arginine deiminase (PAD)(*14, 16*). Although the DDAH from *Pseudomonas aeruginosa* only has 23-30% amino acid identity with mammalian isozymes, the active site residues Cys249, and His162 are conserved and Glu114 replaces Asp (Figure 1.1). Also the DDAH from *Pseudomonas* has been far more tractable for over-expression than its mammalian counterparts, and has resulted in a crystal structure (*17*), making this particular enzyme an excellent model to examine the mechanism of DDAH.

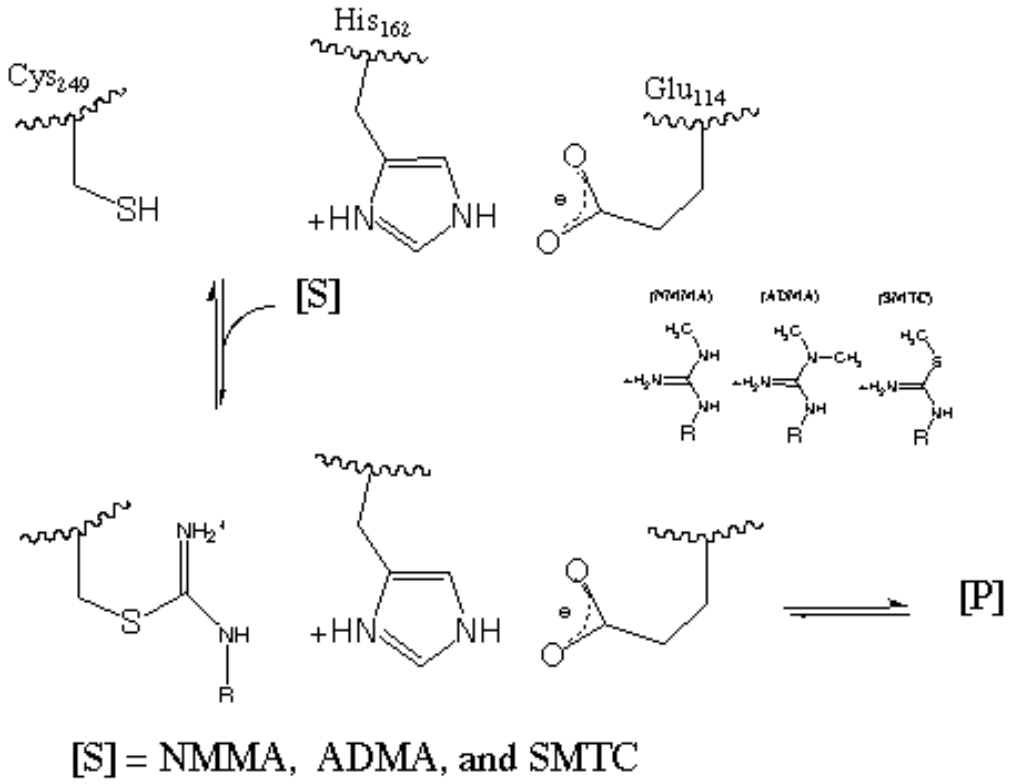

Figure 2.1 DDAH active–site, substrates, and proposed covalent intermediate.

Some members of the amidinotransferase superfamily, such as arginine deiminase, have been shown to use reaction mechanisms that proceed through a covalent intermediate using the conserved active site cysteine as a nucleophile (*24*). However, the mechanism of DDAH has had little characterization, and the role of each conserved active site residue remains to be determined. The experiments detailed here demonstrate that the DDAH–catalyzed hydrolysis reaction does proceed through a covalent intermediate using Cys249 as the active–site nucleophile. We used alternative substrates, mass spectrometry, and steady-state kinetics to explore the specificity and catalytic mechanism of DDAH.

Materials and Methods

CONSTRUCTION OF AN EXPRESSION VECTOR FOR PA DDAH

The coding region for *Pa* DDAH (Protein GI:53727549) was amplified from *Pa aeruginosa* (strain PAO1) genomic DNA (ATCC 470850) using two specific end primers: 5'-CAGGATCCCATATGTTCAAGCACATCATCGCTCG-3' and 5'-CGGAATTC TCAGAAGCGCAGCGACATG-3' (Sigma-GENOSYS, The Woodlands, TX). The forward primer contains an *Nde* I restriction site (underlined) followed by 20 bases corresponding to the coding sequence of the DDAH gene. The reverse primer contains an *Eco* RI restriction site (underlined) followed by 16 bases corresponding to the gene coding sequence. Amplification of the *Pa* DDAH gene was carried out by PCR using an MJ Research (Waltham, MA) PTC 200 thermocycler, along with the aforementioned primers, genomic DNA, dNTPs (New England Biolabs, Beverly, MA), and Triplemaster PCR reagents (Eppendorf, Westbury, NY) following a temperature program: 95º C for 5 min, followed by 30 cycles of 95º C for 30 s, 52º C for 30 s, and 72º C for 1 min, followed by a 3 min hold at 72º C. The PCR-amplified *Pa* DDAH coding sequence was then ligated into a pGEM-T vector (Promega, Madison, WI) and transformed into *Escherichia coli* DH5E cells. The resulting plasmid (pTpaoDDAH) was isolated, and the insert was sequenced to ensure that there were no undesired mutations. The pTpaoDDAH plasmid and the pET-28a expression vector were subsequently digested with *Nde* I and *Eco* RI restriction enzymes followed by gel purification and ligation of the digested *Pa* DDAH coding sequence into the multiple

cloning site of pET-28a. The resulting plasmid (designated pETpaDH) was transformed into *E. coli* DH5 cells for purification and sequencing of the insert.

CONSTRUCTION OF AN EXPRESSION VECTOR FOR C249S DDAH

An oligonucleotide, 5'–CGGAATTCTCAGAAGCGCAGCGAGCAggaACTGAC G-3' (Sigma-GENOSYS) that contained an Eco RI restriction site (underlined) and a mutant codon (lowercase) was designed to introduce a mutation encoding C249S at the end of the DDAH sequence. Because the desired mutation was near the 3' end of the *Pa* DDAH gene, only one PCR was required, using the mutant reverse primer and forward primer described above with the aforementioned reaction conditions. After Qiaquick (Qiagen, Valencia, CA) purification of the C249S PCR product, this insert and a pET-28a expression vector were digested with *Nde* I and *Eco* RI, Qiaquick purified (Qiagen), and ligated together using T4 DNA ligase (Fisher, Pittsburgh, PA). The resulting plasmid (pET-DH-C249S) was concentrated by pellet paint precipitation (Novagen, San Diego, CA) and transformed into *E. coli* DH5E cells for plasmid amplification and purification. DNA sequencing of the coding sequence of the C249S insert indicated that there were no undesired mutations.

OVEREXPRESSION AND PURIFICATION OF WILD-TYPE AND C249S *PA* DDAH

For expression of wild-type and C249S *Pa* DDAH, the expression plasmids were first transformed into *E. coli* BL21 (DE3) cells. Typically, over-expression of *Pa* DDAH was carried out by inoculating 1 L of LB medium containing 30 g/mL kanamycin with 10 mL of inoculant from a saturated overnight culture and shaking at 37° C. IPTG was

added to a final concentration of 0.5 mM when the expression culture reached an OD_{600} of 0.5, and expression was continued for an additional 4 h. Cells were then harvested by centrifugation and stored at –20º C. Frozen cell pellets were re-suspended in pET lysis buffer [10 mM NaH_2PO_4 buffer, 300 mM NaCl, and 10 mM imidazole (pH 8.0)] at 40 mL of buffer/L of culture. Cell suspensions were sonicated on ice for 2 min with 15 s burst/rest cycles followed by centrifugation at 23500 * *g* for 20 min. Approximately 15 mL of supernatant was then loaded directly onto an 8 mL Ni-NTA affinity resin column (Qiagen) and washed with 10 column volumes of lysis buffer (see above), followed by 7 column volumes of 50 mM NaH_2PO_4 buffer, 300 mM NaCl, and 20 mM imidazole (pH 8.0), and finally eluted with 50 mM NaH_2PO_4 buffer, 300 mM NaCl, and 250 mM imidazole (pH 8.0). Fractions (3 mL) were characterized by activity and SDS-PAGE. The wild-type *Pa* DDAH did not require additional purification, but the C249S variant was further purified by loading fractions containing the desired protein onto a DEAE ion-exchange column. This column was washed with 20 mM Tris-HCl buffer (pH 8.0), and then purified protein was eluted stepwise by the addition of a mixture containing 75% of 20 mM Tris-HCl buffer (pH 8.0) and 25% of 20 mM Tris-HCl buffer and 1 M NaCl (pH 8.0). Fractions were characterized by SDS-PAGE, and those containing purified protein were pooled. To remove any extraneously bound metal ions, purified proteins were dialyzed overnight at 4º C in 4 L of 2 mM 1,10-phenanthroline and 100 mM KCl (pH 7), followed by two 4 h dialyses composed of 4 L each of Chelex-100-treated (Bio-Rad, Hercules, CA) 10 mM MES and 100 mM KCl at pH 6.2 and 4º C. The final purification products were made 10% in glycerol and stored in aliquots at –80º C after being flash-frozen in liquid N_2.

CHARACTERIZATION OF *PA* DDAH

The first 15 N-terminal residues of purified wild-type *Pa* DDAH were sequenced by Edman degradation at the Protein Facility (Institute for Cellular and Molecular Biology, The University of Texas). To determine the final metal content, a protein sample (79 μM) and associated dialysis buffer were analyzed by inductively-coupled plasma mass spectrometry (ICP-MS, Department of Geological Sciences, The University of Texas) to quantify the protein's zinc content by subtracting the concentration of zinc found in dialysis buffer from the zinc concentration of the final protein sample and dividing by the protein concentration. To determine protein concentrations, an extinction coefficient was calculated for *Pa* DDAH on the basis of the amino acid sequence (http://workbench.sdsc.edu/) (*25*). All protein concentrations for DDAH were calculated on the basis of the calculated ε_{280} of 17 210 M^{-1} cm^{-1} in a final buffer concentration of 6 M guanidinium hydrochloride and 20 mM phosphate buffer (pH 6.5).

MASS SPECTRUM ANALYSIS OF PRODUCTS FORMED IN THE DDAH REACTION

Because the standard colorimetric assay used for citrulline (*26*) detects ureido groups and is not specific for citrulline formation (*27*), mass spectrometry was used to establish the reaction products of *Pa* DDAH. A Sephadex G-10 spin column was used to exchange a sample of enzyme into 25 mM ammonium bicarbonate buffer (pH 7). An amount (1 μmol) of ADMA was then incubated overnight with 375 pmol of *Pa* DDAH in 25 mM ammonium bicarbonate buffer (pH 7). The subsequent reaction products were analyzed by MALDI-TOF. Two control samples, one lacking enzyme and one lacking substrate, were also analyzed on an Applied Biosystems (Foster City, CA) Voyager-DE

PRO mass spectrometer using α-cyano-4-hydroxycinnamic acid as the matrix as previously described (***12***).

STEADY-STATE KINETIC STUDIES

Using a slightly modified published protocol (*28*) that detects formation of a ureido group, the steady-state catalytic rate constants of Pa DDAH were determined for hydrolysis of various compounds, including creatine, creatinine, argininosuccinate, guanidinoacetate, L–arginine, L–homoarginine, L–canavanine, N-amino- L-arginine, N^{ω}-hydroxy–L-arginine, N^{ω}-methyl–L-arginine (NMMA), N^{ω},N^{ω}-dimethyl–L-arginine (ADMA), and S-methyl–L-thiocitrulline (SMTC) (Sigma-Aldrich Chemical Co., St. Louis, MO). Typically, substrate concentrations ranging from 78 μM – 10 mM were prepared by serial dilution in an assay buffer consisting of Na_2HPO_4 (100 mM) buffer (pH 6.2). Substrate aliquots of 200 μL were placed in 1.5 mL microcentrifuge tubes to which 5 μL of a 79 μM enzyme stock was added. Most reactions were carried out at 25° C for 1 min, and then stopped by addition of 10 μL of 6 N trichloroacetic acid (TCA). Control reactions showed that citrulline production under these conditions is linear for more than 5 min. Slower substrates such as L-arginine were assayed at 25° C for longer periods of time (2 h) with increased enzyme concentrations (4.5 nM). Compounds that displayed no turnover were further tested at 25° C for activity by incubating each compound (5 mM) with a higher concentration of enzyme (6 μM) for 1 h. A control reaction without the enzyme was also performed at each substrate concentration, enabling background citrulline levels to be subtracted. A series of standards for quantifying final citrulline concentrations was prepared by serially diluting citrulline to a final concentration range

of 0-313 μM in 100 mM Na_2HPO_4 buffer (pH 6.2) and aliquoting these samples in 200 μL portions in 1.5 mL microcentrifuge tubes. To the citrulline standards, enzyme reaction mixtures, and controls was added 1 mL of freshly prepared color-developing reagent (*28*), and the tubes were placed in a boiling water bath for 15 min and then cooled for 10 min at 25 C. The absorbance at 540.5 nm was measured for each sample using a Cary 50 UV-vis spectrophotometer (Varian Inc., Walnut Creek, CA) and then converted into citrulline concentrations by using a standard curve. The resulting data, after background subtraction, were fit directly to the Michaelis–Menten equation using KaleidaGraph (Synergy Software, Reading, PA). All reactions were carried out in at least triplicate. Activity tests for the C249S variant were also performed using 10 mM substrates (NMMA, ADMA, and SMTC) for 1 h at 37° C to maximize the chance of detecting any citrulline that might be formed.

MASS SPECTRUM ANALYSIS OF COVALENTLY MODIFIED PA DDAH

To characterize a covalent enzyme-substrate intermediate that might accumulate during steady-state reactions, incubations of NMMA, ADMA, or SMTC and DDAH were quenched with acid during turnover. Samples were typically prepared by incubating 20–60 μM enzyme and 10-45 mM substrate in 10 mM MES buffer, 100 mM KCl, and 10% (v/v) glycerol (pH 6.2) at 25° C, followed by quenching with 1 M trifluoroacetic acid to a final concentration of 83 mM after reaction for 0, 1, 5, and 30 min. A control lacking substrate was included for every reaction. Samples were then desalted on a protein trap (Protein MicroTrap, Michrom, Auburn, CA) and analyzed by electrospray ionization mass spectrometry (ESI-MS) on a ThermoFinnigan LCQ (San Jose, CA) ion

trap mass spectrometer as described previously (*29*) using a 10 min 5 – 95% B gradient delivered by a Michrom Magic 2002 HPLC system.

IDENTIFICATION OF COVALENTLY MODIFIED PEPTIDE

Steady-state reaction mixtures of *Pa* DDAH and SMTC were prepared and the reactions quenched with acid as described above. A Sephadex G–10 spin column was then used to exchange these reaction mixtures into 50 mM ammonium acetate buffer (pH 4) where the covalent adduct is stable (data not shown) and where an acid stable protease would be active. The resulting product was subsequently digested with Glu–C endoproteinase (Roche, Indianapolis, IN) in a 20:1 (w/w) ratio for 18 h at room temperature. Digestion products were analyzed using MALDI-TOF and MALDI-PSD on an Applied Biosystems Voyager-DE PRO system using α-cyano-4-hydroxycinnamic acid as the matrix as previously described (*30*). Theoretical digest masses were calculated with MS-Digest in the Protein Prospector suite using two missed cleavages (*31*).

Results

EXPRESSION AND CHARACTERIZATION OF WILD-TYPE AND C249S PA DDAH

The *Pa* DDAH coding sequence was amplified from genomic DNA and cloned into a pET-28a expression vector without any undesired mutations. The resulting N-terminal His_6-tagged protein was overproduced in BL21 (DE3) *E. coli*, and a single affinity chromatography step resulted in homogeneous wild-type *Pa* DDAH (>98% homogeneous) as assessed by SDS-PAGE. Characterization of the purified protein by ESI-MS showed a major peak at 30 495 ± 10 Da, which matches (within error) the mass

calculated from the amino acid sequence (30 503 Da) of His_6-tagged *Pa* DDAH when the N-terminal methionine residue had been removed (Figure 1A). The first 15 amino acids of the purified protein were identified by N–terminal sequencing to give a GSSHHHHHHSSGLVP sequence, confirming that the N–terminal methionine had been removed. ESI-MS of protein samples gauged to be homogeneous by SDS-PAGE did reveal a minor peak that carries an additional 177 ± 10 Da adduct and a small peak indicating an additional 254 ± 10 Da adduct, both of which are consistent with a minor fraction of the purified DDAH carrying a nonenzymatic modification at the N-terminus from □-gluconoylation and □-6-phosphogluconoylation, respectively, both of which have previously been characterized in other recombinant proteins containing polyhistidine tags (*32*). The total amount of gluconoylation varied among enzyme preparations, but was always only a minor component. The modified and unmodified N-terminal His_6 tags were not removed for these tests because the crystal structure of this enzyme places the N-terminus distant from both the active site (*17*) and the dimer interface (*33*), the His_6 fusion was previously shown to be active (*15*), and short N-terminal extensions of other DDAH isoforms do not significantly affect their kinetics (*34*). Unlike the wild-type protein, the C249S variant required an additional purification step. Hence, ion-exchange chromatography followed the initial affinity column and resulted in >95% purity as assessed by SDS-PAGE. Because zinc has been shown to inhibit the activity of bovine brain DDAH (*21, 35*), chelation and dialysis steps were carried out at the end of the purification to remove any remaining zinc ions. For both the wild type and the C249S variant, less than 0.001 equiv. of zinc was found in the final purified proteins.

MASS SPECTRAL ANALYSIS OF SUBSTRATE DIGESTION PRODUCTS

The substrate ADMA was completely hydrolyzed by purified DDAH, and the reaction products were analyzed by MALDI-TOF. A control reaction, lacking enzyme, was used to determine the mass of unhydrolyzed ADMA: $M{\cdot}H^+$ obs , 203.1 ± 0.1 Da; $M{\cdot}H^+$ calc, 203.14 Da. MALDI-TOF of reaction mixtures in which ADMA was incubated with purified DDAH showed a loss of this 203.1 Da peak and the appearance of two new peaks at 46.0 ± 0.1 and 176.1 ± 0.1 Da, corresponding to the calculated masses of dimethylamine ($M{\cdot}H^+$ calc , 46.06) and citrulline ($M{\cdot}H^+$ calc , 176.10).

DETERMINING THE STEADY-STATE KINETIC CONSTANTS

An established discontinuous assay for citrulline production (*28*) was used to follow any hydrolysis reactions observed with varying concentrations of different compounds as catalyzed by the purified wild-type *Pa* DDAH (Table 2.1). This enzyme was shown to prefer ADMA over NMMA (indicated by a 3.9-fold increase in k_{cat}/K_M), but the artificial substrate SMTC had the highest k_{cat} (1.5-fold increase) and the lowest K_M (2.2-fold decrease) of all of the substrates that were tested. An apparent substrate inhibition was observed with NMMA, ADMA, N□–hydroxy–L-arginine, and N□–amino–L–arginine at concentrations above 10 mM, but SMTC did not show any substrate inhibition at concentrations up to 40 mM (data not shown). Further experiments will be required to determine the mechanism of substrate inhibition, so concentrations of <10 mM were typically used for these studies.

Table 2.1 Steady-state Rate Constants for DDAH-Catalyzed Hydrolysis of Substrates, Ranked by Increasing k_{cat}/K_M Values

Substrate	k_{cat} (min^{-1})	K_M (□M)	k_{cat}/K_M (min^{-1} mM^{-1})
L-Arginine [a]	0.10 ± 0.02	940 ± 50	0.11 ± 0.03
N□-Amino-L-arginine [a]	7.2 ± 0.1	1110 ± 60	6.5 ± 0.4
N□-Hydroxy-L-arginine [a]	20 ± 2	2300 ± 400	9 ± 2
NMMA (**1**); Rat DDAH [b]	5.6	360 ± 10	16
NMMA (**1**) [a]	18.6 ± 0.6	670 ± 60	28 ± 3
ADMA (**2**); Rat DDAH [b]	9.2	180 ± 10	51
ADMA (**2**) [a]	33.6 ± 0.6	310 ± 20	108 ± 9
SMTC (**3**) [a]	50.4 ± 0.6	143 ± 5	350 ± 20

[a.] Reactions are carried out with *Pa* DDAH at 25° C and at pH 6.2.

[b.] Values are from (*14*), and were carried out with rat kidney DDAH at 37° C and at pH 6.5.

Less active substrates include *N*-hydroxy- L-arginine, *N*-amino- L-arginine, and L-arginine that have k_{cat}/K_M values 8-, 17-, and 1000-fold lower, respectively, than that of ADMA. Creatine, creatinine, argininosuccinate, guanidinoacetate, L-homoarginine, and L-canavanine were not good substrates, exhibiting either no activity or less activity than L-arginine. We were unable to detect any activity for the C249S variant-catalyzed hydrolysis of compounds (NMMA, ADMA, and SMTC) under the conditions described above, indicating that the k_{cat} of this variant must be lowered by at least 5 orders of magnitude.

MASS SPECTROMETRY OF ACID-QUENCHED STEADY-STATE REACTIONS

To obtain evidence for a transient covalent adduct, reactions were acid-quenched at various time points before, during, and after turnover and then analyzed by ESI-MS. The deconvoluted mass spectrum of a control reaction, quenched before addition of substrate, results in a major peak at 30 495 ± 10 Da (Figure 2.2 A) matching that of unmodified *Pa* DDAH (see above). The minor peak seen at 30 672 Da is assigned to the fraction of DDAH with □-gluconoylation at the N-terminus. Analysis of a steady-state reaction between SMTC and DDAH that was quenched after 1 min of turnover clearly shows that the major peak shifts 158 Da higher to 30 653 ± 10 Da, with only a minor amount of the unmodified 30 496 Da peak remaining (Figure 2.2 B). The small peak due to the fraction of enzyme that is □-N-gluconoylated also shifts an equivalent amount (156 ± 10 Da) and maintains a similar ratio to the major peak throughout the reaction. A reaction quenched after 5 min of turnover (Figure 2.2 C) results in essentially the same peaks that are seen in the 1 min sample, but the relative peak heights of the major peak

(30 654 Da) and the unmodified enzyme peak (30 495 Da) have changed, showing an increase in the unmodified enzyme peak after reaction for 5 min. Finally, after a 30 min reaction (Figure 2.2 D), the spectrum does not show any peaks different from those observed in the starting sample (Figure 2.2 A).

The progress curve for *Pa* DDAH–catalyzed conversion of SMTC (20 mM) to citrulline was determined for a reaction using the same conditions that were used for preparing the ESI-MS samples described above (Figure 2.2 E). It should be noted that these experiments involve much more enzyme than is normally used when measuring initial rates. Citrulline is produced at the highest rate during the first 1 min, which corresponds to the ESI–MS spectrum showing the largest 158 ± 10 Da adduct peak (Figure 1B). After the reaction has progressed for 5 min, the rate of citrulline production is slowed, most likely due to product inhibition (*36*) under these conditions, and corresponds to the ESI-MS spectrum in which less of the 159 ± 10 Da adduct is seen relative to the unmodified enzyme (Figure 2.2 C). Finally, after 30 min, the reaction slows because the conversion of SMTC to citrulline is nearly complete, and this corresponds to the ESI-MS spectrum (Figure 2.2 D) that is nearly identical to that taken before the reaction was started (Figure 2.2 A). In short, a covalent adduct of 158 ± 10 Da transiently appears during *Pa* DDAH-catalyzed turnover of SMTC. The ratio of this adduct to the unmodified enzyme is the largest during the fastest initial hydrolysis rates, decreases when less enzyme is available to react with the substrate (probably due to product inhibition), and disappears when the conversion is complete.

Despite its lack of activity, the C249S variant was also tested for possible formation of a covalent adduct upon incubation with SMTC. ESI-MS of the quenched

incubations only showed one major peak at 30 481 ± 10 Da, consistent with a calculated mass of 30 487 Da for the C249S variant after removal of the N-terminal methionine.

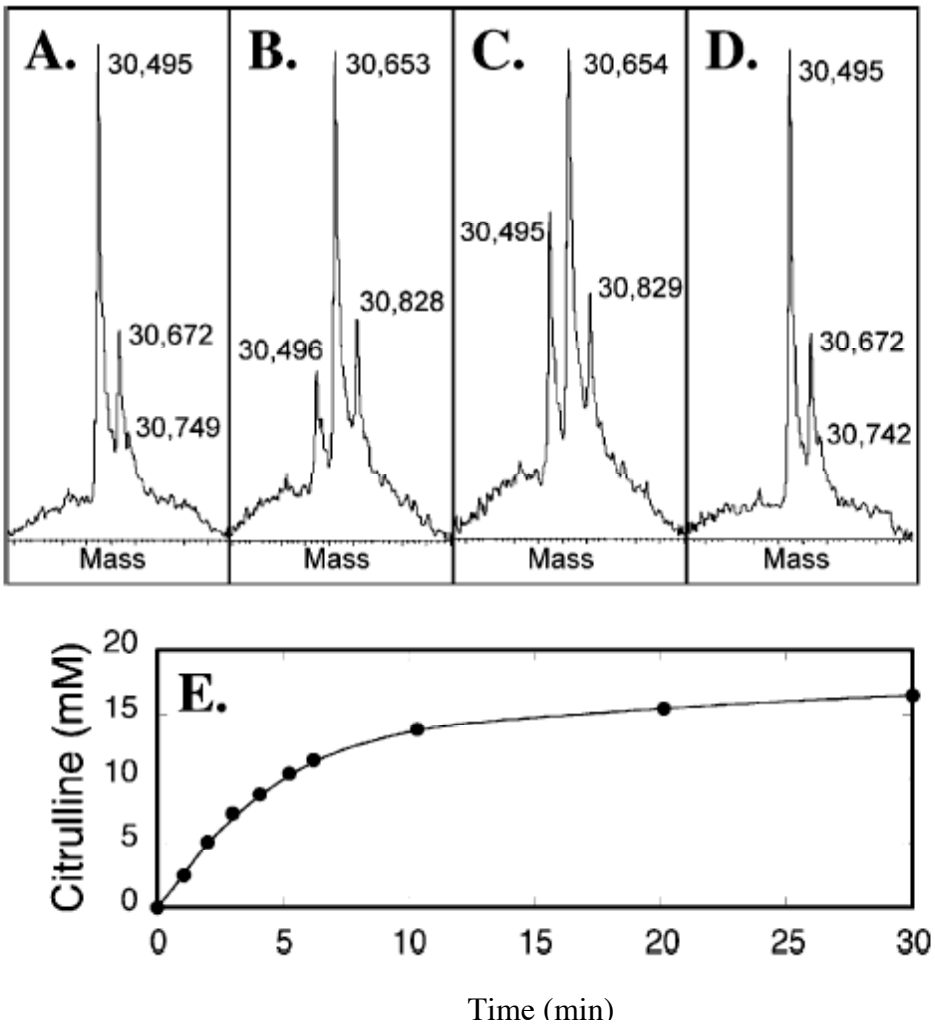

Figure 2.2 Deconvoluted ESI-MS of quenched DDAH reactions with S-methyl-L-thiocitrulline (SMTC)

Reactions are acid-quenched before (A) and after addition of SMTC with subsequent turnover for (B) 1, (C) 5, and (D) 30, min. The minor peaks that consistently contain a 178 Da adduct throughout the reaction reflect a fraction of the enzyme that is □-N-gluconoylated during expression (*32*). (E) A progress curve showing hydrolysis of SMTC (20 mM) to citrulline under the same conditions that were used for the trapping experiments in panels A-D indicates that the fastest rate of hydrolysis corresponds with the sample containing the most 157 Da adduct and that, after turnover is finished, the enzyme does not contain this 157 Da adduct.

IDENTIFICATION OF THE COVALENTLY MODIFIED PEPTIDE

To determine both the residue that is transiently modified and a more precise mass of the covalent adduct, an acid-trapped reaction mixture containing both the unmodified enzyme and the enzyme containing the 158 Da adduct was digested by Glu-C endoproteinase and the resulting peptides were detected by using MALDI-TOF in both linear and reflectron modes. The theoretical digest peptide molecular masses were compared to the observed MS data, and 24 different peptides covering 74% of the total sequence were successfully detected, including peptides containing active site residues Cys249, His162, Glu114, and Thr165 (Table 2.2). An N-terminal peptide was detected and corresponds to the mass of the first 52 residues without the N-terminal methionine, again showing removal of the N-terminal methionine during expression and purification of His 6-tagged *Pa* DDAH. A minor peak corresponding to this same N-terminal peptide but with an additional 178 ± 1 Da was also observed, consistent with a small amount of DDAH undergoing nonenzymatic N-terminal α–gluconoylation during expression as reported with other recombinant proteins (*32*). A small amount of a 258 Da adduct to this peptide was also observed (data not shown) in our samples, consistent with the presence of a very minor fraction of an α-N-6-phosphogluconoyl modification usually found in small amounts when this nonenzymatic gluconoylation occurs during overexpression (*32*).

Importantly for the detection of a covalent adduct, the linear MALDI spectrum of the digestion mixture shows a peptide at *m/z* 1732.9, corresponding to the average mass of the C-terminal DDAH peptide following Glu-C cleavage ($_{240}$YRKIDGGVSCMSLRF$_{254}$). This C–terminal peptide contains the active site Cys249

residue. The same spectrum also shows a peptide at *m/z* 1890.2, which does not correspond to the mass of any predicted DDAH Glu-C cleavage peptide, but is 157.3 ± 0.4 Da higher than the DDAH C-terminal peptide mass. This postulated adduct is consistent with the 158 ± 10 Da adduct found when the undigested protein was analyzed by ESI-MS. The peptide at *m/z* 1890 is not seen in the MALDI reflectron spectrum, demonstrating that it contains a bond that readily fragments after ionization. No mass increase was found for any of the 23 other peptides found in the digest. Comparison of the C–terminal adduct to the ESI-MS results of the intact protein indicates that there is just a single modification, excluding the missing peptides in the digest as sites for multiple attachments.

To identify the modified residue, ions from the MALDI post source decay (PSD) fragmentation spectra of both the native C-terminal peptide at *m/z* 1733 and the modified peptide at *m/z* 1890 were compared (Table 2.2). Immonium ions, b ions, and y ions (see ref (*37*) for nomenclature) from each parent confirm that both peptides are derived from the same amino acid sequence. The primary fragments for the *m/z* 1733 peptide are b_5 and y_{10} ions produced by fragmentation after an Asp residue. The *m/z* 1890 peptide undergoes a dominant fragmentation involving neutral loss of 157 and 190 Da to produce the *m/z* 1733 and 1700 fragments, respectively, consistent with fragmentation on either side of a sulfur atom (Figure 2.3). The sum of these observations shows that modification occurs at the only cysteine residue found within this peptide, Cys249.

Table 2.2 Summary of Proteolytic Cleavage of DDAH with Glu-C Endoproteinase[a]

DDAH Sequence # plus leader (-18 to 0)	Calculated average peptide mass (Da)	Observed peptide mass (Da) [b]
(-18)-33	5657.4	5658.1
(-18)-33 + Glc[c]	5835.5	5835.8
34-56	2627.0	
57-65	1096.2	
66-83	1903.2	
84-88	604.6	
89-90	249.2	
91-93	374.4	
94-94	148.1	
95-105	1323.7*	1323.7*
95-114	2277.6	2277.4
95-129	3914.5	3914.4
106-108	417.5	
109-114	573.6	
115-129	1655.9	1655.7
115-146	3469.0	3468.7
130-136	748.8	
130-146	1832.1	1831.9
130-158	3095.6	
137-146	1101.6*	1101.6*
147-158	1281.7*	1281.7*
147-171	2749.3	2749.0
147-180	3669.3	3669.0
147-186	4357.1	4356.8

159-171	1485.8	1485.8
159-180	2405.8	2405.7
159-186	3093.6	3094.0
187-194	1026.1	
195-197	358.4	
198-210	1528.6	1528.9
200-210	1270.4	
211-223	1546.8	1546.7
211-234	2846.4	2846.3
211-239	3378.0	3377.7
224-234	1317.8*	1317.8*
235-254	2264.6	2264.3
240-254	1733.1	1733.1
240-254 + IMO[d]	1890.2	1890.3

[a] Comparing calculated peptide masses (MS-Digest in Protein Prospector) with experimental results by MALDI-TOF for digestion with up to two missed cleavages. Amino acid numbering is assigned to match that of 1H70.pdb (*17*).

[b] Mass accuracy is 200 ppm.

[c] Glc stands for *N*-terminal -gluconoylation (*32*).

[d] IMO stands for the 1-(iminomethyl)-L-ornithine fragment of the covalent adduct (Figure 2.3 B).

* Denotes monoisotopic mass.

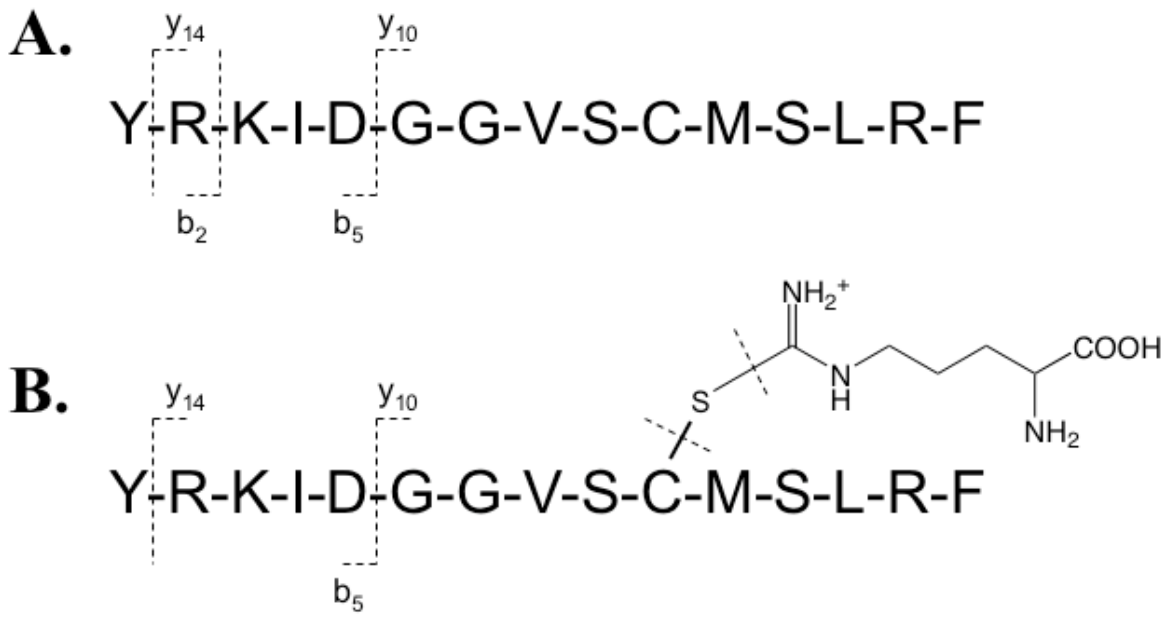

Figure 2.3 Fragmentation patterns from MALDI-PSD

(A) The 1733 Da peptide shows y_{14}, y_{10}, b_2, and b_5 fragments. (B) The 1890 Da peptide shows the same b_5 fragment, but y_{14} and y_{10} also contain an additional adduct. Fragmentation on either side of a sulfur atom implicates a cysteine side chain as the point of attachment.

Discussion

DDAH plays an important role in regulating endogenous pools of the NOS inhibitors ADMA and NMMA in mammals, so understanding its catalytic mechanism is of significant interest. Why a bacterium that is not known to produce methylated arginines has a DDAH gene is not yet well understood. However this enzyme will serve as a model system for investigating the mechanism of DDAH. The colorimetric assay used to determine activity is not specific to citrulline alone (*27*), so we sought to determine the actual reaction products to ensure that *Pa* DDAH is the functional equivalent of the mammalian isozymes. For a counter example, instead of the N^{ω}–nitrogen, related amidinotransferases in the same superfamily use the ornithine side chain rather than dimethylamine as the leaving group (*38*). If *Pa* DDAH breaks a similar bond in its NMMA substrate, the resulting reaction products would be L–ornithine and *N*-methylurea, which would be indistinguishable from citrulline when using the colorimetric assay. In order to rule out this possibility, MALDI–TOF–MS was used to characterize the reaction products after complete hydrolysis of ADMA by purified *Pa* DDAH. The MS analysis identified citrulline and dimethylamine as two new products, unambiguously identifying dimethylamine as the leaving group in the reaction catalyzed by this bacterial enzyme and demonstrating that the products are the same as those found with the mammalian DDAH enzymes (*14*). There was no evidence of either L–ornithine or *N*-methylurea being formed.

Having established the reaction products, the steady-state kinetic constants for *Pa* DDAH catalyzed hydrolysis were determined for a variety of common guanidino-containing compounds by using a published discontinuous diacetyl monoxime

derivatization assay (*28*). Supporting the proposition that this enzyme is a true DDAH, asymmetric methylated arginine analogs are shown to be the preferred substrates (Table 1). In fact, the k_{cat}/K_M values for hydrolysis of ADMA and NMMA are both nearly 2-fold higher than those reported for mammalian DDAH isolated from rat kidney (Table 1) (*14*). ADMA is the preferred substrate for *Pa* DDAH (*15*) as reflected in a 1.8–fold increase in k_{cat} and a 2.1-fold decrease in K_M when compared to NMMA. A similar result to that of rat kidney DDAH which shows a 1.6-fold increase in k_{cat} and a 2.0-fold decrease in K_M when comparing ADMA and NMMA as substrates (*14*). The presence of an N^{ω}-substitution appears to be important for catalysis. N^{ω}-hydroxy-L-arginine and N^{ω}-amino-L-arginine are moderate substrates, but L-arginine is a very poor substrate with a k_{cat}/K_M value three orders of magnitude lower than that of ADMA. Interestingly, the NOS inhibitor SMTC (*39*) proved to be the best substrate tested so far with a 2.7-fold faster k_{cat} and 4.7 fold lower K_M at pH 6.2 as compared with its natural analog NMMA.

Other guanidino compounds commonly found in metabolism are not effectively processed as substrates, further supporting the proposed function of this enzyme as a DDAH. Despite the lack of known methyl arginine production in *Pseudomonas sp*., the observation that ADMA is a preferred substrate, and the determination that reaction products and rate constants are comparable to a known mammalian DDAH enzyme, are consistent with the assignment of this bacterial enzyme as an authentic DDAH.

Two other guanidino modifying enzymes in the superfamily, arginine deiminase (*24, 40*) and arginine:glycine amidinotransferase (*41, 42*), have been shown to utilize a covalent intermediate in their reaction mechanisms. The amidinotransferase reaction was studied through the use of radiolabeled L-arginine and acid trapping, and the arginine

deiminase reaction was elucidated through acid trapping, pre-steady-state kinetics (*24*) and X-ray crystallography (*43*). In a similar fashion we attempted to acid trap a transient covalent intermediate formed during steady-state turnover with the naturally occurring substrates ADMA and NMMA, but only found a single peak by ESI-MS with the same mass as unmodified enzyme. We hypothesized that either the rate of intermediate formation was rate determining thus limiting detectable amount of adduct, or that the DDAH catalyzed reaction does not use a covalent intermediate in its mechanism. A non-covalent mechanism would not be totally be unprecedented because at least one guanidino hydrolase, creatine amidinohydrolase, uses histidine as a general base to generate a hydroxide nucleophile (*44*). We then tried acid trapping with the substrate analogue SMTC, which has a 1.5 fold higher k_{cat} than ADMA (Table 2.1). Reactions of SMTC turnover by *Pa* DDAH were quenched at different time points to trap any covalent intermediate that accumulates. Points were taken throughout an entire progress curve at 0, 1, 5, and 30 min to insure that any adduct observed is transient in nature, and not the result of time-dependent inactivation. In contrast to our results with methylated arginines, the ESI-MS of a reaction mixture after 1 min of turnover (Figure 2.1B) showed appearance of a new major peak, indicating the formation of a new covalent adduct of 158 ± 10 Da (Figure 1B). The mass of this adduct is consistent with the expected mass increase (157.09 Da) after loss of a proton from an amino acid side chain and formation of a covalent bond between *Pa* DDAH and the remaining 1-(iminomethyl)-L-ornithine portion of the SMTC substrate after loss of its methanethiol leaving group. After 5 min of turnover (Figure 2.1C) the major peak is still that of the 158 Da adduct, but the amount of free enzyme has increased, and after 30 min of turnover (Figure 2.1D) the major peak

has returned to all free enzyme. A progress curve following citrulline production was taken under identical conditions as the acid-trapping experiment (Figure 2.1E) and shows that the rates observed parallel the relative amounts of enzyme-intermediate observed by ESI–MS in Figure 2.1 A–D. (For both the progress curve and the acid-trapping experiments, enzyme concentrations are much higher than those commonly used for determining initial rates.) Unrelated to the transient covalent adduct, a constant minor peak resulting from an *N*-terminal 178 Da adduct is seen at all time points and is due to non-enzymatic □-gluconoylation of the protein during expression (*32*); the ratio of this +□178 Da peak to the major peak is constant throughout the entire progress curve, providing further evidence that small differences in the *N*-terminus do not have significant catalytic consequences.

In order to map out the site of the covalent adduct, quenched reactions were digested with Glu–C endoproteinase at pH 4 where the *S*–alkylthiouronium intermediate is expected to be stable. This digest was analyzed by MALDI–TOF, resulting in 24 observed peptides covering 74% of the total sequence, including peptides containing the active site residues Cys_{249}, His_{162}, Glu_{114} and most of the other residues within 6 Å of the ureido group of citrulline complexed with *Pa* DDAH (*17*). MS analysis was able to identify 24 different peptides covering 74% of the total sequence, including peptides containing the active site residues Cys_{249}, His_{162}, and Glu_{114}. The linear MALDI spectrum of the digestion mixture shows a peptide at *m*/*z* 1732.9, corresponding to the average mass of the *C*-terminal DDAH peptide following Glu–C cleavage ($_{240}$YRKIDGGVSCMSLRF$_{254}$). This *C*-terminal peptide also contains the active–site Cys_{249} residue. The same spectrum also shows a peptide at *m*/*z* 1890.2, which does not

correspond to the predicted mass of any DDAH Glu-C cleavage peptide, but is 157.3 Da higher than the DDAH *C*-terminal peptide mass, consistent with the proposed intermediate. The peptide at *m*/*z* 1890 is not seen in the MALDI reflectron spectrum, demonstrating that it contains a bond that readily fragments after ionization, such as would be expected for a sulfide–carbamide bond. No increase of 157 Da was found for any other peptides in the digest. The immonium ion, b and y ions for the adducted peptide are similar to those of the unmodified peptide, confirming that the same peptide sequence is involved in both cases. The adducted peptide PSD shows modified y_{10}^{*} ions that appear as a pair of peaks separated by 34 Da. They represent dual fragmentation products with both backbone fragmentation and loss of the unstable adduct, again fragmenting on either side of the sulfide bond and implicating Cys249 as the point of attachment (Figure 2.3).

To corroborate the importance of Cys249, a C249S mutation was constructed and purified. A crystal structure of this variant shows that it folds properly and is capable of binding substrate (*17*). This mutant enzyme does not hydrolyze NMMA, ADMA, (*17*) nor SMTC, and acid quenched mixtures of SMTC and C249S only resulted in one major peak by ESI–MS, with a mass matching that of unmodified mutant enzyme.

Together these results show that the *Pa* DDAH is indeed a member of the superfamily of guanido modifying enzymes. Despite their being no evidence for *Pseudomonas* species that can produce methyl arginines, this bacterium is shown to have a gene product capable of catalyzing the identical reaction chemistry, and similar substrate specificity as its mammalian counterparts. The use of the activated substrate analogue SMTC, reveals that, like arginine deiminase and arginine:glycine

amidinotransferase, the DDAH catalyzed reaction proceeds through attack of an active–site cysteine nucleophile, forming a transient *S*–alkylthiouronium intermediate, and thus further relating it to the superfamily of guanido modifying enzymes. The mechanistic information from the experiments detailed here will greatly facilitate design of inhibitors for DDAH and perhaps other superfamily members that are potential drug targets.

Chapter 3 A New Continuous Assay for DDAH Activity and Quantification of Product Inhibition

Introduction

Dimethylarginine dimethylaminohydrolase (DDAH) is found in both prokaryotes and eukaryotes and catalyzes the hydrolysis of N^{ω}-methyl-L-arginine (NMMA, Scheme 3.1 A) and asymmetric N^{ω},N^{ω}–dimethyl–L–arginine (ADMA) to L-citrulline and either methylamine or dimethylamine, respectively (*14, 15, 45*). In mammalian systems, ADMA and NMMA are endogenous inhibitors of nitric-oxide synthase, making DDAH an attractive target for therapeutic intervention because of its regulation of nitric oxide production through control of ADMA and NMMA concentrations (*12*). To date, the only reported methods for monitoring DDAH activity have been discontinuous assays. The use of radiolabeled substrates (*13*), HPLC (*46*), or derivatization to detect dimethylamine production (*47*) have been reported, but the most commonly used procedure to assay DDAH activity relies on diacetyl monoxime (DAMO) derivatization of the ureido group in L-citrulline (Scheme 3.1 A) to form a colored product (*26, 27*). This assay has been optimized for monitoring DDAH activity in a 96-well format (*28*), but still requires several laborious steps that can introduce error and hazard, including the addition of strong acids and prolonged incubation of sealed tubes or microtiter plates at 95° C. This method also suffers from the instability of the final chromophore to light (*26*), the inability to distinguish L-citrulline from other compounds that have ureido groups, and

the discontinuous nature of the assay which requires approximately 25 min to develop and analyze a sample.

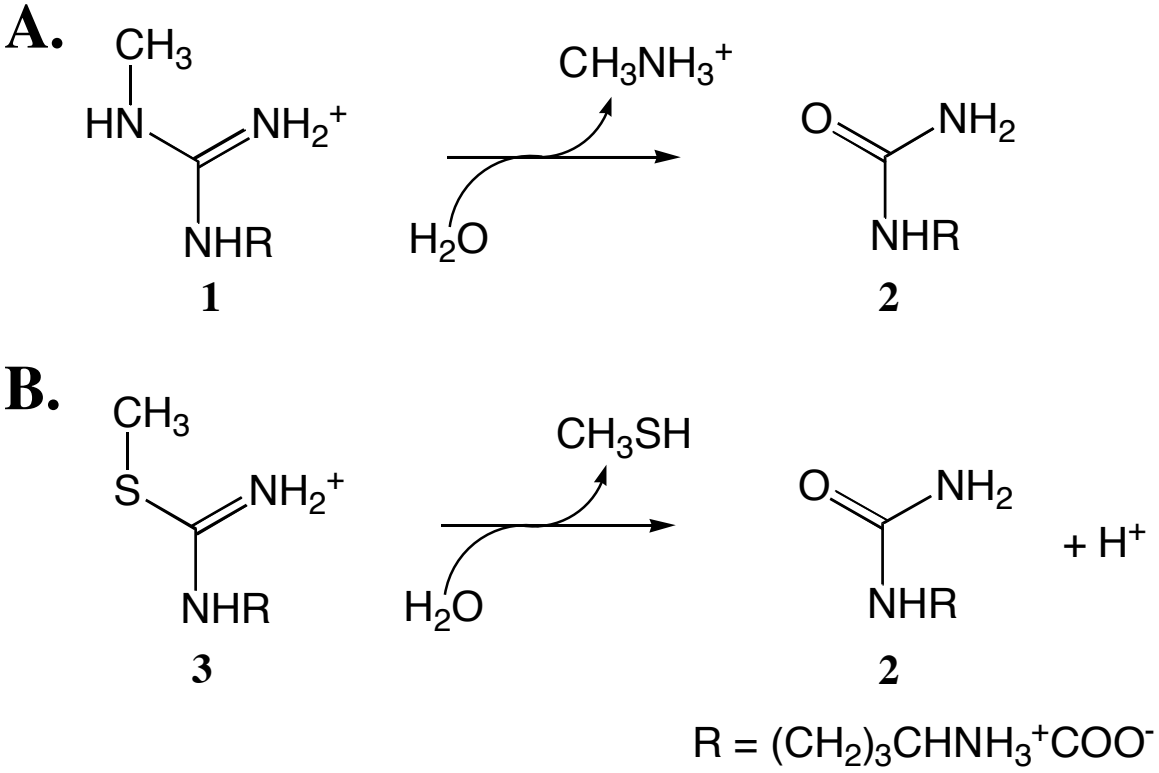

Scheme 3.1 DDAH catalyzed reaction products of NMMA and SMTC

We therefore developed a new assay for DDAH activity based on the use of the alternative substrate, *S*-methyl-L-thiocitrulline (SMTC), that, upon hydrolysis, is proposed to produce methanethiol (Scheme 3.1 B) which can easily be quantified by 5,5'-dithiobis(2-nitrobenzoic acid) (DTNB) in a continuous spectrophotometric assay. Because of the similar reactions catalyzed by this superfamily of enzymes, it is likely that this strategy could be more widely applied.

This alternative substrate, SMTC, is commercially available (Sigma-Aldrich Chemical Co., St. Louis, MO), and similar in structure and charge (the pK_a of *S*-methylthiourea is 9.8 (*48*)) to NMMA (the pK_a of *N,N'*-dimethylguanidine is 13.6 (*48*)), a natural substrate of DDAH. Previous studies (Chapter 2) using the DAMO assay demonstrated that SMTC serves as a good substrate for the DDAH from *PA aeruginosa*, and that this bacterial DDAH which shares 29-30 % amino acid identity with human, rat and bovine DDAH-1, and 23% identity with human and rat DDAH-2, processes NMMA and ADMA with comparable rates to those reported for mammalian DDAH isozymes (*14, 35, 49*). In this study we compared the kinetics of DDAH–catalyzed hydrolysis of SMTC as assayed by the discontinuous DAMO derivatization assay to follow L-citrulline production, and as assayed using DTNB to follow methanethiol production in a continuous spectrophotometric assay. We also demonstrated the utility of this new assay method by determining the K_i of product inhibition by L-citrulline, a measurement not readily made using the DAMO derivatization assay.

Materials and Methods

STEADY–STATE KINETICS OF SMTC HYDROLYSIS AS DETERMINED BY DAMO DERIVATIZATION ASSAY

The DAMO derivatization assay for L–citrulline production (*28*) was used, with minor modification, to determine the k_{cat} and K_M values for SMTC hydrolysis by *Pa aeruginosa* DDAH (*49*) under the same conditions as used for the continuous assay described below. Briefly, concentrations of SMTC (0 – 10 mM) were prepared in assay buffer consisting of 0.1 M phosphate buffer, pH 7.27, containing 1 mM EDTA to chelate

any trace metals that could catalyze unwanted thiol oxidation. Substrate aliquots of 200 μL were placed in 1.5 mL microcentrifuge tubes to which 5 μL portions of a stock solution of purified recombinant His_6-DDAH from *PA aeruginosa* (79 μM) (*49*) were added to initiate the reactions. Substrate and enzyme were incubated at 25° C for 1 min and then quenched with 10 μL of trichloroacetic acid (6N) to stop the reaction. Control reactions without enzyme were included for each substrate concentration. Standards containing L–citrulline (0 to 313 μM) were also prepared in 0.1 M phosphate buffer, 1 mM EDTA, pH 7.27, and used to construct a linear standard curve. To the standards and quenched reactions, a 1 mL aliquot of a color developing reagent containing DAMO and other components (*28*) was added. Reaction tubes were sealed and placed in a boiling water bath for 15 min, and then cooled to 25° C over a 10 min period. The absorbance at 540 nm was measured for each sample using a Cary 50 UV-Vis spectrophotometer (Varian Instruments, Walnut Creek, CA). The resulting absorbance values, after background correction, were converted to L-citrulline concentrations using a standard curve and the initial rates of product formation at each substrate concentration were fit directly to the Michaelis-Menten equation (Kaleidagraph; Synergy Software, Reading PA).

STEADY–STATE KINETICS OF SMTC HYDROLYSIS AS DETERMINED BY CONTINUOUS ASSAY

The steady-state DDAH-catalyzed hydrolysis of SMTC was measured, but instead of the discontinuous assay, DTNB was used to monitor methanethiol release in a continuous manner. Briefly, stock concentrations of SMTC (0 - 10 mM) were prepared in assay buffer containing 0.1 M phosphate buffer, 1 mM EDTA, pH 7.27 and a stock

solution of DTNB (5 mM), as described (*50*). To a microcuvette, 300 μL of a substrate stock and 10 μL of DTNB reagent were mixed and the reaction was initiated by the addition of 2.5 μL of enzyme stock (79 μM). Changes in absorbance at 412 nm were monitored continuously. At 10-fold lower enzyme concentrations and sufficient substrate and DTNB concentrations, increases in absorbance due to substrate hydrolysis were found to be linear for times longer than 10 min, indicating that, despite the five cysteine residues found in *Pa* DDAH, enzyme activity is not adversely effected by incubation with DTNB on this timescale. Similar incubations at 37º C were also linear, but showed some loss of activity at times longer than 6 min, suggesting that at increased temperatures, this enzyme is more susceptible to modification by DTNB. Typically, after a short initial mixing period (less than 20 s) reactions were followed at 25º C for 2-5 min and the linear portions of the curves were plotted to obtain an observed rate for hydrolysis of SMTC at each concentration. These observed steady-state rates (AU/min) were converted to units of μM/s using a published molar absorption coefficient of 14,150 M^{-1} cm^{-1} (*50*). This extinction coefficient is sensitive to pH, temperature, and some other experimental conditions (*50-53*), so these must be carefully controlled. The resulting data were fit directly to the Michaelis-Menten equation as described above (Figure 3.1, inset).

COMPETITIVE INHIBITION OF DDAH BY L-CITRULLINE WITH THE CONTINUOUS ASSAY

Briefly, assay solutions were prepared containing varying SMTC (9 – 313 μM) and L-citrulline (1.2 - 17 mM) concentrations, all in 1 mM EDTA, 0.1M phosphate buffer, pH 7.27. To a microcuvette, 290 μL of a substrate / inhibitor mixture and 10 μL of the DTNB reagent were mixed, and the reaction was initiated by the addition of 2.5 μL

from an enzyme stock solution (79 μM). Production of methanethiol and its subsequent reaction with DTNB was monitored continuously at 412 nm as described above.

Results

STEADY–STATE KINETICS OF SMTC HYDROLYSIS AS DETERMINED BY DAMO DERIVATIZATION AND BY CONTINUOUS ASSAY

These two dissimilar assay methods for steady-state hydrolysis of SMTC by DDAH gave comparable results and these data were well fit by the Michaelis-Menten equation. The steady-state rate constants were found to be consistent whether measured by the discontinuous DAMO assay that follows L-citrulline production (K_M = 23 ± 3 μM; k_{cat} = 48.6 ± 0.6 min^{-1}) or by the DTNB detection of methanethiol release (K_M = 19 ± 1 μM; k_{cat} = 72 ± 0.6 min^{-1}). These results illustrate that a continuous assay for DDAH can be easily used for quantifying the catalytic activity of this enzyme and gives results comparable to existing assays. These corroborating results indicate that significant amounts of methanethiol are not lost to evaporation or oxidation before reacting with DTNB, and that factors other than enzyme activity are not limiting under these conditions.

COMPETITIVE INHIBITION OF DDAH BY L-CITRULLINE WITH THE CONTINUOUS ASSAY

For easy visual interpretation, Lineweaver-Burk plots of DDAH inhibition by L-citrulline were plotted and show that, at high substrate concentrations, the extrapolation of $1/v_o$ values from all of the substrate concentrations at each inhibitor concentration intersect at $1/V_{max}$, indicating that inhibition is competitive with substrate (Figure 3.1) (*54,*

55), and that L-citrulline binds at the active site, consistent with the crystallographic observation (*17*). To obtain a numerical value for K_i, the initial rate data were fit directly to the equation for competitive inhibition, $v_o = ((V_{max}[S])/(\alpha K_M + [S]))$, by fitting V_{max} and α while constraining the K_M of SMTC to the value determined above. The values calculated for α were then plotted versus L-citrulline concentrations and the slope was determined to give the value of K_i, ($\alpha = 1 + [I]/K_i$) (*54*). Using this method, the K_i determined for L-citrulline inhibition of *PA aeruginosa* DDAH is 8.4 ± 0.5 mM, a result comparable to the reported K_i (3.0 mM) for product inhibition of rat DDAH-1 (*14*).

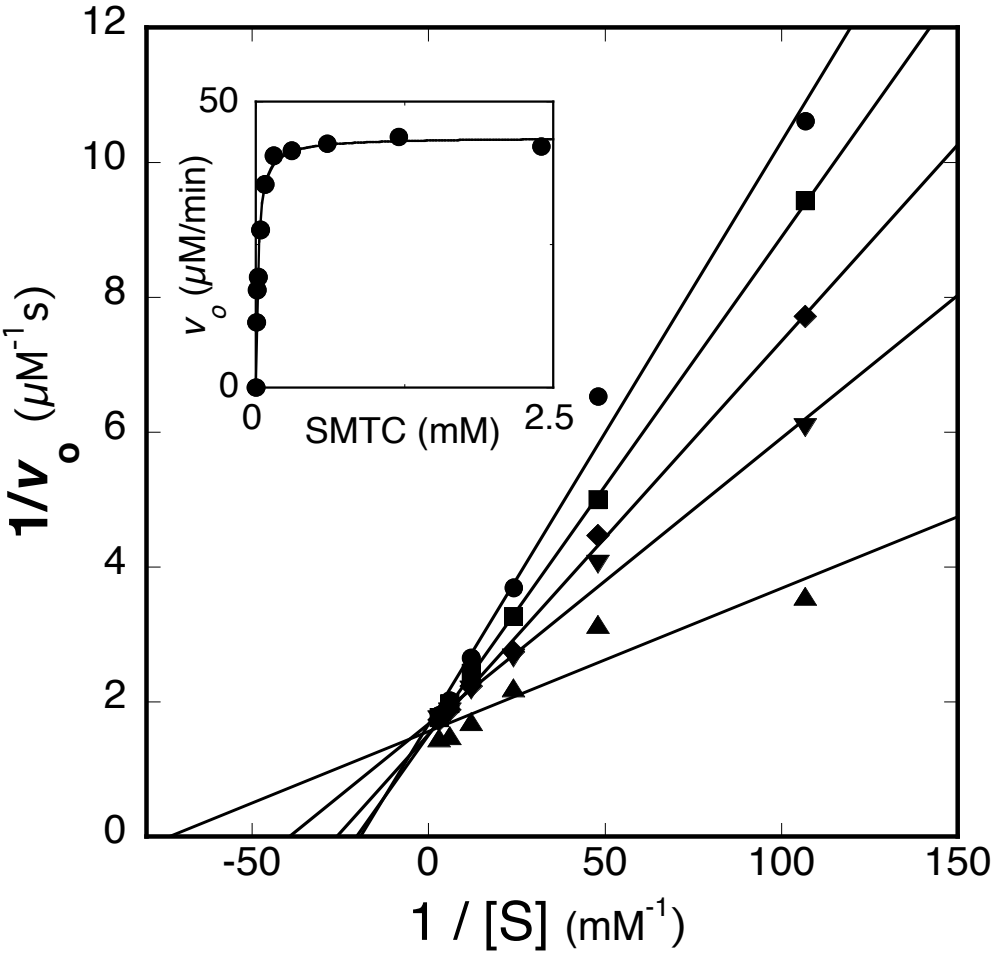

Figure 3.1 Lineweaver-Burk Plot for L-Citrulline Inhibition of DDAH

L-Citrulline is included in assay mixtures at concentrations of 0 (▲), 2.13 (▼), 4.26 (✦), 8.52 (■), and 17.04 (●) mM. The inset shows uninhibited DDAH-catalyzed hydrolysis of SMTC as monitored by the DTNB assay (●) and a fit of this data to the Michaelis–Menten equation (solid line).

Discussion

This novel continuous assay has other advantages over the DAMO derivatization procedure. For example, a crystal structure of L-citrulline bound to a mutant *Pa aeruginosa* DDAH active site has been published, but the inhibition constant was not reported. Because the DAMO derivatization assay detects ureido groups, determining the inhibition constant of L-citrulline is problematic due to the small amounts of L-citrulline produced by enzyme in comparison with the concentrations used for inhibition studies. However, the continuous assay greatly facilitates these experiments.

Although this new continuous assay has many advantages, it is not expected to fully supplant the existing DAMO assay for several reasons. DDAH isozymes from different sources likely display varying sensitivities to thiol–modifying reagents (*14, 35*) and this sensitivity will have to be assessed before using the DTNB-based assay. Moreover, an artificial substrate must be used rather than the naturally occurring ADMA and NMMA. Also, a variety of experimental conditions are known to interfere with DTNB-based assays and attempts to overcome these drawbacks are well described (*50-53, 56*). Despite these caveats, this new continuous assay represents a significant advance from the known discontinuous assays of DDAH activity. In general, DTNB-based assays are amenable to high–throughput formats (*57*), so the assay reported here could allow facile screening of both inhibitor and mutant DDAH enzyme libraries. In addition, unlike the DAMO derivatization assay, this continuous assay is insensitive to compounds containing ureido groups, allowing a wider variety of inhibitors to be easily assayed. Because of the similarity of reactions catalyzed by other superfamily members,

it is likely that this assay strategy could have wider applicability. In conclusion, the use of a commercially-available alternative substrate, SMTC, allows a quantifiable, continuous, spectrophotometric assay of enzyme activity, which will greatly facilitate studies of DDAH.

Chapter 4 Active–site Directed Inactivation of DDAH

Introduction

The finding that DDAH isoforms regulate endogenous concentrations of N^{ω}-methyl-L-arginine (NMMA) and N^{ω}, N^{ω}-dimethyl-L-arginine (ADMA) (*16*) which serve as nitric oxide synthase inhibitors, has made DDAH an attractive drug target. Overproduction of nitric oxide is implicated in various disease states including septic shock, neuronal damage during stroke, and angiogenesis (*2*). Thus, understanding the normal physiological control mechanisms of nitric oxide production is of great interest as is the ability to regulate the concentrations of endogenous methylated arginines through the selective inhibition of DDAH activity. The DDAH from *Pseudomonas aeruginosa* (*Pa*) may also have a pathogenic function – one report suggests that nitric oxide may mediate respiratory tissue damage during infection, an effect limited by ADMA (*58*), but possibly encouraged by *Pa* DDAH. Hence, inhibitors for both human and microbial DDAH isoforms are desired. Inhibitors known to target the active-site specifically include L-citrulline (*17, 36*), L-homocysteine (*59*), *S*-nitroso-L-homocysteine (*60*), zinc (II) (*21*), and synthetic arginine analogs (*61*). However, few specific irreversible inhibitors have been described.

The work described here shows that 2-chloroacetamidine (Figure 4.1)(CAA), with a substrate–like amidinium group and a chloromethylene moiety, is a time–dependent, active–site directed inactivator of *Pa* DDAH. Through kinetic analysis, site–directed mutants and mass spectrum analysis, a mechanism of inactivation is proposed.

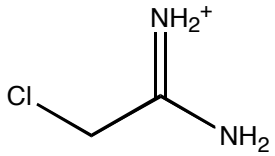

Figure 4.1 Structure of 2–chloroacetamidine (CAA)

Materials and Methods

Materials. Synthetic DNA primers were from Sigma-Genosys (The Woodlands, TX). Restriction enzymes and dNTPs were from New England Biolabs (Beverly, MA). Triplemaster polymerase was from Eppendorf (Westbury, NY). Qiaquick purification kits were from Qiagen (Valencia, CA). Glu-C endoproteinase was from Roche (Indianapolis, IN). 2-Chloroacetamidine was from Lancaster (Windham, NH). Chelex-100 was from BioRad (Hercules, CA). Unless noted otherwise, all other chemicals and buffers are from Sigma-Aldrich Chemical Co. (St. Louis, MO).

CONSTRUCTION OF AN EXPRESSION VECTOR FOR MUTANT H162G DDAH, PROTEIN EXPRESSION AND PURIFICATION

Two complementary mutagenic oligonucleotides, (forward) 5′-CGCCTGGAAAAGGTCCTGggcCTGAAGACCGGGCTCGCC–3′ and (reverse) 5′-GGCGAGCCCGGTCTTCAGgccCAGGACCTTTTCCAGGCG–3′ were designed to introduce a mutant codon (lowercase) encoding a H162G mutation in the DDAH sequence by overlap extension PCR (*62*). Briefly a 3′ H162G megaprimer was produced by PCR amplification from a pETpaDH template (*49*) using the forward mutagenic primer and an outside T7 terminator primer (New England Biolabs) in an MJ Research

PTC 200 thermocycler (Waltham, MA), along with dNTPs, Triplemaster polymerase and Hi-Fidelity Buffer (Eppendorf), with a temperature program of 95° C for 5 min, followed by 30 cycles of 95° C for 30□s, 52° C for 30□s, and 72° C for 1 min. Construction of the 5□ H162G megaprimer required slightly different conditions to optimize product. Amplification was carried out by the PCR using pETpaDH as a template, the reverse mutagenic primer described above, a specific outside primer described previously (*49*), dNTPs, Triplemaster polymerase and Tuning Buffer according to protocols for GC–rich templates (Eppendorf) by using a temperature program of 98° C for 5 min, followed by 45 cycles of 98° C for 20□s, 53° C for 10□s, and 72° C for 90□s. After Qiaquick purification, the 5□and 3□megaprimers, the specific outside end primers described previously, dNTPs, Triplemaster polymerase, and Tuning Buffer, were combined in a PCR with a temperature program of 98° C for 5 min, followed by 45 cycles of 98° C for 20□s, 53° C for 10□s, and 72° C for 90□s. The resulting H162G *Pa* DDAH coding sequence was subsequently cloned between the *Nde*I and *Eco*RI restriction enzyme sites of a pET-28a expression vector as described previously (*49*). Expression and purification of mutant H162G *Pa* His_6-DDAH as well as C249S and wild-type *Pa* His_6-DDAH was completed as described previously (*49*).

TIME-DEPENDENT INACTIVATION OF DDAH BY 2-CHLOROACETAMIDINE (CAA)

Purified recombinant *Pa* His_6-DDAH (7.9 □M) was incubated with KCl (100 mM) and 2-chloroacetamidine (CAA, 0 – 10.5 mM) at pH 6.2 and 25° C in MES buffer (10 mM) that was previously treated with Chelex–100 (BioRad, Hercules, CA) to remove trace metal ions. To test for time-dependent loss of activity, aliquots were removed from

these incubations at time points (0 – 40 min) and diluted into an assay solution containing an excess (1 mM) of the alternative substrate, *S*-methyl-L-thiocitrulline (*49*). The remaining enzyme activity was assayed by detecting methanethiol release upon substrate hydrolysis using dithio-bis(2-nitrobenzoic acid), as described elsewhere (*36*). Inactivation rates in preincubation mixtures including enzyme, CAA, and an excess of the substrate N^{ω}-methyl-L-arginine (10 mM) were assessed to determine whether CAA acts at the active-site of the enzyme. To avoid errors inherent in fitting linearized semi-log plots, the observed pseudo first order inactivation rate constants (k_{obs}) were determined by direct fitting of the inactivation plots to a single exponential equation. The resulting k_{obs} values were plotted against inactivator concentration and directly fit to $k_{obs} = (k_{inact}*[I])/(K_I + [I])$ to obtain K_I and k_{inact} values (*63*). All fits were calculated using KaleidaGraph software (Synergy Software, Reading, PA). To further assay the irreversibility of inhibition by CAA, fully inhibited DDAH was dialyzed for 24 h at 4 ºC with MES buffer (10 mM) and KCl (100 mM) at pH 6.2 and the resulting activity was assayed as described above. Control reactions were run in parallel to insure that uninhibited DDAH retained activity under these conditions.

MASS SPECTRUM ANALYSIS OF INACTIVATED DDAH AND DDAH VARIANTS

In order to characterize any covalent adducts formed during enzyme inactivation, 30 min incubations of CAA (1 mM) with *Pa* His_6-DDAH were carried out at 25 °C under the same conditions used in the preincubations described above and quenched with 0.5 M trichloroacetic acid. Similar incubations were carried out using the C249S and H162G mutant DDAH enzymes, and a wild type DDAH that had previously been denatured in

MES buffer (20 mM) containing 8 M urea at a pH of 6.2. Control reactions omitting CAA were also run in parallel. Samples were then desalted and analyzed by ESI-MS on a ThermoFinnigan LCQ (San Jose, CA) ion trap mass spectrometer as described previously (*49*). A control digest of untreated DDAH was also conducted and analyzed in parallel.

IDENTIFICATION OF A COVALENTLY MODIFIED DDAH PEPTIDE

In order to determine the amino acid that is modified by CAA, the inactivated DDAH was exchanged into 50 mM ammonium acetate buffer (pH 4) by passing through a Sephadex G-10 spin column, digested with Glu-C endoproteinase, and the products analyzed using MALDI-TOF and MALDI-PSD on an Applied Biosystems Voyager-DE Pro as previously described (*49*) (*30*). Theoretical digest masses were calculated by the MS-Digest program in the Protein Prospector suite using two missed cleavages (*31*).

INCUBATION OF DDAH WITH 2-CHLOROACETAMIDE

Incubations containing DDAH (30 μM), KCl (100 mM) and 3 mM of 2-chloroacetamide, a neutral analog of CAA were prepared at pH 6.2 and 25 ºC in MES buffer (10 mM) that was previously treated with Chelex-100 to remove trace metal ions. To test for time-dependent loss of activity, aliquots were removed from these incubations at time points between 0 – 15 min and assayed as described above. Control reactions were completed in the absence of 2-chloroacetamide. All reactions were performed at least in triplicate, and the data fit as described above.

Results

CLONING, EXPRESSION, AND PURIFICATION OF MUTANT AND WILD-TYPE DDAH ENZYMES

DNA sequencing of the H162G variant indicated that the desired mutagenic codon was successfully incorporated and no inadvertent mutations were introduced into the protein coding region. The resulting vector was used to express mutant H162G DDAH in BL21(DE3) *E.coli*. This variant, as well as the C249S and wild-type DDAH, were purified using published procedures to greater than 95% homogeneity as assessed by SDS-PAGE and determined to contain less than 0.01 equiv zinc by inductively-coupled plasma mass spectrometry (Department of Geological Sciences, The University of Texas) (*49*).

TIME-DEPENDENT INACTIVATION OF DDAH BY (CAA) AND BY 2-CHLOROACETAMIDE

Preincubation mixtures of DDAH with CAA result in time- and concentration-dependent enzyme inactivation, with K_I and k_{inact} values of 3.1 ± 0.8 mM and 1.2 ± 0.1 min^{-1}, respectively (Figure 4.2). Co-incubation with excess substrate (uninhibited k_{cat} = 19 min^{-1}, K_M = 670 □M) protects against inactivation, indicating that CAA acts at the active-site of the enzyme. Inhibition is observed after dilution of the preincubation mixtures into a large excess of substrate and after dialysis to remove non-covalently bound inhibitors, consistent with an irreversible mechanism. Preincubations with the neutral 2-chloroacetamide did not show any time-dependent inactivation relative to controls.

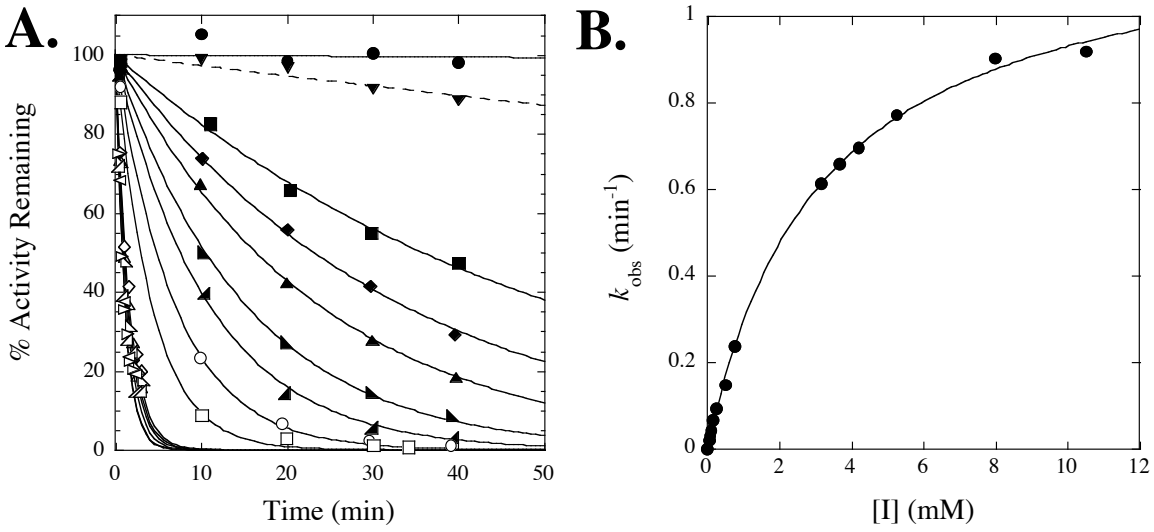

Figure 4.2 Time- and concentration-dependent inactivation of DDAH by CAA

(A) Exponential fits to the observed inactivation at pH 6.3, 25 °C by different concentrations of CAA: 0 (●), 0.05 (■), 0.075 (◆), 0.1 (▲), 0.15(filled right triangle pointing left), 0.25(filled right triangle pointing right), 0.5(○), 0.75(□), 3.2 (▯), 3.7 (▯), 4.2 (empty triangle pointing left) 5.3(empty triangle pointing right), 8 (equilateral triangle pointing left) and 10.5 mM (equilateral triangle pointing right). The dashed line (▼) indicates fits to inactivation by CAA (0.1 mM) in the presence of 10 mM substrate, $N^{\square}$-methyl-L-arginine. B. Concentration dependence of the pseudo-first order k_{obs} values for inactivation.

Table 4.1 Summary of major ions observed in ESI-MS spectra of control and inactivated DDAH

DDAH Preparation	Theoretical Calculated mass (Da)	Control Incubations with no inactivator Observed mass (Da)[a]	Incubations with CAA Observed mass (Da)[a]
Wild Type	30503	30499	30556
Urea-denatured	30503	30497	30495
C249S	30487	30478	30479
H162G	30423	30415	30471

[a] The major ion peaks from deconvoluted ESI-MS spectra are reported with errors of ± 10 Da.

MASS SPECTRUM ANALYSIS OF INACTIVATED DDAH AND DDAH VARIANTS

The deconvoluted mass spectrum of a control reaction including wild-type DDAH but no inactivator results in one major peak at 30499 ± 10 Da, matching the mass calculated from the protein sequence, after removal of the N-terminal methionine residue (30503 Da) (Table 4.1). Fully inactivated DDAH results in one major peak at a different mass of 30556 ± 10 Da, indicating the addition of a covalent adduct of 57 ± 10 Da. Incubation mixtures with CAA and C249S DDAH, or urea-denatured DDAH do not result in peaks that differ significantly from that predicted for unmodified protein (Table 1). However, incubation mixtures with CAA and H162G DDAH do result in one major peak at 30471± 10 Da, indicating a mass increase (56 ± 10 Da) over control incubations that do not contain inactivator (30415 ± 10 Da).

IDENTIFICATION OF A COVALENTLY MODIFIED DDAH PEPTIDE

In order to determine which amino acid of DDAH is modified during inactivation, and to get a more precise mass of the covalent adduct, inactivated wild-type DDAH containing the + 56 Da adduct was digested by Glu-C endoproteinase and the resulting peptides were detected using MALDI-TOF. Sixteen different peptides were identified by comparison with peptide molecular masses calculated from a theoretical digest. The observed peptides cover 66 % of the total protein sequence and include the active-site residues Cys249, His162, Glu114, and Thr165 (Table 2). The digestion mixture also shows a peptide at *m*/*z* 1789.1, which does not correspond to the mass of any predicted peptide after digestion, but is 56.1 ± 0.2 Da higher than the C-terminal peptide of DDAH ($_{240}$YRKIDGGVSCMSLRF$_{254}$) after digestion by Glu-C endoproteinase. This proposed adduct is consistent with the 57 ± 10 Da adduct found in undigested inactivated DDAH using ESI-MS. Similar mass increases were not observed for any other peptides in the digest, including the peptide containing the active site histidine residue (His162). A control Glu-C digest of DDAH lacking CAA did not contain any signal at *m*/*z* 1789, but did contain the unmodified C-terminal peptide at *m*/*z* 1733.

Table 4.2 Summary of proteolytic cleavage of inactivated DDAH with endoprotease Glu-C[a]

DDAH sequence positions plus leader (-18 to 0)	Calculated peptide mass (Da)	Observed peptide mass (Da)[b]
(-18) to 33	5657.4	5656.9
95-105	1324.5	1324.5
95-114	2277.6	2277.5
95-129	3914.5	3914.1
106-114	972.1	972.1
115-129	1655.9	1655.8
130-146	1832.1	1832.1
137-146	1102.3	1102.3
147-158	1282.5	1282.5
159-171	1485.8	1485.8
159-186	3093.6	3093.4
172-186	1626.8	1626.7
211-223	1546.8	1546.8
211-234	2846.4	2846.3
224-234	1318.6	1318.7
240-254	1733.1	1733.0
240-254 + Acam[c]	1789.2	1789.1

[a] Comparison of average calculated average peptide masses (MS-Digest in Protein Prospector) for up to two missed cleavages with experimental linear MALDI-TOF results. Amino acid numbering is assigned to match that of Protein Data Bank entry 1H70 (*17*).

[b.] Mass accuracy is 100 ppm, after smoothing of spectrum and internal calibration.

[c.] Acam stands for the acetamidine adduct shown in Figure 4.3.

Table 4.3 Summary of major ions observed in MALDI-PSD fragmentation spectra from *m/z* 1789 parent ion: YRKIDGGVSCMSLRF+Acam[a]

Ion	Calculated *m/z*	Observed *m/z*[b]
R	70	70
K	84	84
I/L	86	86
K	129	129
Y	136	136
RK-NH_3	268.3	268.1
b_2-NH_3	303.3	302.8
y_5	653.8	653.3
b_5	676.8	676.4
y_{10}	1057.3	--
y_{10}*+(Acam)[a]	1113.4	1113.9
y_{10}*-(Acam+S)	1023.2	1024.0
MH^+-(Acam+S)	1699.0	1699.1

a. Acam stands for the acetamidine fragment shown in Figure 4.3

b. Mass accuracy is 1500 ppm. Average masses are reported.

Ions from MALDI post source decay (PSD) fragmentation spectra of the modified C-terminal peptide at *m/z* 1789 were used to provide information about the site of attachment (Table 4.3, Figure 4.3). Ions found at *m/z* 84 and at *m/z* 129 are consistent with the singly charged multiple immonium and related ions characteristic of lysine and glutamine residues (*64*), but are both assigned here as lysine-derived ions (Table 4.3)

because there are no glutamine residues found in the parent peptide. The b_2-NH_3, b_5 and y_5 daughter ions match those expected from unmodified peptide. However, a y_{10}* ion is found as a fragment containing the 56.6 ± 1.7 Da adduct. These results localize the adduct to a residue within the $_{245}$GGVSC$_{249}$ sequence. Additional fragmentation shows a neutral loss of 90 Da from the y^{10}* ion, providing additional information about the site of attachment (Figure 4.3).

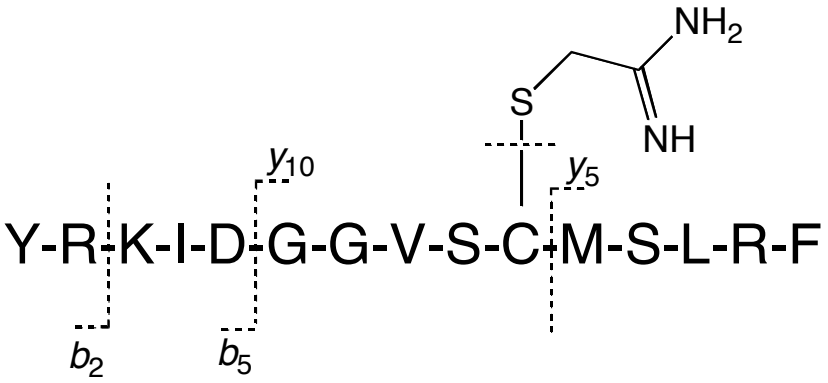

Figure 4.3 Summary of fragmentation pattern from MALDI-PSD

A 1789 Da peptide shows b_2-NH_3, b_5, y_5, and y_{10}* fragments. The y_{10}* fragment ions have an additional mass shift of 56.6 Da due to the presence of the acetamidine adduct. Secondary fragmentation involving neutral loss of the acetamidine modified cysteinyl sulfur implicates Cys249 as the point of attachment.

Discussion

2-chloroacetamidine (CAA) has a substrate–like group amidinium coupled to a chloromethylene leaving group. Thus we hypothesized that (CAA) might have potential as an active–site directed inactivator of DDAH. Indeed, pre–incubation mixtures of *PA aeruginosa* DDAH with CAA resulted in a time- and concentration-dependent enzyme inactivation, with K_I and k_{inact} values of 3.1 ± 0.8 mM and 1.2 ± 0.1 min^{-1}, respectively (Figure 4.2). Inhibition is observed even after dilution of the pre–incubation mixtures into large excesses of substrate and after dialysis to remove any non-covalently bound inhibitors, consistent with an irreversible mechanism. Also, co–incubation with excess substrate protects against inactivation, indicating that CAA acts at the active–site of DDAH.

To determine how inactivation by CAA occurs, we analyzed reaction mixtures of CAA with wild–type DDAH, a C249S variant and a H162G variant by ESI-MS. The deconvoluted mass spectrum of a control reaction of wild–type DDAH without CAA resulted in one major peak at 30499 ± 10 Da, matching the mass calculated from the protein sequence, after removal of the *N*-terminal methionine residue (30503 Da). Inactivated DDAH resulted in one major peak at a different mass of 30556 ± 10 Da, indicating the addition of a covalent adduct of 57 ± 10 Da. This mass increase is consistent with the covalent addition of only one equivalent of CAA with the loss of a Cl^- ion from CAA, and a proton from the enzyme (56.08 Da).

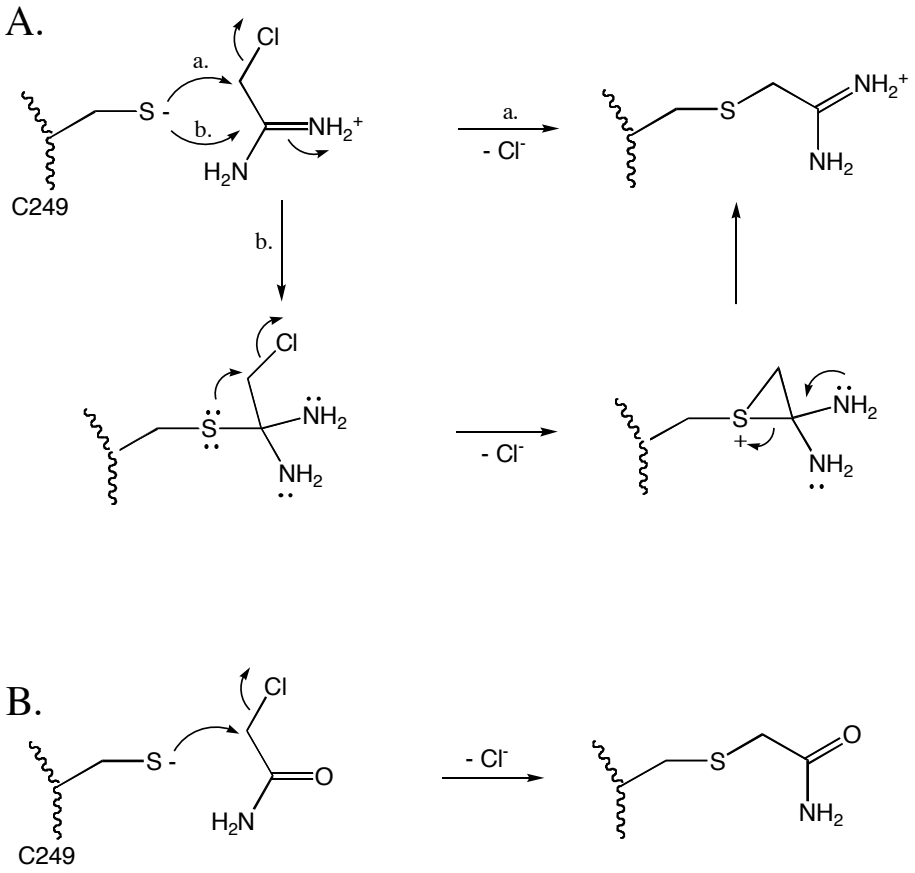

Scheme 4.1 Possible mechanisms for modification of Cys249 by (A) CAA or by (B) 2-chloroacetamide

Incubations of the C249S variant with CAA did not result in formation of adduct, implicating that the nucleophilicity of this residue is important to the inactivation mechanism. However, incubations of the H162G variant with CAA resulted in formation of a +56 Da adduct (Table 4.1), demonstrating that His_{162} is not involved in formation of adduct.

To further investigate the inactivation mechanism, we determined which residue of DDAH is modified by CAA**,** by using protease digestion of control and inactivated wild-type enzyme and subsequent MALDI-TOF MS to identify the resulting peptide

fragments. The linear MALDI spectrum of inactivated DDAH showed a new peak at 1789.1 ± 0.2 Da, corresponding to the mass of a C-terminal peptide containing the active-site cysteine, ($_{240}$YRKIDGGVSCMSLRF$_{254}$), plus a 56.1 ± 0.2 Da adduct. Similar mass increases were not observed for any other peptides in the digest, including the peptide containing the active–site His_{162}, and were not observed in control incubations lacking CAA. This result gave strong evidence that the single covalent modification observed above was attached to a residue within this peptide, most likely the active–site Cys249. This is consistent with the observation that the C249S does not react with CAA. The 100 ppm mass accuracy of the MALDI-MS measurements also allowed us to distinguish between a covalent acetamidine adduct with a calculated mass difference of 56.08 Da (Scheme 4.1 A), and a covalent acetamide adduct with a calculated mass addition of 57.06 Da (Scheme 4.1 B) in the singly charged peptide ions. The acetamide adduct could potentially arise through hydrolysis of the amidine either before (Scheme 4.1 B) or after (not shown) inactivation. Although only a small difference of 1 Da is predicted between these two adducts, accurate MS measurements can easily distinguish the 1 Da difference between arginine and citrulline residues arising from post-translational modifications (*65*). Here, the observed *m*/*z* increase of 56.1 ± 0.2 Da upon inactivation is consistent with formation of a covalently attached acetamidine adduct (Scheme 4.1 A) and not consistent with an acetamide adduct (Scheme 4.1 B). In support of this conclusion, no time-dependent inhibition was observed upon preincubation of DDAH with the neutral 2-chloroacetamide under experimental conditions similar to those used for inactivation of DDAH by CAA. The positive charge of CAA clearly either enhances the nucleophilicity

of Cys249, or is far more capable of binding in the active site as compared to the neutral 2-chloroacetamide.

The finding that CAA is a time dependent, active–site directed inactivator of DDAH makes it a promising lead compound in developing a pharmacophore for inhibiting this superfamily of enzymes (*66*). We also applied CAA to a different superfamily member peptidyl arginine deiminase IV (PAD4) and found a similar time– and concentration– dependent inactivation, that was protected by substrate, with K_I and k_{inact} values of 20 ± 5 mM and 0.7 ± 0.1 min^{-1}, respectively.

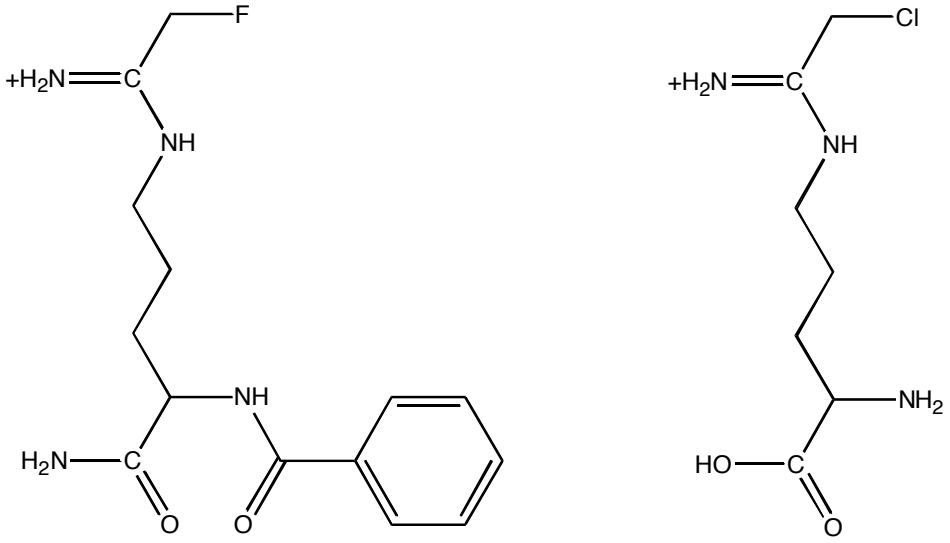

N-α-benzoyl-N5-(2-fluoro-1-iminoethyl)-L-ornithineamide 2-chloro-1-iminoethyl-L-ornithine

Figure 4.4 Structure of N-α-benzoyl-N^5-(2-fluoro-1-iminoethyl)-L-ornithineamide, and 2–chloro-1-iminoethyl-L-ornithine

Shortly after publishing our results, Luo et al., demonstrated that the substrate–like N-α-benzoyl-N^5-(2-fluoro-1-iminoethyl)-L-ornithineamide (F-amidine) (Figure 4.4) also inactivates PAD–4, in a time and concentration dependent manner, with a K_I and k_{inact} values of 330 μM and 1 min^{-1} respectively (*67*). Thus in the case of

PAD–4, the substrate like features of F-amidine yielded a k_{inact}/K_I of 3000 M^{-1} min^{-1}, or nearly 100 fold higher than the k_{inact}/K_I of 35 M^{-1} min^{-1} for CAA. The rather high K_I and slow k_{inact} values of DDAH inactivation by CAA, 3.1 ± 0.8 mM and 1.2 ± 0.1 min^{-1} respectively, will likely be similarly improved by the addition of an α–NH_2/COOH moiety and a substrate–like side chain length. An inactivator with these is proposed: 2–chloro-1-iminoethyl-L-ornithine (Figure 4.4).

These results demonstrate that the haloacetamidine moiety is effective for general targeting of the guanidino modifying superfamily, but other structural factors will have to be incorporated in order to achieve inactivation of specific enzymes and lower K_I values.

Chapter 5 Protonation States of Cys249 and His162 During DDAH Catalysis

Introduction

Previously we showed that hydrolysis of an activated substrate (SMTC) by *Pa* DDAH catalyzed reaction proceeds through a covalent thiouronium intermediate formed by the active–site nucleophile, Cys249 (Chapter 2). However, the mechanism of nucleophilic activation has not been well addressed. Murray-Rust et al. hypothesized that the active site Cys249 and His162 of DDAH may form a thiolate-imidazolium ion pair as seen in cysteine proteases (*17*). However, $Cys^{-}His^{+}$ ion pair formation is unlikely because the structure shows a distance greater than 6.5 Å between them, and the substrate physically separates Cys249 and His162. While exploring active site–directed inhibitors of DDAH (Chapter 4) we noted that the positively charged 2-chloroacetamidine is a vastly superior inactivator compared to its neutral analog 2–chloroacetamide. We hypothesized that the positively charged guanidino group of substrates (i.e. ADMA or NMMA) may be integral in deprotonating Cys249 for nucleophilic attack, perhaps by forming a substrate–Cys249 ion pair. Herein, we determined that Cys249 exists as the protonated thiol in the enzymes' resting state (near physiological pH), but becomes activated to the anionic thiolate upon binding cationic ligands. Data obtained through pH profiles and an H162G variant also indicates that His162 is important for both formation of the covalent intermediate and for its decay. Finally, a second alternative method for continuously monitoring DDAH activity is described.

Materials and Methods

Materials. Unless noted otherwise, all chemicals are from Sigma-Aldrich Chemical Co. (St. Louis, MO). All enzymes, including wild-type *Pa* DDAH and the catalytically inactive C249S and H162G *Pa* DDAH variants, were purified and assayed as described previously(*28, 36, 49, 66*).

pH Dependence of *Pa* DDAH-catalyzed Hydrolysis of S-Methyl-L-thiocitrulline

Because thiol reactivity changes with pH, the continuous assay for DDAH based on 5, 5'-dithiobis-(2-nitrobenzoic acid) (*36*) was not used for these experiments. Instead, a new assay based upon the inherent spectral differences between *S*-methyl-L-thiocitrulline and the products, methanethiol and L-citrulline, was used to directly monitor substrate hydrolysis in a continuous manner by following absorbance decreases in the UV spectrum. Multiple wavelengths were monitored to quantify different concentration ranges, typically using 260 nm for high substrate concentrations (0.6 – 8 mM), 245 nm for lower concentrations (0.125 – 0.6 mM), and 235 nm for the lowest concentrations (0.015 – 0.125 mM). Standard curves were prepared either using *S*-methyl-L-thiocitrulline or using equimolar mixtures of L-citrulline and methanethiol in order to quantify the observed absorbance changes. Including methanethiol in these standard curves is particularly important at alkaline pH values because thiolates have a higher absorbance than protonated thiols. The accuracy of this method was verified through comparison with parallel reactions at one selected pH (7.3), that were assayed using both a discontinuous assay for citrulline production (*28*) and a continuous spectrophotometric assay (*36*). Typically, reactions of *Pa* DDAH (1 – 3.5 □M) with *S*-

methyl-L-thiocitrulline (concentrations from 0 - 10 × K_M) were prepared at various pH values (4.5 – 9.5) using the following buffers: at pH 4.5 – 5, sodium acetate (250 mM); at pH 5.5 - 6.5, MES (250 mM); at pH 7 - 7.5, HEPES (250 mM); at pH 8 - 8.5, Tris HCl (250 mM); at pH 9 - 9.5, sodium borate (250 mM). All buffers contain KCl (250 mM). All reactions were done at least in triplicate at each pH value and the observed rates were fit to the Michaelis-Menten equation using Kaleidagraph software (Synergy) to obtain the steady-state rate constants.

pH Dependence of *Pa* DDAH-catalyzed Hydrolysis of N$^{\omega}$-Methyl-L-arginine

A previously published discontinuous assay for L-ctirulline production (*28*) was used to determine the steady-state rate constants for *Pa* DDAH-catalyzed hydrolysis of N^{ω}-methyl-L-arginine using the same conditions as described for *S*-methyl-L-thiocitrulline. All reactions were performed at least in triplicate and the observed results were fit directly to the Michaelis-Menten equation.

Fitting the steady-state pH-rate data

Fits to the resulting k_{cat}/K_M values (Figure 1A) and k_{cat} values (Figure 1B) for hydrolysis of both substrates at each pH were calculated as described below. Bell-shaped curves were fit with a two pK_a model (equation 1), rearranged as shown in equation 2, in which y is substituted by either k_{cat}/K_M or k_{cat}, accordingly (*54, 55*), and a lower limiting term, y_{min}, was added to allow for a non-zero plateau at low pH values. This y_{min} term was fixed at zero when fitting data from N^{ω}-methyl-L-arginine hydrolysis, but was left unconstrained to obtain good fits to data from *S*-methyl-L-thiocitrulline hydrolysis. Because fits to two pK_a values closer than 3.5 units tend to underestimate y_{max}, Segel's

method (equations 3, 4) was used to calculate corrected pK_a values for each limb of the k_{cat}/K_M profiles (*54, 55*).

$$\log[y_{obs}] = \log[y_{max}] - \log\left(1 + \frac{[H^+]}{K_1} + \frac{K_2}{[H^+]}\right) \quad (1)$$

$$\log[y_{obs}] = \log\left(y_{min} + \frac{(y_{max} - y_{min})}{(1 + 10^{(pK_{a1} - pH)} + 10^{(pH - pK_{a2})})}\right) \quad (2)$$

$${}_1[H^+]_{1/2} + {}_2[H^+]_{1/2} = K_1 + 4[H^+]_{opt} \quad (3)$$

$$[H^+]_{opt} = \sqrt{K_1 K_2} \quad (4)$$

Fits to the k_{cat} values for *S*-methyl-L-thiocitrulline hydrolysis at each pH were calculated using a single pK_a model including a lower limiting term, k_{min}, to account for the non-zero plateau at low pH as described in equation 5.

$$\log[k_{cat}] = \log\left(k_{min} + \frac{(k_{max} - k_{min})}{(1 + 10^{(pK_a - pH)})}\right) \quad (5)$$

UV-VIS DIFFERENCE SPECTROSCOPY OF APO PROTEINS

Stock solutions of His_6-tagged *Pa* DDAH (70 μM) and His_6-tagged *Pa* C249S DDAH (120 μM) were prepared as described earlier (*49*) and then diluted to final concentrations of 8.3 μM and 14.1 μM, respectively, using various buffers with pH values between 6 and 10. The following buffers were used at the pH ranges as indicated: at pH 5.5 – 6.5, MES (20 mM); at pH 7 – 8, HEPES (20 mM), at pH 8.5 – 10, CHES (20 mM). All buffers contain KCl (100 mM). The absorbance of each sample at 240 and 280 nm was measured in at least three separate experiments using a quartz micro-cuvette and a Cary 50 UV-vis spectrophotometer (Varian, Inc., Walnut Creek, CA), after baseline correction using the appropriate buffer as a blank. The resulting absorbance values at

240 nm were normalized using the 280 nm readings and then averaged for each pH value. The (Abs_{240}/Abs_{280}) ratio for the C249S variant was then subtracted from the (Abs_{240}/Abs_{280}) ratio determined for wild-type *Pa* DDAH at each pH, and then multiplied by the calculated native extinction coefficient for *Pa* DDAH (ε_{280} = 20 240 M^{-1} cm^{-1}) in order to determine the observed $\Delta\varepsilon_{240}$ values at each pH. The Grubbs test, calculated with an alpha value of 0.05 using the GraphPad outlier calculator available free of charge from http://www.graphpad.com/quickcalcs/Grubbs1.cfm, was used to remove any outlying data points. In order to determine the observed pK_a for the absorbance changes at 240 nm, the program KaleidaGraph (Synergy Software, Reading, PA) was used to fit equation 6, in a procedure similar to that reported previously (*68*).

$$\varepsilon_{240(obs)} = \varepsilon_{240(min)} + \frac{(\varepsilon_{240(max)} - \varepsilon_{240(min)})}{(1 + 10^{(pK_a - pH)})} \qquad (6)$$

pH Dependence of *Pa* DDAH Inactivation by Iodoacetamide

Preincubation mixtures of *Pa* DDAH (11 μM) with varying concentrations of iodoacetamide (0 – 2.5 mM) were prepared at various pH values (5.5 – 10) in the buffers described above. At pH values from 5.5 – 7.5, aliquots of the preincubation mixtures were withdrawn at successive time points, diluted 26-fold into an assay buffer containing an excess of the alternative substrate *S*-methyl-L-thiocitrulline (1 mM), potassium phosphate (100 mM), EDTA (1 mM), 5, 5'-dithiobis-(2-nitrobenzoic acid) (200 mM), at pH 7.3, and the remaining enzyme activity was monitored using a continuous spectrophotometric assay as described previously (*66*). Under these conditions, the diluted iodoacetamide does not significantly interfere with our activity assay. At pH values greater than 8, only single time points were assayed due to the increased rate of

inactivation. A form of the second order rate equation (equation 7) was used to obtain rate constants for inactivation in a procedure similar to that described elsewhere (*69*). Act_{obs} and Act_{inital} are the observed and initial percent enzyme activities, [I] is the initial iodoacetamide concentration, and t is the preincubation time.

$$A_{obs} = A_{initial} e^{-k[I]t} \quad (7)$$

In order to determine the observed pK_a for inactivation by iodoacetamide, the resulting $k_{inact(obs)}$ values, determined at each pH, were fitted with a single apparent pK_a value (equation 8). All experiments and controls were performed at least in triplicate.

$$k_{inact(obs)} = \frac{(k_{inact(max)})}{(1 + 10^{(pK_a - pH)})} \quad (8)$$

SUBSTRATE PROTECTION AGAINST INACTIVATION BY IODOACETAMIDE

In order to determine whether inactivation of *Pa* DDAH by iodoacetamide occurs by modification at the active–site, a substrate-protection experiment was carried out. Solutions of *Pa* DDAH (14 □□) in Tris buffer (250 mM) and KCl (250 mM) at pH 8.5, were co-incubated with either iodoacetamide (1 mM) alone, or with iodoacetamide (1 mM) and *N*□-methyl-L-arginine (2.5 mM). As a control, *Pa* DDAH was incubated in buffer alone. At time points between 0 and 6 min, aliquots of the incubation mixtures were diluted 26-fold into a buffer containing potassium phosphate (100 mM), EDTA (1 mM), 5, 5'-dithiobis-(2-nitrobenzoic acid) (180 mM), and *S*-methyl-L-thiocitrulline (1 mM) and assayed as described previously . Observed rates were plotted as a percent of the original activity against time and fit to a single exponential equation (Figure 5.5).

MASS SPECTROMETRY OF QUENCHED REACTIONS

Typically, steady-state reactions with *Pa* DDAH (final concentration of 50 μM) and substrate (5 mM) were incubated for 20 – 30 s at 25° C before addition of trifluoroacetic acid (final concentration of 1 M), which quenches the reactions during turnover and traps any acid-stable covalent intermediates that accumulate. Incubations at two different pH values were prepared in the following buffers: at pH 5.5, MES (200 mM) and at pH 8, Tris HCl (200 mM). Both buffers contain KCl (200 mM). Quenched reactions were analyzed by ESI–MS as described previously (*49*). Incubations with the H162G variant (25 - 50 μM), were also completed using slightly more substrate (5 - 10 mM), and longer reaction times (3 – 10 min), and even repeated at a higher pH (9.5) in order to maximize the chance of trapping potential intermediates during incubations with N^{ω},N^{ω}-dimethyl-L-arginine.

INHIBITION OF *PA* DDAH BY L-LYSINE

The steady-state rates of *Pa* DDAH (670 nM)-catalyzed hydrolysis of *S*-methyl-L-thiocitrulline (8 – 1000 mM) were determined in varying concentrations of L-lysine (1.25 – 15 mM) in K_2HPO_4 (0.1 M) buffer, EDTA (1 mM), at 25º C and pH 7.3, using a continuous assay as described earlier (*36*). All reactions were done in triplicate and the results directly fit using KaleidaGraph software (Synergy) to equation 9 for competitive inhibition (*70*) where $\alpha = (1 + [I]/K_i)$:

$$v = \frac{k_{cat} \cdot [S] \cdot [E]_{total}}{(\alpha K_M + [S])} \qquad (9)$$

UV-VIS DIFFERENCE SPECTROSCOPY OF LIGAND-BOUND PROTEINS

Using a quartz micro-cuvette and a Cary 50 UV-vis spectrophotometer (Varian Inc.), absorbance scans (230 -300 nm) were recorded for wild-type and C249S variant *Pa* DDAH (4 – 5 μM) in K_2HPO_4 buffer (100 mM), EDTA (1 mM), pH 7.3, in the presence of either L-lysine (10 mM) or L-citrulline (20 mM) at concentrations required to achieve approximately 70 % saturation. Baseline corrections were made using control solutions in which the protein component was omitted. All experiments were repeated at least in triplicate and an average observed extinction coefficient was calculated at each wavelength as described above. The ligand-dependent changes in the observed extinction coefficient at each wavelength were then calculated for both wild-type and C249S mutant *Pa* DDAH by subtracting the results from the L-citrulline-bound proteins from those of the L-lysine-bound proteins at each wavelength.

Results

pH DEPENDENCE OF *PA* DDAH-CATALYZED SUBSTRATE HYDROLYSIS

The k_{cat}/K_M values determined for *S*-methyl-L-thiocitrulline and N^{ω}-methyl-L-arginine hydrolysis (Figure 1A) both showed a bell-shaped pH dependence that was fit to two apparent pK_a values. The fitted pK_a values for *S*-methyl-L-thiocitrulline were 7.4 ± 0.2 for the ascending limb (slope of 0.8) and 8.8 ± 0.2 for the descending limb, with a limiting non-zero plateau (0.2 $s^{-1}mM^{-1}$) at low pH. The fitted pK_a values for N^{ω}-methyl-L-arginine were 7.9 ± 0.3 for the ascending limb (slope of 1) and 9.3 ± 0.6 for the descending limb. Because these pairs of fitted pK_a values are closer than 3 units, Segel's

method was used to calculate corrected pK_a values of 8.0 and 8.2 for *S*-methyl-L-thiocitrulline hydrolysis and 8.5 and 8.7 for $N^{\square}$-methyl-L-arginine hydrolysis.

The k_{cat} values determined for $N^{\square}$-methyl-L-arginine hydrolysis (Figure 1B) showed bell-shaped pH dependence that was fit to two apparent pK_a values: 6.1 ± 0.1 for the ascending limb (slope of 1) and 9.4 ± 0.1 for the descending limb. The k_{cat} values determined for *S*-methyl-L-thiocitrulline hydrolysis (Figure 1B) were best fit to one apparent pK_a of 5.6 ± 0.1 for the ascending limb (slope of 0.2) and a limiting non-zero plateau (k_{min} = 0.6 s^{-1}) at low pH values. *Pa* DDAH showed linear initial rates for substrate hydrolysis between pH values of 4.5 - 9.5, but at more acidic or alkaline pH values, the enzyme was not active or displayed non-linear kinetics, suggesting enzyme inactivation.

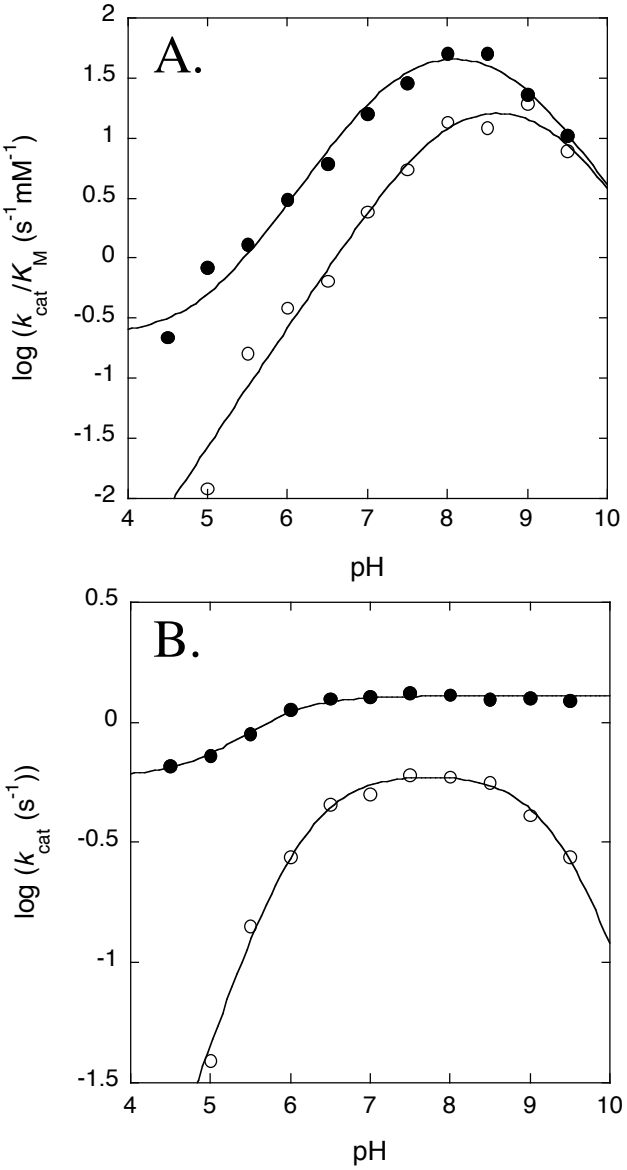

Figure 5.1 pH–Rate profiles for substrate hydrolysis by wild-type *Pa* DDAH

A. The k_{cat}/K_M values for *S*-methyl-L-thiocitrulline (●) are fit to two corrected apparent pK_a values of 8.0 and 8.2, and the k_{cat}/K_M values for $N^{\square}$-methyl-L-arginine (○) are fit to two corrected pK_a values of 8.5 and 8.7 (see materials and methods for details). B. The k_{cat} values for hydrolysis of *S*-methyl-L-thiocitrulline (●) are fit to one apparent pK_a of 5.6 for the ascending limb (slope of 0.2) and a non-zero plateau (0.6 s^{-1}) at low pH. The k_{cat} values for hydrolysis of $N^{\square}$-methyl-L-arginine (○) are fit to apparent pK_a values of 6.1 for the ascending limb (slope of 1) and 9.4 for the descending limb.

UV-VIS DIFFERENCE SPECTROSCOPY OF APO PROTEINS

In order to follow the absorbance change at 240 nm due to pH-induced deprotonation at the thiol side chain of Cys249, differences in absorbance at 240 nm between wild-type and a C249S mutant *Pa* DDAH were determined (Figure 2A). A pH-dependent increase in absorbance at 240 nm was observed with an apparent pK_a of 8.9 ± 0.2, and $\Delta\varepsilon_{240(max)}$ of 3600 ± 100 $M^{-1}cm^{-1}$. These experimentally determined values are consistent with typical pK_a values for unperturbed non-catalytic cysteine residues (*70*) and with ε_{240} values for one equiv of thiolate (*71*).

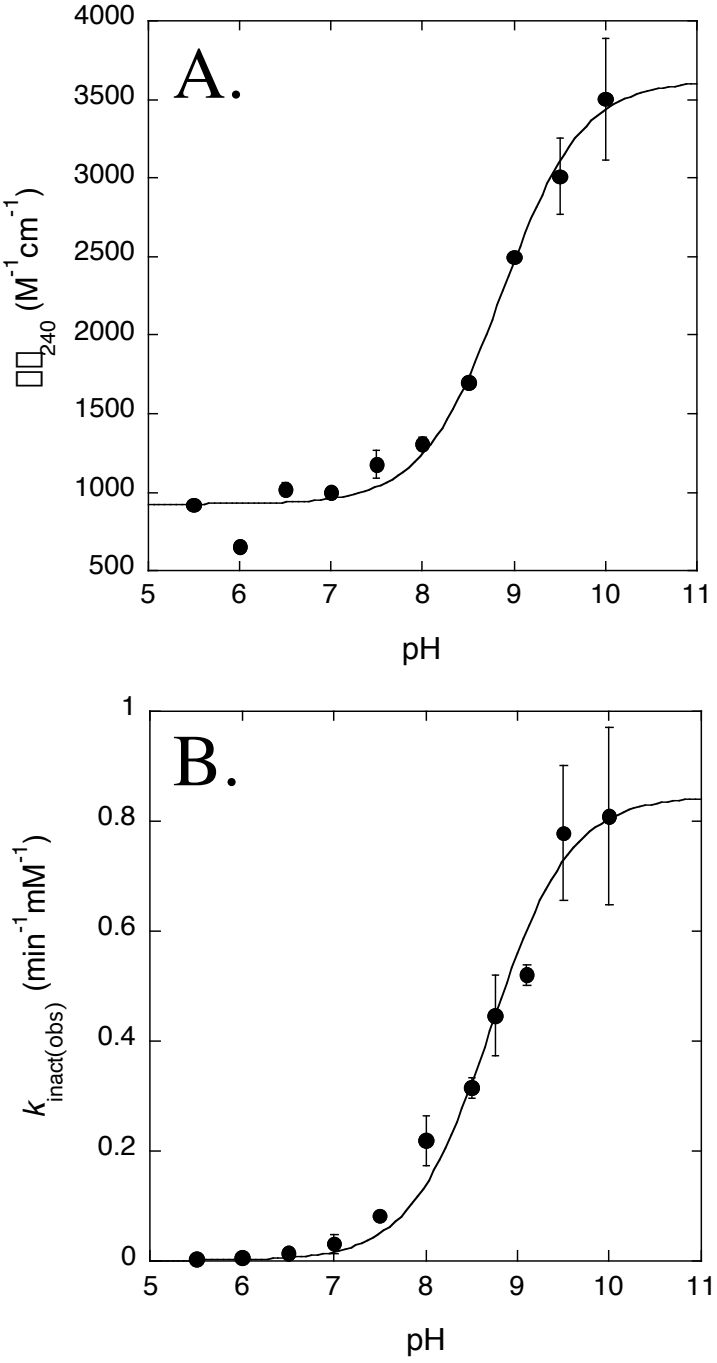

Figure 5.2 Determination of the pK_a of Cys249

A. UV-Vis difference spectroscopy at 240 nm between wild-type *Pa* DDAH and the C249S variant showing a pH-dependent increase in absorbance with an apparent pK_a of 8.9 due to thiolate formation. B. Observed rates for inactivation of wild-type *Pa* DDAH by the thiol modification reagent iodoacetamide showing a pH-dependent increase with an apparent pK_a of 8.7.

pH Dependence of *Pa* DDAH Inactivation by Iodoacetamide

Under our experimental conditions, plots of the pseudo first order inactivation rate constants with respect to iodoacetamide concentration were linear, indicating second order kinetics. Consequently, the second order rate constants for inactivation at various pH values were determined. Addition of N^{ω}-methyl-L-arginine (2.5 mM) to an incubation mixture at pH 8.5 can prevent inactivation by iodoacetamide (supporting information), indicating that inactivation is due to modification at the active–site. The rate of *Pa* DDAH inactivation by iodoacetamide increased at higher pH values (Figure 2B) and showed one apparent pK_a value of 8.7 ± 0.1, matching the apparent pK_a observed for the active-site Cys249 using UV–vis difference spectroscopy (Figure 2A). Fits of this data to a two- pK_a model did not result in a statistically significant improvement (F–test). Using similar methods, attempts to obtain pseudo first order rate constants for inactivation by 2-chloroacetamidine, a known affinity label, were unsuccessful due to the rapid inactivation rates at high pH.

Mass Spectrometry of Quenched Reactions

Previous studies have shown that steady-state reactions of *Pa* DDAH with an activated substrate, *S*-methyl-L-thiocitrulline, can be acid-quenched to trap a transient covalent adduct of + 157 Da that accumulates during turnover and may be a catalytic intermediate in the enzymatic mechanism (Scheme 5.1) (*49*). Here, incubation mixtures of both the wild–type and H162G proteins with the activated substrate *S*-methyl-L-thiocitrulline, show the presence of the + 157 Da adduct, within error (Table 1). However, incubation of these proteins with the naturally-occurring substrate N^{ω},N^{ω}-dimethyl-L-arginine only resulted in accumulation of a + 157 Da adduct with the wild-

type protein. Incubations of this natural substrate with the H162G variant only resulted in a mass matching that of unmodified enzyme, even when incubations were repeated at a pH value (9.5) higher than an unperturbed thiol pK_a.

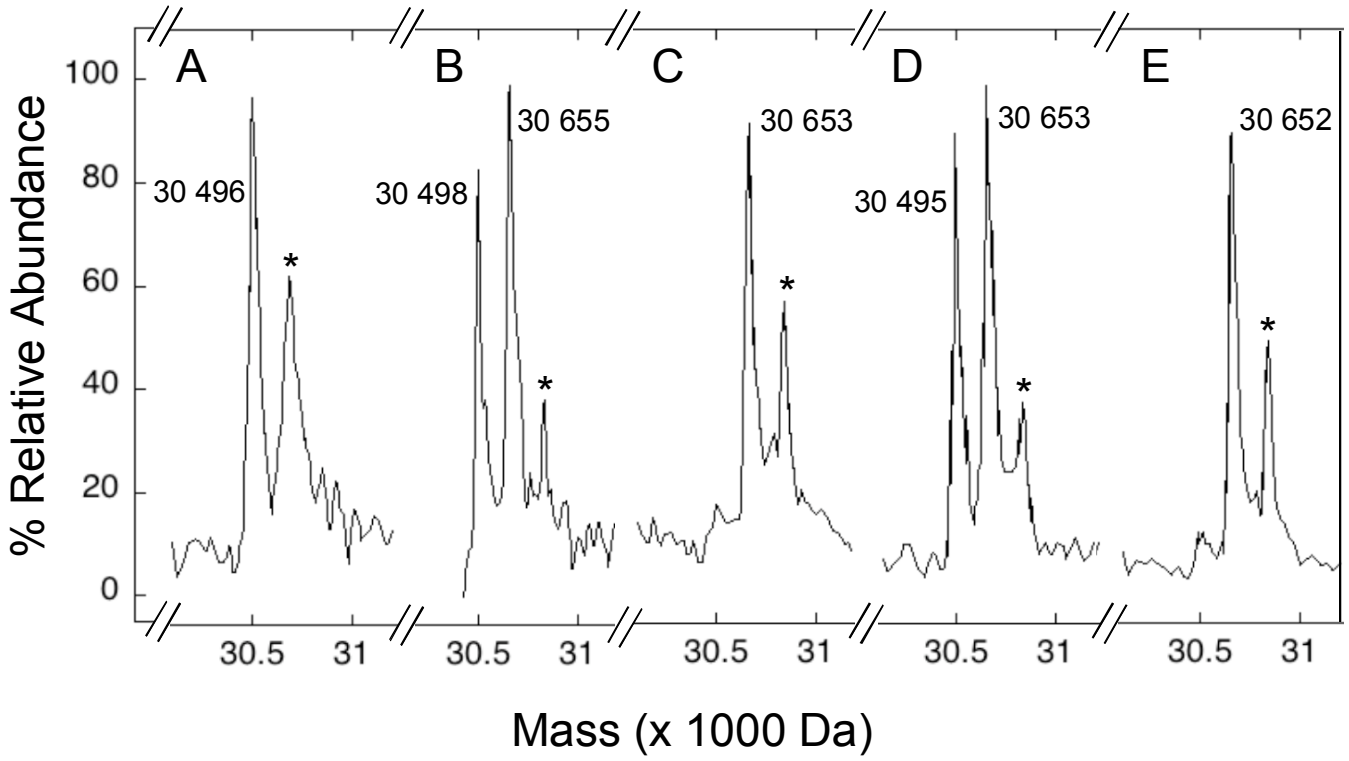

Figure 5.3 Deconvoluted ESI-MS spectra of trapped reactions with wild-type *Pa* DDAH

Steady-state reactions of wild-type *Pa* DDAH and $N^{\square}$-methyl-L-arginine at pH 5.5 (A) and pH 8.0 (B), $N^{\square}$, $N^{\square}$-dimethyl-L-arginine at pH 8.0 (C), and *S*-methyl-L-thiocitrulline at pH 5.5 (D) and 8.0 (E) were acid-trapped and then analyzed by ESI-MS to detect any accumulation of a covalent adduct during turnover. Marked (*) peaks are attributable to a smaller fraction of non-enzymatically $N^{\square}$-gluconoylated protein modified during expression. The calculated mass for unmodified wild-type *Pa* DDAH after removal of the N-terminal methionine is 30 503 Da. The expected mass of the proposed covalent intermediate is 30 660 Da. Representative ESI-MS plots are shown and typically have an error of ± 10 Da.

This trapping technique was also used to identify the major species that accumulate during steady-state turnover by wild-type *Pa* DDAH at two different pH

values (Figure 5.3). At pH 5.5, trapping steady-state reactions of N^{ω}-methyl-L-arginine during turnover results only in protein that does not contain the + 157 Da adduct (Figure 3A). However, when repeated at pH 8.0, trapping of these reactions results in a significant fraction of the enzyme in which the + 157 Da covalent adduct accumulates (Figure 3B). At pH 5.5, trapping of reactions with *S*-methyl-L-thiocitrulline shows that a mixture of unmodified enzyme and covalent adduct is present (Figure 3D), but in reactions at a higher pH (8.0), almost all of the enzyme is trapped as the + 157 Da covalent adduct (Figure 3E). At pH 8.0, trapping of reactions with N^{ω},N^{ω}-dimethyl-L-arginine (Figure 3 C) also result in trapping almost all of the enzyme with the covalent adduct. Because the amount of covalent adduct that accumulates at high pH varies with substrate, the k_{cat} and K_M values for N^{ω}-methyl-L-arginine (0.59 ± 0.01 s^{-1}, 44 ± 4 μM), N^{ω},N^{ω}-dimethyl-L-arginine (1.27 ± 0.04 s^{-1}, 39 ± 9 μM), and *S*-methyl-L-thiocitrulline (1.30 ± 0.04 s^{-1}, 26 ± 4 μM) were all determined at a single pH of 8.0 for comparison.

Table 5.1 Summary of major ions observed in ESI-MS spectra of acid-quenched steady-state reactions with wild–type or H162G *Pa* DDAH and various substrates

Substrate used in Incubations	Incubations with wild-type *Pa* DDAH [a] Observed mass (Da) [b]	Incubations with H162G *Pa* DDAH [a] Observed mass (Da) [b]
Control (without substrate)	30 495	30 415
N^{ω}, N^{ω}-dimethyl-L-arginine	30 652	30 416
S-methyl-L-thiocitrulline	30 653	30 573

[a] The theoretical calc'd mass for wild-type *Pa* DDAH is 30 403, and H162G mutant *Pa* DDAH is 30 423.

[b] The major ion peaks from deconvoluted ESI-MS spectra are reported with errors of ± 10 Da. All reactions were completed at pH 8 prior to the acid quench.

INHIBITION OF *PA* DDAH BY L-LYSINE

L-Lysine was examined as a potential competitive inhibitor. A double reciprocal plot of $(1/v_o)\times$[E] versus 1/[S], determined at different L-lysine concentrations showed linear fits that intersect at the y-axis, consistent with competitive inhibition. Non-linear fits to a competitive inhibition model determined a K_i for L-lysine inhibition of 4.0 ± 0.3 mM at pH 7.3. Previously, L-citrulline was determined to be a competitive inhibitor of *Pa* DDAH (*17*) with a K_i of 8.4 ± 0.5 mM at pH 7.3 (*36*).

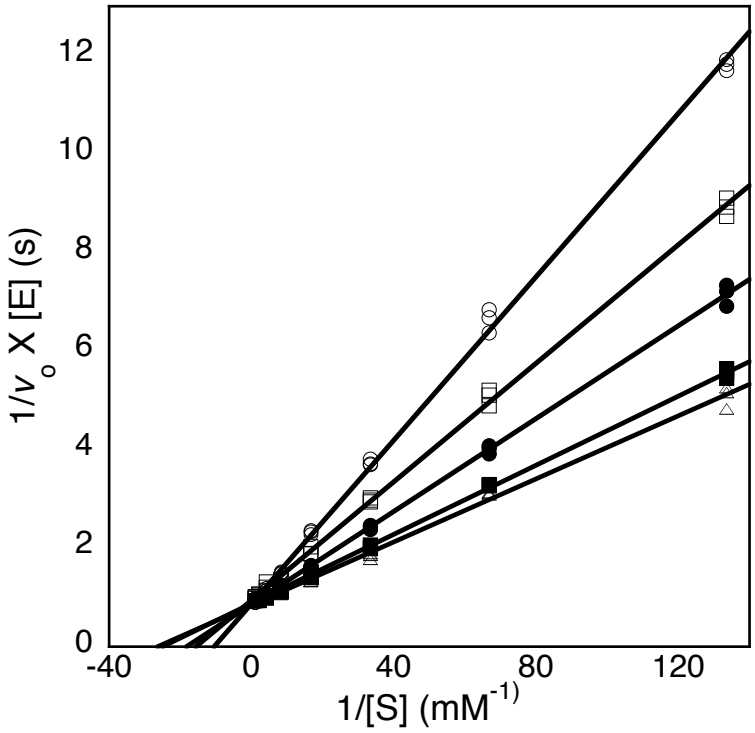

Figure 5.4 Competitive inhibition of wild-type *Pa* DDAH by L-lysine

For display purposes, a double-reciprocal plot is shown for inhibition of *S*-methyl-L-thiocitrulline hydrolysis by 1.25 (□), 2.5 (■), 5 (●), 10 (□), and 15 (○) mM L-lysine. Non-linear fits for competitive inhibition indicate a K_i value of 4.0 ± 0.3 mM at pH 7.3. See materials and methods for experimental details.

SUBSTRATE PROTECTS AGAINST INACTIVATION BY IODOACETAMIDE

In order to determine whether inactivation of *Pa* DDAH by iodoacetamide occurs by modification at the active–site, a substrate-protection experiment was carried out. The observed rate of *Pa* DDAH inactivation by iodoacetamide was significantly slowed by co-incubation with substrate, suggesting that inactivation occurs through modification at the active–site.

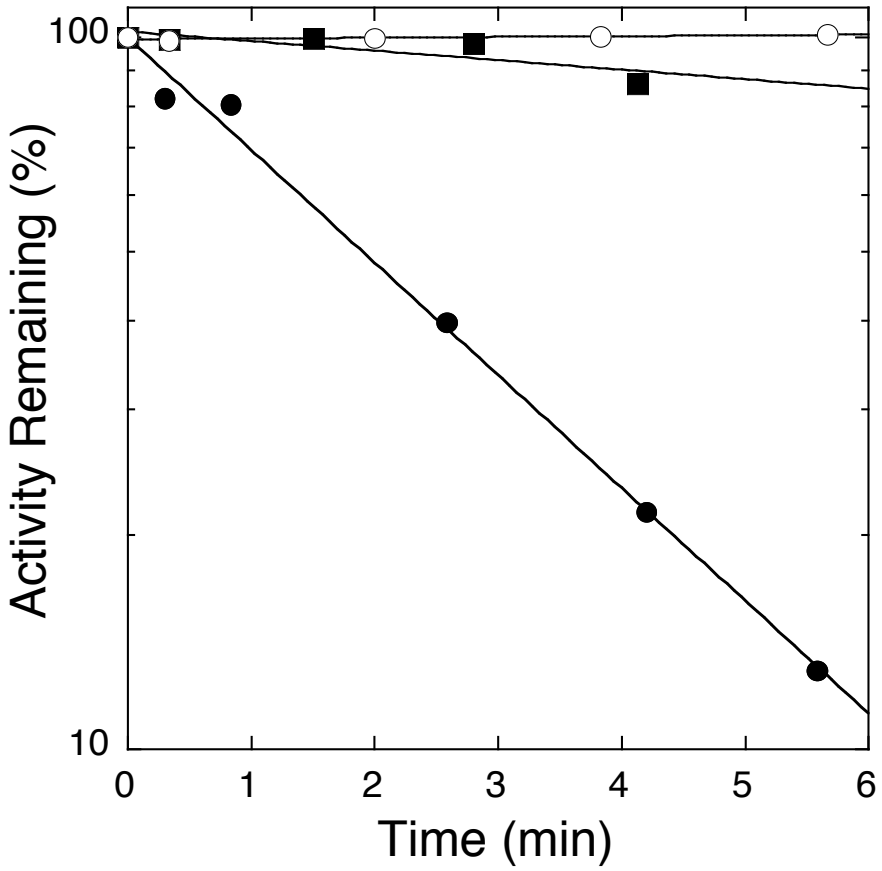

Figure 5.5 Substrate protects against *Pa* DDAH inactivation by iodoacetamide

Control incubations of *Pa* DDAH (open circles) show no loss of activity. Incubations with iodoacetamide (closed circles) show time-dependent inactivation. Incubations with iodoacetamide and $N^{\square}$-methyl-L-arginine (closed squares) show that substrate protects against inactivation.

UV-VIS DIFFERENCE SPECTROSCOPY OF LIGAND-BOUND PROTEINS

Changes in absorbance near 240 nm, which are reflective of thiol deprotonation (*71*), were determined by subtracting spectra of L-citrulline-bound *Pa* DDAH from L-lysine-bound *Pa* DDAH. The ligand concentrations used were 2.5-fold higher than their K_i values as determined by competitive inhibition, resulting in ~ 70 % saturation. These difference spectra showed a relative increase in absorbance with a λ_{max} near 235 nm and an apparent extinction coefficient of 3 000 M^{-1} cm^{-1} (calc'd 4 300 M^{-1} cm^{-1} at full occupancy), consistent with deprotonation of one equiv of thiol upon L-lysine binding (Figure 4). Parallel experiments with the C249S variant did not show a similar increase in absorbance, indicating that Cys249 is likely the thiol that becomes deprotonated upon ligand binding. The structure of C249S *Pa* DDAH has previously been reported and shows that this protein structure is comparable to wild-type and capable of binding L-citrulline at the active-site (*17*).

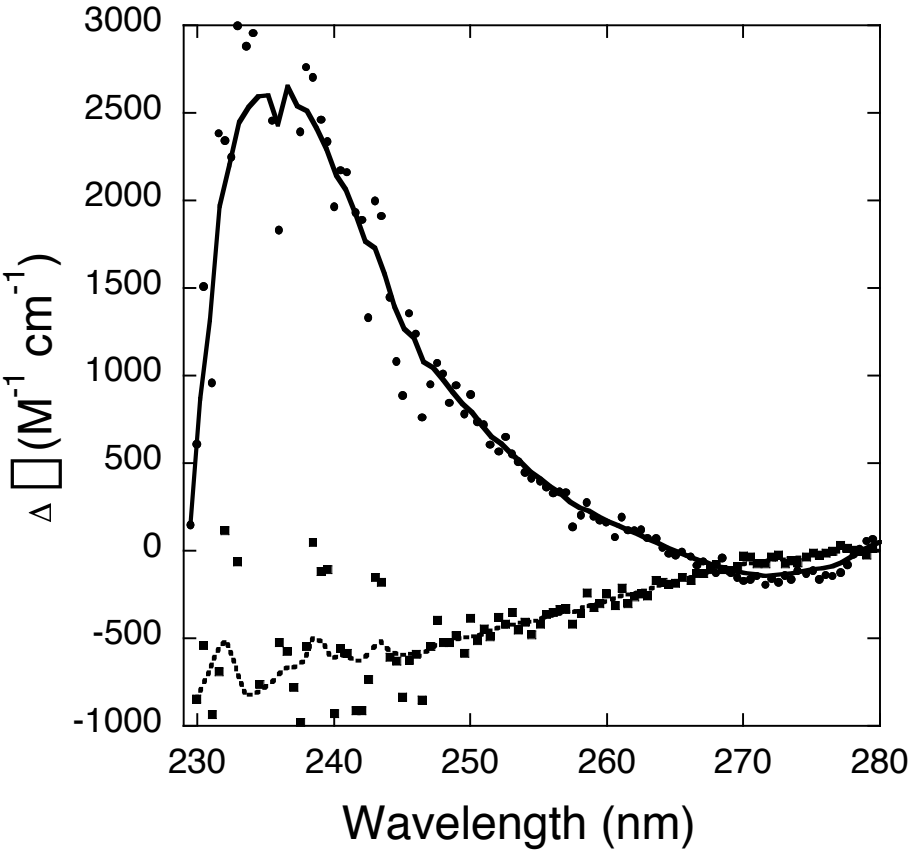

Figure 5.6 UV-Vis difference spectra of *Pa* DDAH upon ligand binding

Spectra of L-citrulline-bound proteins are subtracted from L-lysine-bound proteins using both wild-type (●, solid line) and C249S variant (■, dashed line) *Pa* DDAH, indicating an increase of absorbance at 235 nm upon L-lysine binding to wild-type *Pa* DDAH at pH 7.3.

Discussion

The mechanism of nucleophilic activation in the amidinotransferase superfamily has not been well studied. Murray–Rust et al. suggested that DDAH might have a preformed $Cys^{-}His^{+}$ ion pair, but the structure of a *Pa* C249S DDAH variant shows that product binds between these two residues (*17*). Also the Nδ of His162 is more than 6 Å from the Cys249 side chain. A $Cys^{-}His^{+}$ ion pair is therefore unlikely unless there are significant conformational changes in the ligand–free enzyme. Previously, we had noted (Chapter 4) that at pH 6.3, DDAH is inactivated with the positively charged 2–chloroacetamidine but not the neutral analog 2–chloroacetamide (*66*). The ionization state of Cys249 has not previously been reported, despite the importance of this knowledge for understanding the catalytic mechanism and inhibitor design.

We first looked at the pH dependence of k_{cat}/K_M to follow ionizations in the free–enzyme and free–substrate. The activated substrate, SMTC, and the naturally occurring substrate NMMA both exhibited narrow bell–shaped curves with corrected pK_a values of 8.0 and 8.2 for SMTC and 8.5 and 8.7 for NMMA (Figure 5.1). This is indicative of Cys249 being predominantly neutral at physiological pH values. However, assigning one of these pK_a values to Cys249 ionization is ambiguous because of the possibility of pH dependent changes in the rate–limiting step (*72*).

To obtain more direct evidence for the pH–dependence of Cys249 ionization in the resting enzyme we measured UV–vis difference spectra between wild–type *Pa* DDAH and a C249S variant. Thiolate anions absorb more strongly ($\varepsilon_{240} \approx 4000$ M^{-1} cm^{-1}) than neutral protonated thiols ($\varepsilon_{240} \approx 50$ M^{-1} cm^{-1}) (*71*) and UV–vis difference spectroscopy of wild-type and C249S variant enzymes allow the measurement of

absorbance differences due specifically to changes in ionization at Cys249, eliminating interference from other protein residues. This experiment resulted in an apparent pK_a of 8.9 (Figure 5.2 A), which can be specifically assigned to Cys249. We corroborated this result by following the pH dependence of DDAH inactivation by the neutral inactivator iodoacetamide where we determined an apparent pK_a of 8.7 (Figure 5.2 B). These pK_a values are consistent with the typical ionization values seen with non–catalytic cysteine residues. Thus at physiological pH values, Cys249 is predominantly in the neutral protonated state.

We also examined the pH rate dependence of DDAH catalysis of SMTC and NMMA hydrolysis under k_{cat} conditions where ionizations reflect the enzyme–substrate complex. The pH rate curves for both substrates had similar ascending limbs (Figure 5.1 B) with an apparent pK_a of 5.6 for SMTC and an apparent pK_a of 6.1 for NMMA. One hypothesis for these observed results is that binding of the substrate assists in ionizing Cys249. Adjacent binding of the positively charged substrate guanidinium next to Cys249 would be expected to cause a substantial shift in pK_a. If this interpretation is correct, then binding of substrate would be responsible for lowering the Cys249 pK_a value by 2.8 units (from 8.9 to 6.1) reflecting a $\Delta\Delta G_{Ka}$ of 3.8 kcal/mol, similar to the typical range of $\Delta\Delta G$ values (3-5 kcal/mol) reported for buried salt bridges (*70*).

However, instead of reflecting the ionization of particular groups, steady-state pH rate curves can also reflect kinetic pK_a values, which are instead due to changes in the rate-limiting step of the overall reaction (*70*). This seems likely to be the case for reactions with both SMTC and NMMA. Acid quenched steady–state reactions with NMMA show no observable covalent adduct at pH 5.5, but a significant amount (~40%) of adduct is observed at pH 8 (Figure 5.3 A, B respectively). Quenched reactions with

SMTC show approximately 45% covalent adduct at pH 5.5 and nearly 100% adduct at pH 8 (Figure 5.3 D, E respectively). The accumulation of covalent adduct at high pH values indicates that intermediate decay is at least partially rate–limiting. (It should be noted that at the pH optimum of *Pa* DDAH, we are able to trap a covalent adduct that accumulates during steady-state turnover of NMMA and asymmetrical ADMA (Figure 5.3 B, C), demonstrating that the proposed covalent intermediate can be trapped using naturally occurring substrates and not only with an activated artificial substrate (*49*).)

We therefore used a direct approach to determine that binding cationic ligands can induce Cys249 ionization. We find that the positively charged (side–chain) L–lysine is a competitive inhibitor of *Pa* DDAH (Figure 5.4), as well as the previously described neutral (side–chain) L-citrulline (*36*). This pair of ligands was used for difference UV–vis spectroscopy with wild–type, and C249S DDAH. Binding of a cationic ligand at the active–site of wild–type DDAH results in an increase of absorbance near 240 nm relative to binding a neutral ligand, with a magnitude consistent with the ionization of one cysteine side chain (Figure 5.6). Difference spectroscopy with the C249S variant did not show a similar change (Figure 5.6), indicating that the observed thiolate signal is from Cys249. These results directly show that binding a positively-charged ligand stabilizes the anionic form of Cys249, and are consistent with a substrate-assisted mechanism where binding of a cationic ligand lowers the pK_a of the active site cysteine, favoring deprotonation and activation of this residue as a catalytic anionic nucleophile.

The pH–rate analysis of DDAH also provides information about the role of His162 in the catalytic mechanism. The k_{cat} versus pH profiles of SMTC and NMMA are strikingly different at alkaline pH values. The k_{cat} rates for SMTC show a pH independent plateau at alkaline pH values while rates for NMMA show a descending limb with an

apparent pK_a of 9.4 (Figure 5.1 B). The main difference between these two substrates is their leaving groups, methanethiol and methylamine. Protonation of the methanethiol leaving group may not be strictly required for catalysis, but protonation of the methylamine leaving group is likely essential prior to or concomitant with cleavage of the C–N bond. This difference is reflected in the pH rate behavior, where hydrolysis of NMMA slows at alkaline pH values, likely due to lack of protonation of the leaving group. The crystal structure of *Pa* DDAH suggests that His162 is well placed to act as an acid in protonating the leaving group, and perhaps as a base in generating a hydroxide for attack on the covalent intermediate (*17*). Murray–Rust et al. previously reported that a H162N DDAH variant was incapable of turnover, demonstrating that His162 is essential to catalysis (*17*). Because the alternative substrate SMTC does not likely require leaving group protonation for intermediate formation, we hypothesized that a H162 variant may be able to accumulate a covalent adduct with this substrate. We incubated an H162G DDAH variant with SMTC and found that it accumulates a covalent adduct that does not decay (Table 5.1). Conversely, incubations with the natural substrate ADMA and H162G DDAH did not result in accumulation of a covalent adduct. This result indicates that His162 is both a general acid and general base in the DDAH catalytic mechanism. The finding that no covalent intermediate can be formed upon incubations with H162G and ADMA further suggests that His162 acts as a general acid. Because a stable covalent reaction intermediate can form with the H162G variant shows that His162 is essential for generating a hydroxide for intermediate hydrolysis. Therefore the apparent pK_a of 9.4 for the descending limb of k_{cat} versus pH profile for NMMA hydrolysis can be assigned to His162.

The results reported here indicate that substrate assists in the mechanism of *Pa* DDAH, depressing the pK_a of Cys249 sufficiently for activation of this nucleophile (Scheme 5.1). This mechanism has also been proposed for ubiquitin–conjugating enymes where a catalytic cysteine is not deprotonated until substrate is bound (*73*). Ligand induced cysteine activation should be also considered in inhibitor design, because inactivation rates of *Pa* DDAH by the positively charged 2–chloroacetamidine are significantly higher than the neutral iodoacetamide, despite having a worse leaving group (data not shown).

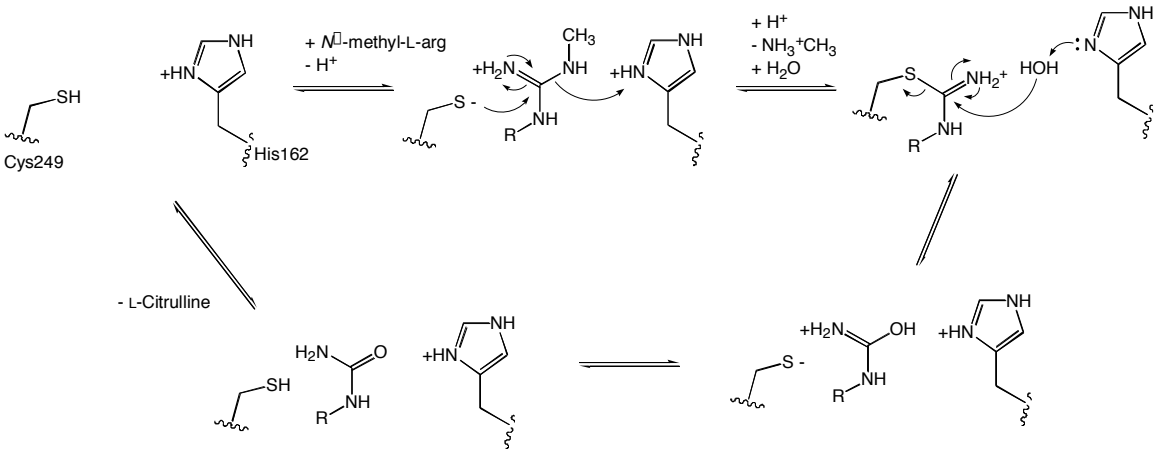

Scheme 5.1 Proposed substrate–assisted activation of Cys249 and His162 as general acid and general base in the mechanism of *Pa* DDAH

Chapter 6 The Role of Glu114 in the Mechanism of DDAH

Introduction

The DDAH from *Pseudomonas aeurginosa* has a highly conserved active–site containing Cys249, His162, and Glu114, although sequence alignments show that aspartate often replaces glutamate in other related enzymes. The structures from *PA aeurginosa* and bovine DDAH suggest that the carboxyl group from Glu114 (or Asp129, respectively) forms an ion pair with the active–site His and may be important to catalysis (*17, 18*). Murray-Rust et al. briefly investigated the *PA aeurginosa* DDAH active–site Glu114 by making an E114Q variant, and reported that there was no observable activity with the substrate ADMA (*17*). In contrast, we have determined that an active–site variant, H162G, is capable of completing a half reaction with the activated substrate SMTC, and stably accumulates a covalent intermediate with release of the methane–thiol leaving group (*74*). We hypothesized that the use of SMTC might allow us to tease out the role of His162 as a general acid or general base, and the effect of Glu114 as a potential modulator of His162. Therefore, we constructed E114Q, E114D, and E114G substituted enzymes to more fully explore the role of Glu114.

We used the aforementioned mutant enzymes, the activated substrate SMTC, steady–state kinetics, pH profiles, mass spectrum analysis, and metal binding studies to elucidate the contribution of Glu114 to catalysis.

Materials and Methods

CREATING AN EXPRESSION VECTOR FOR E114G DDAH

Two complementary oligonucleotides, (Sigma GENOSYS) (forward) `5–GGCACGGTGggtGCCGGCGAC–`3, and (reverse) `5–GTCGCCGGCaccCACCGTGCC–`3 were used to introduce a mutant codon (lowercase) coding for E114G in the *Pa* DDAH sequence. The *Pa* DDAH gene was amplified using an MJ Research PTC 200 thermocycler along with a plasmid containing the wild–type DDAH coding sequence, dNTPs, 10x reaction buffer, and pfu-Turbo polymerase (Stratagene). The reaction conditions for the PCR used a temperature program of 98° C for 30 s, followed by 16 cycles of 98° C for 30 s, 55° C for 1 min, and 12 min at 68° C. The PCR-amplified products were then digested with *Dpn* I and concentrated using a Qiaquick spin column (Qiagen). The digestion product was transformed into *E.coli* DH5E cells for plasmid amplification and isolation. The resulting plasmid (designated pETpaE114G) was purified using a Qiaquick spin column (Qiagen) and the coding region was sequenced to confirm that there were no undesired mutations.

CREATING AN EXPRESSION VECTOR FOR E114D DDAH

Two complementary oligonucleotides, (Sigma GENOSYS) (forward) `5–GGCACGGTGgacGCCGGCGAC–`3, and (reverse) `5–GTCGCCGGCgtcCACCGTGCC–`3 were used to introduce a mutant codon (lowercase) coding for E114D in the *Pa* DDAH sequence. Amplification of the *Pa* DDAH gene was performed as described above using the new mutant primers and a

modified temperature program: 98°C for 30 s, followed by 16 cycles of 98°C for 30 s, a gradient of 45–54°C for 1 min, and 12 min at 68°C. The PCR-amplified products from all annealing temperatures were combined, and digested with *Dpn* I, transformed into *E.coli* DH5E cells for plasmid amplification and isolation. The coding region in the resulting plasmid (designated pETpaE114D) was sequenced to verify that only the desired mutation had been incorporated.

CREATING AN EXPRESSION VECTOR FOR E114Q DDAH

The plasmid, pETpaE114Q, containing the gene for E114Q DDAH was constructed by J. Momb, in the Fast lab. The coding region of the resulting plasmid was sequenced to verify that only the desired mutation had been incorporated.

OVEREXPRESSION AND PURIFICATION OF E114G, E114D, AND E114Q *PA* DDAH

Expression and purification of mutant E114G His_6-DDAH as well as the E114D and E114Q enzymes was completed as described previously (*49*), with the exception of extending the expression time from 4 hr to 12 hr, because this was found to reduce or eliminate the fraction of protein that undergoes post–translational N–terminal gluconoylation (*32*).

STEADY–STATE KINETICS OF E114G AND E114D *PA* DDAH

The steady–state rate constants were determined for E114G and E114D DDAH–catalyzed hydrolysis of SMTC using a previously published continuous assay that measures spectral changes in DTNB upon reaction with methanethiol (*36*). The

E114D mutant was assayed by addition of enzyme (920 nM) to serial dilutions of SMTC (7□M – 1□mM) in a Na_2HPO_4 buffer (100 mM), DNTB (160 □M), EDTA (1 mM), at pH 7.3. (*36*). The E114G variant was assayed by addition of enzyme (1.9 □M) to serial dilutions of SMTC (16□M – 1□mM) in Tris buffer (250 mM), KCl (250 mM), DNTB (185 □M), EDTA (1 mM), at pH 7.5. The resulting data were fit directly to the Michaelis-Menten equation using KaleidaGraph software (Synergy Software, Reading, PA). All reactions were carried out at least in triplicate.

pH DEPENDENCE OF *PA* DDAH E114G & E114Q–CATALYZED HYDROLYSIS OF SMTC

The pH rate dependence of E114G DDAH hydrolyzed SMTC was followed under V_{max} conditions with E114G DDAH (3.7□M) and SMTC (740□M) from pH 5 – 9.5 with buffer conditions and a continuous DNTB based assay described previously (*74*). All reactions were completed at least in triplicate and the resulting rates were plotted against pH and fit to equation 6.1 to assign apparent pK_a values. These reactions were carried out under saturating substrate conditions allowing k_{cat} to be estimated by the relationship $k_{cat} = V_{max}/[E]$.

$$k_{cat} = \left[k_{min} + \frac{(k_{max} - k_{min})}{(1 + 10^{(pK_a - pH)})} \right] \qquad (6.1)$$

The pH rate dependence of E114Q DDAH–catalyzed hydrolysis of SMTC was followed under V_{max} conditions using E114Q DDAH (5.6 □M) and SMTC (740□M) at pH 6 – 9.5 as described above. The results were fit to equation 6.1.

pH Dependence of E114G DDAH Catalyzed Hydrolysis of NMMA

Because different substrates can reveal different steps in the catalytic mechanism, we also analyzed the ability of E114G DDAH to hydrolyze NMMA. A previously published discontinuous assay for L-citrulline production (*28*) was used to determine a k_{cat} (estimated by V_{max}/[E]) value for E114G DDAH catalyzed hydrolysis of NMMA as described above for SMTC. Typically E114G DDAH (1.2 □M), NMMA (2.4 mM), and 200□L of each buffer were incubated 2 h at 25° C, with the exception of reactions at pH 5 which were incubated with higher concentrations (12□mM) of NMMA. All reactions were performed at least in triplicate and the observed rates were fit to equation 6.2 which describe a two pK_a model.

$$k_{cat} = \left[k_{min} + \frac{(k_{max} \square k_{min})}{(1 + 10^{(pK_{a1} \square pH)} + 10^{(pH\text{-}pK_{a2})})} \right] \qquad (6.2)$$

Mass Spectrum Analysis of Steady–State Reactions of E114G and E114Q Pa DDAH with SMTC

Mixtures of E114G DDAH (45□M) or E114Q DDAH (134□M) and SMTC (0 or 10 mM) were reacted (1 min) at 25^{O} C in a HEPES buffer (10 mM), KCl (100 mM), and 10 % glycerol (v/v), at pH 7.3 before being quenched by addition of trifluoroacetic acid to a final concentration of 1.2 M. Samples were analyzed by ESI–MS as described previously (Chapter 2) (*49*).

UV-VIS SPECTROSCOPY OF COBALT (II)-BOUND *PA* DDAH

Using a quartz micro-cuvette and a Cary 50 UV-vis spectrophotometer (Varian Inc.), absorbance scans (300 - 800 nm) were recorded for wild-type (260 μM), C249S variant (190 μM), E114G variant (50 μM), and E114Q variant (150 μM) *Pa* DDAH in HEPES buffer (10 mM), KCl (100 mM), at 25º C and pH 7.3, upon addition of $CoCl_2$ (40 – 860 μM). Baseline corrections were made using control solutions prepared without the protein component. To obtain difference spectra, the absorption values of the protein samples were subtracted, at each wavelength, from the resulting absorbance values after addition of $CoCl_2$. In order to determine the apparent extinction coefficients for absorbance changes at 340 and 600 nm, and to obtain the apparent dissociation constant for cobalt (II) binding, the absorbance changes at each of these two wavelengths, determined in three separate experiments, were fit to Beer's law (equation 6.3), where ℓ is the pathlength of the cuvette (1 cm), and $[E \bullet Co^{2+}]$ is defined by equation 6.4 (*74*) because the protein and ligand concentrations are of similar magnitude:

$$\text{Abs} = \Delta\varepsilon \cdot \ell \cdot [E \bullet Co^{2+}] \tag{6.3}$$

$$[E \bullet Co^{2+}] = \frac{([E] + [CoCl_2] + K_d) - \sqrt{([E] + [CoCl_2] + K_d)^2 - 4 \cdot [E][CoCl_2]}}{2} \tag{6.4}$$

Results

CLONING AND EXPRESSION OF GLU114 PA DDAH VARIANTS

Sequencing verified that there were no undesired mutations in any of the coding regions for the three variants constructed. The resulting *N*-terminal His_6-tagged proteins were each overexpressed in BL21 (DE3) *E. coli* cells, and in each case a single affinity chromatography step resulted in purified mutant DDAH (95–98% homogeneous) as assessed by SDS-PAGE. Typical yields ranged between 15–45 mg/L expression culture.

STEADY–STATE KINETICS OF E114G AND E114D DDAH

The steady–state rate constants for E114G and E114D DDAH–catalyzed hydrolysis of SMTC were determined using a previously published DNTB based assay (*36*). The E114D mutant displayed virtually identical kinetics to wild–type DDAH with a k_{cat} of 1.12 ± 0.01 s^{-1}, and K_M of 17□±□1□M, while E114G had a reduced k_{cat} of 0.12 ± 0.01 s^{-1}, and retained a similar K_M of 38□±□3□M.

Table 6.1 Summary of k_{cat} (s^{-1}) values for wild–type and Glu114 mutant DDAH

	(NMMA)[a]	(SMTC)[b]
wild–type [c]	0.28 ± 0.01	1.33 ± 0.03
E114D	nd[d]	1.12 ± 0.01
E114G	0.0024 ± 0.0004	0.15 ± 0.01
E114Q	nd[d]	0.010 ± 0.001

[a] k_{cat} was determined at pH 6, 25º C
[b] k_{cat} was determined at pH 7.5, 25º C
[c] Values from ref. (*74*)
[d] (Not determined)

pH Dependence of DDAH E114G and E114Q Hydrolysis of SMTC

The k_{cat} values determined for E114G catalysis of SMTC (Figure 6.1) fit well to one apparent pK_a of 6.0 ± 0.1, a similar result to the pH rate profile of the wild–type enzyme (Chapter 5). The effect of this mutation results in approximately a 40–fold reduction in k_{cat} values at pH 5. At optimum pH (≥ 7.5) k_{cat} values are only 8–fold less than that of wild–type DDAH.

The k_{cat} values obtained for E114Q hydrolysis of SMTC were plotted against pH and fit to equation 6.1. However the resulting curve shows only an ascending limb with no plateau, yielding an estimated pK_a of 10. At pH 6, E114Q is approximately 1500–fold slower than wild–type DDAH, but activity increases with pH, to within 4–fold of wild–type values at pH 9.5. pH values greater than 9.5 inactivate DDAH, so assays at more alkaline pH values were not attempted.

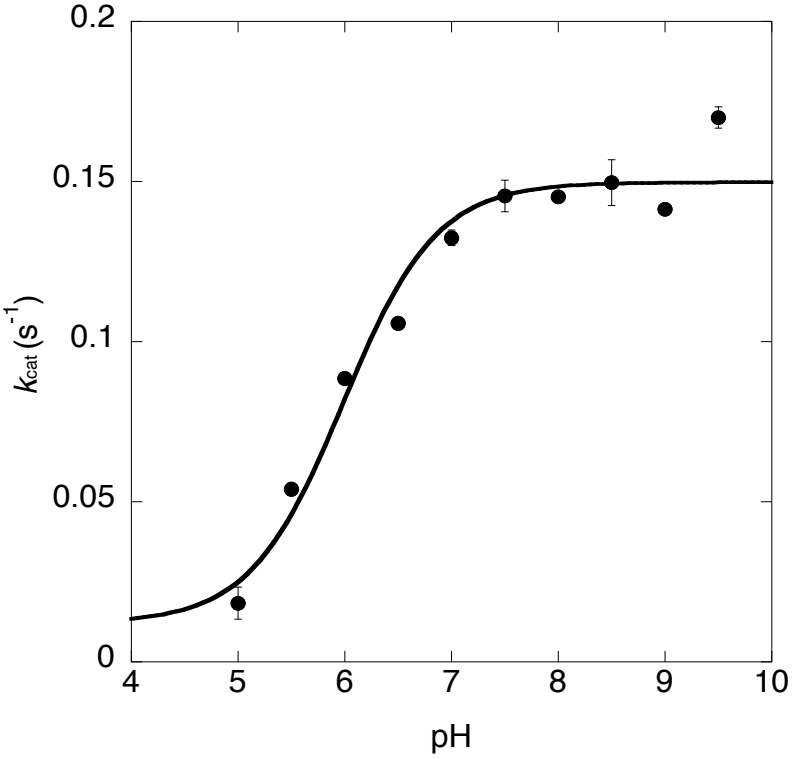

Figure 6.1 The pH rate dependence of E114G DDAH hydrolysis of SMTC

The k_{cat} values are fit to one apparent pK_a of 6□±□0.1 (Equation 6.1) (Log plot slope of 0.7) for the ascending limb.

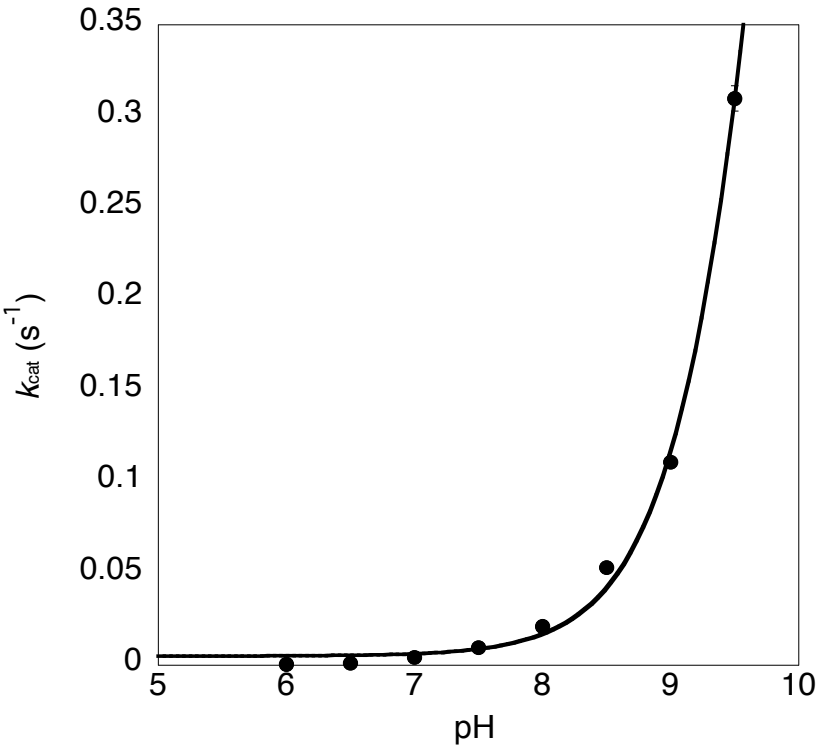

Figure 6.2 pH rate dependence of E114Q DDAH hydrolysis of SMTC

The k_{cat} values are fit to one estimated pK_a of 10□(Log plot slope of 0.8) for the ascending limb.

pH Dependence of Pa E114G DDAH Hydrolysis of NMMA

The apparent k_{cat} values obtained for E114G DDAH–catalyzed hydrolysis of NMMA were plotted against pH and result in a narrow bell–shaped curve (Figure 6.3). Fits to equation 6.2 yielded a pK_a of 6.3 ± 0.1 for the ascending limb and a second pK_a of 8.1 ± 0.1 for the descending limb. In general, fits to two pK_a values closer than 3 units apart tend to underestimate V_{max} at the pH optimum, so Segel's method (*55*) (Chapter 5, equations 5.3, 5.4) was used to calculate corrected pK_a values of 6.6 and 7.8, respectively. The k_{cat} value observed for E114G catalyzed hydrolysis of NMMA was found to be approximately 100–fold slower than that of wild–type DDAH at its pH optimum.

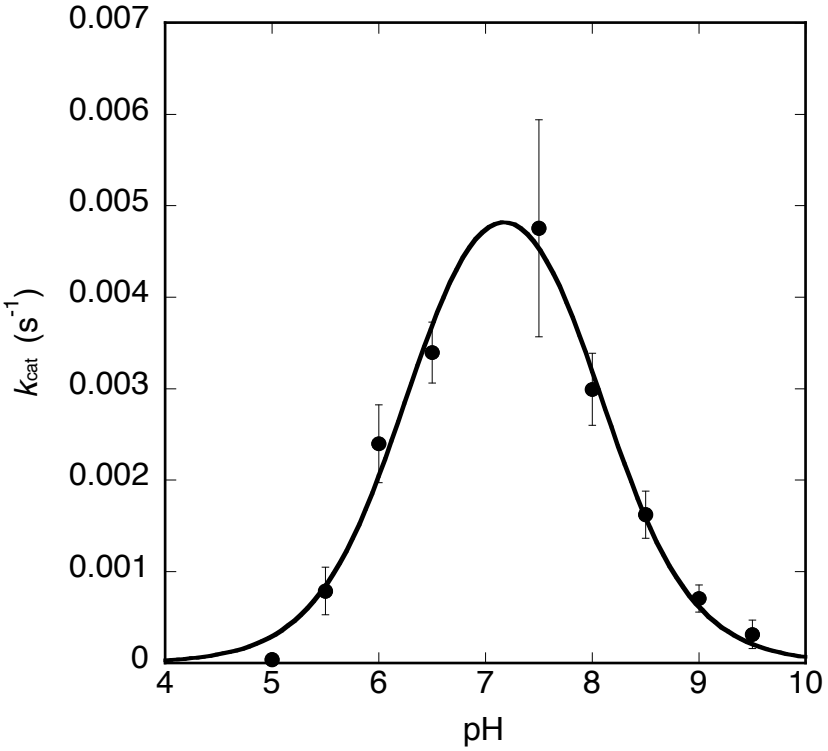

Figure 6.3 pH rate dependence of E114G DDAH catalyzed hydrolysis of NMMA

The fitted k_{cat} values yield two apparent pK_a values of 6.3±0.1 (log plot slope of 1) for the ascending limb and 8.1±0.1 (log plot slope of 0.6) for the descending limb. Because pairs of pK_a values that are closer than 3 units apart tend to underestimate V_{max}, Segel's method (*55*) was used calculate the corrected pK_a values of 6.6 and 7.8.

MASS SPECTRUM ANALYSIS OF STEADY–STATE REACTIONS OF E114G AND E114Q PA DDAH WITH SMTC

Mass spectrum analysis of control reactions (lacking substrate) of E114G DDAH resulted in one major peak with a mass of 30424 ± 10 Da, consistent with the calculated mass of 30431 Da, minus the *N*–terminal methionine for this mutant DDAH. Incubations of E114G with SMTC resulted in the appearance of a new major peak with a mass of 30582 ± 10 Da, reflecting a net increase of 158 Da, consistent with the formation of the *S*–alkylthiouronium reaction intermediate observed previously for wild–type and H162G DDAH (*49, 74*). Control incubations of E114Q DDAH without substrate resulted in one major peak with a mass of 30496 ± 10 Da, consistent with the calculated mass of 30502 Da, minus the *N*–terminal methionine for this mutant DDAH. Incubations of E114Q DDAH with SMTC resulted in a new major peak with a mass of 30652 ± 10 Da, yielding a net increase of 156 Da, consistent with the formation of the expected covalent reaction intermediate. Acid–quenched steady–state reactions of both E114G and E114Q mutant DDAH with SMTC result in formation of nearly 100 % enzyme–adduct species, demonstrating that the decay of the *S*–alkylthiouronium intermediate is rate limiting during catalysis of SMTC by both of these enzymes.

UV-VIS SPECTROSCOPY OF COBALT (II)-BOUND PA DDAH

Spectral changes upon addition of $CoCl_2$ to wild–type *Pa* DDAH show the formation of a new absorbance band at 340 nm and a broad absorption band at 500 – 650 nm (Figure 6.4 A). The features at 340 and 600 nm both appear to saturate with

matching apparent K_d values for cobalt (II) binding of 80 ± 10 μM and 80 ± 20 μM, respectively (Figure 6.4 B). The apparent extinction coefficient at 340 nm is calculated to be 860 ± 30 M^{-1} cm^{-1}, similar in magnitude to the extinction coefficients reported for one equiv of thiolate binding to cobalt (II) (*75*) (*76*). Additionally, the broad feature between 500 – 650 nm has a calculated extinction coefficient at 600 nm of 270 ± 10 M^{-1} cm^{-1}, which has a magnitude consistent with 4- or 5-coordinate cobalt (II) complexes (*75*) (*77*) . Parallel experiments with a C249S mutant do not show either of the spectral features at 340 or 600 nm (Figure 6.4 C), indicating that cobalt (II) binding likely occurs at the active–site. Precipitation is obvious at concentrations of $CoCl_2$ greater than 1 mM, precluding experiments at higher metal concentrations. Spectral changes upon addition of $CoCl_2$ to E114Q DDAH show the formation of a new absorbance band at 340 nm and a broad absorption band at 500 – 650 nm. Observed features at 340 and 605 nm both appear to saturate with similar apparent K_d values for cobalt (II) binding of 14 ± 8 μM and 9 ± 5 μM, respectively (Figure 6.5) with a combined average of 12 μM. The apparent extinction coefficient at 340 nm is calculated to be 850 ± 60 M^{-1} cm^{-1}, similar in magnitude to the extinction coefficients reported for one equivalent of thiolate binding to cobalt (II) (*75*) (*76*). Additionally, the broad feature between 500 – 650 nm has a calculated extinction coefficient at 605 nm of 380 ± 20 M^{-1} cm^{-1}, which has a magnitude consistent with 4- or 5-coordinate cobalt (II) complexes (*75*) (*77*). Experiments with E114G did not show any spectral features at 340 or 605 nm, indicating that this mutant does not bind cobalt (II) at the active–site. Protein precipitation was obvious at concentrations of $CoCl_2$ greater than 250 μM, precluding experiments at these higher metal concentrations.

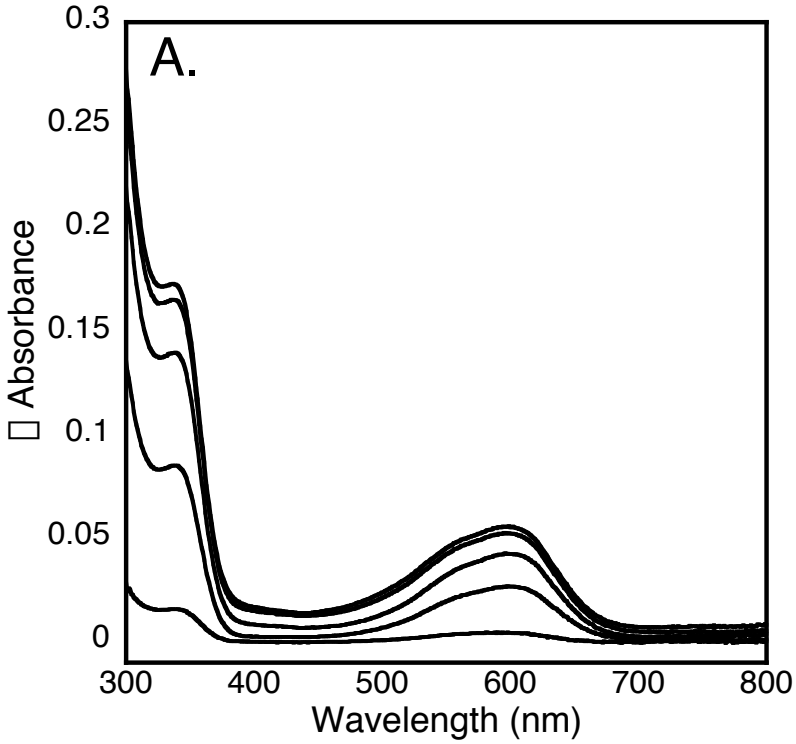
A.
0.3
0.25
0.2
0.15
0.1
0.05
0
Absorbance
300
400
500
600
700
800
Wavelength (nm)

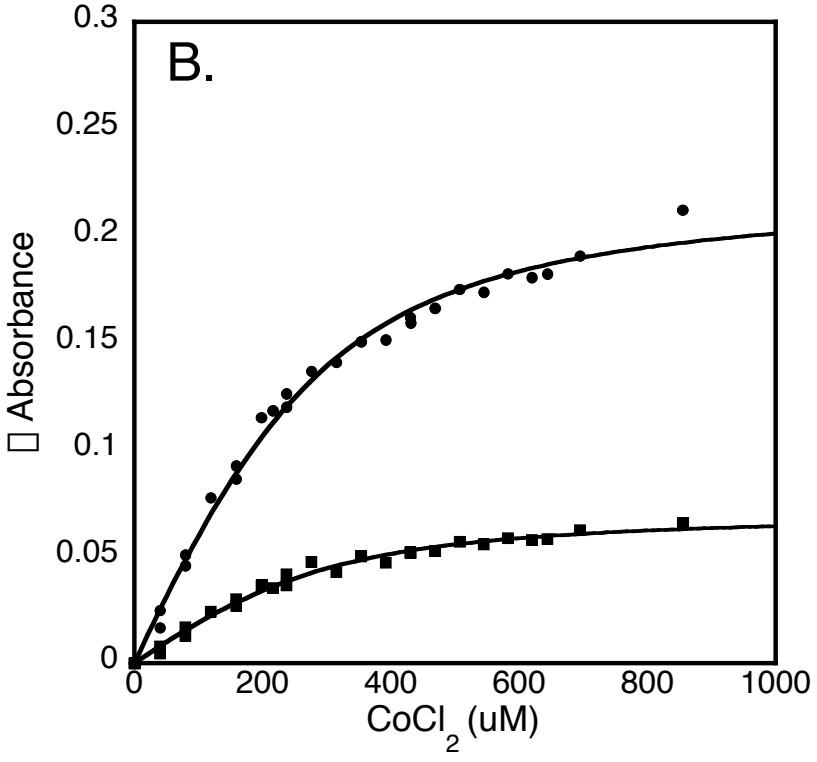
B.
0.3
0.25
0.2
0.15
0.1
0.05
0
Absorbance
0
200
400
600
800
1000
CoCl2 (uM)

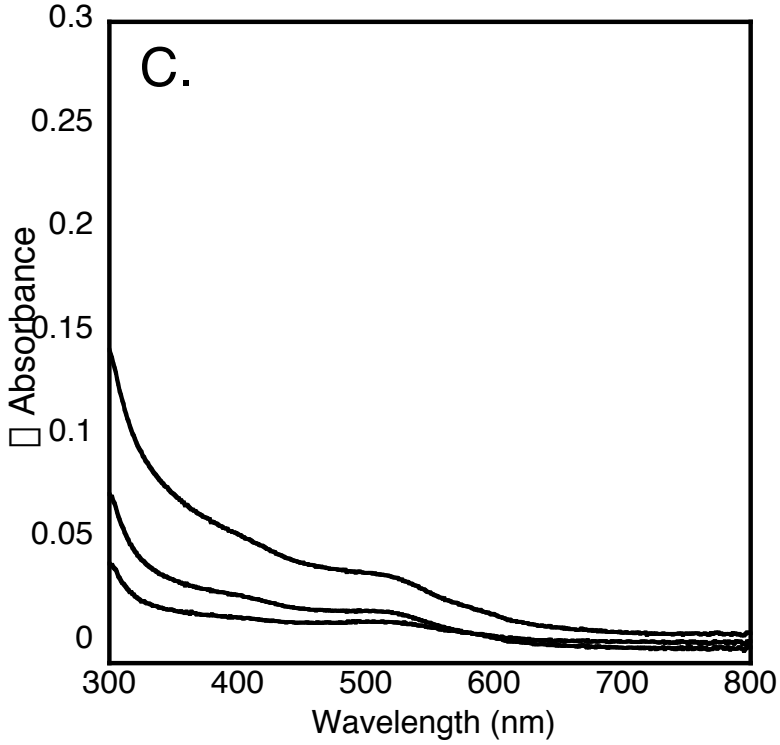
C.
0.3
0.25
0.2
0.15
0.1
0.05
0
Absorbance
300
400
500
600
700
800
Wavelength (nm)

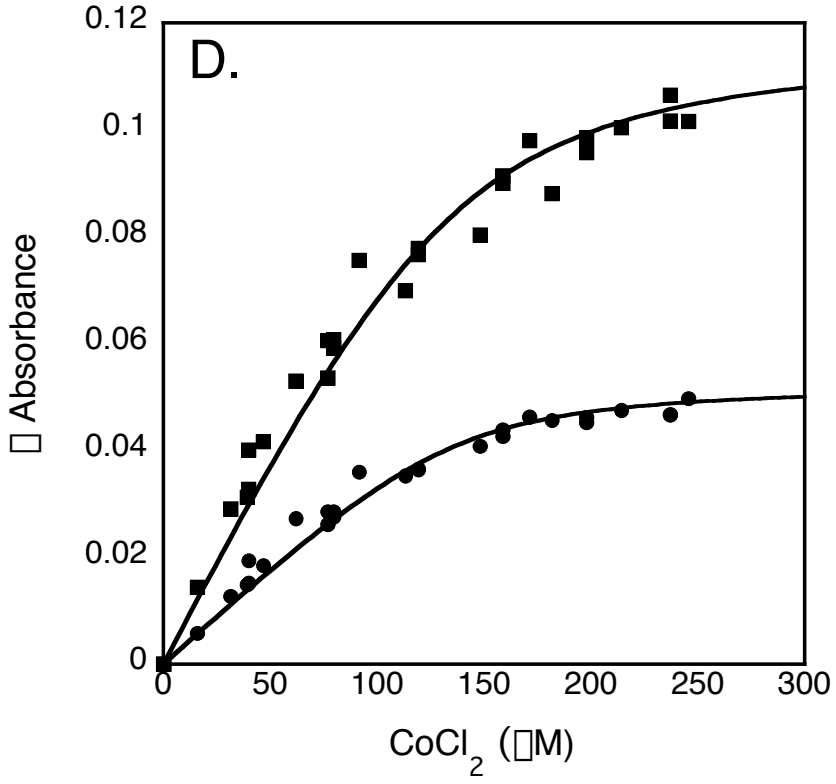

Figure 6.4 UV–Vis spectra of cobalt (II) binding to *Pa* DDAH

A. UV-Vis difference spectra are determined by subtracting the spectrum of apo *Pa* DDAH from samples containing *Pa* DDAH (260 M) and 40, 160, 320, 470, and 540 M $CoCl_2$, resulting in increases in increasing absorbance values. B. Increases in absorbance at 340 (●) and 600 nm (■) upon addition of $CoCl_2$ to *Pa* DDAH are fit as described in materials and methods to yield apparent extinction coefficients of $_{340}$ (860 ± 30 M^{-1} cm^{-1}) and $_{600}$ (270 ± 10 M^{-1} cm^{-1}) and a K_d (80 ± 20 M) for cobalt (II) binding. C. UV-Vis difference spectroscopy subtracting the spectrum of apo C249S *Pa* DDAH from samples containing C249S *Pa* DDAH (190 M) and 220, 430, and 640 M $CoCl_2$. Some protein precipitation is observed at higher $CoCl_2$ concentrations as evidenced by the increase in baseline. D. Increases in absorbance at 340 (■) and 605 nm (●) upon addition of $CoCl_2$ to E114Q DDAH are fit as described in materials and methods to yield apparent extinction coefficients of $_{340}$ (850 ± 60 M^{-1} cm^{-1}) and $_{605}$ (380 ± 20 M^{-1} cm^{-1}) and an average K_d of 12 M for cobalt (II) binding.

Discussion

We sought to determine the contribution of Glu114 to catalysis by DDAH. The structure of a C249S mutant (pdb 1H70) complexed with citrulline shows that Glu114 makes an apparent ion pair with His162 with an interatomic distance of 2.8 Å observed between the N$^{\delta}$ of His162 and an oxygen of the Glu114 carboxyl. We hypothesized that Glu114 might be responsible for properly positioning and ionizing His162 for this histidine's role as general acid/base. The E114D mutation is one methylene group shorter and could possibly reposition His162, affecting its function. However, this mutation appeared to have virtually no effect on catalytic activity, displaying k_{cat} and K_M values nearly identical to those of wild–type DDAH. Sequence analysis of the amidinotransferase superfamily shows that Asp often substitutes for Glu at this position. For example, a recent structure of bovine DDAH–1 (2C6Z), has an Asp instead of Glu at this position and gives an Asp^{-}–His^{+} distance of 2.6 Å, showing a structurally conserved interaction between these two residues (*18*). One interesting exception is peptidyl arginine deiminase IV (PAD4), which has a serine at the same structural position as Glu114.

In DDAH, a carboxylate at position 114 is quite important. E114G and E114Q are very catalytically impaired. Profiles of the pH dependence of k_{cat} values for E114G DDAH catalyzed hydrolysis of SMTC yielded a single pK_a of 6 ± 0.1 with a pH independent plateau at alkaline pH values. The k_{cat} values at the pH optimum are only 8–fold less than wild–type DDAH. Mass spectral analysis of E114G incubated with SMTC at pH 7.3 showed one major peak consistent with the mass of the covalent intermediate

previously characterized for the wild–type enzyme (*49*). This shows that at basic pH values, the rate limiting step for E114G catalysis of SMTC is decay of the covalent adduct (k_3 Scheme 6.1), similar to that seen with wild–type DDAH (*49*).

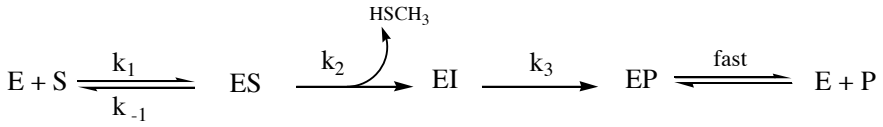

Scheme 6.1

Thus, because wild–type DDAH and the E114G mutant show the same rate–limiting step the effect of an active site carboxyl on k_3 can be calculated to be a $\Delta\Delta G^{\ddagger}$ ~1.4 kcal/mol ($\Delta\Delta G^{\ddagger} = -RT\ln(k_{cat(wt)}/k_{cat(mut)})$. The pH plots of k_{cat} values for E114G DDAH catalyzed hydrolysis of NMMA (Figure 6.3) showed a bell shaped curve similar to that seen with wild–type DDAH, but the curve was more narrow with an apparent pK_a of 6.3 for the ascending limb and 8.1 for the descending limb. In comparison the wild–type DDAH pH dependence is much broader and has apparent pK_a values of 6.1 and 9.4 respectively (*74*). This is consistent with Glu114 stabilizing the general acid form of His162, raising its pK_a and extends the alkaline limb from 8.1 to 9.4. Intriguingly, superfamily member PAD–4, which has a Ser (S406) (PDB 1WD8) at the structural position of Glu114 has a very narrow pH rate profile, remarkably similar to that of E114G DDAH, with apparent pK_a values of 6.2 and 7.9 (*78*). The lack of an active–site His^+carboxyl$^-$ ion pair in PAD-4 likely explains its narrow pH rate profile. The Ser406 residue of PAD–4 is ~3.5 Å from the active–site His (His471), suggesting that it may orient His471 in a productive position, thus partially fulfilling the role of Glu/Asp normally seen at this structural position, but not effecting the ionization of His471.

At non–optimal pH values (6.0) a different step in DDAH catalysis becomes rate limiting. Mass spectral analysis of wild–type DDAH incubations with NMMA show no observable accumulation of covalent intermediate (data not shown). This indicates that formation of the *S*-alkylthiouronium intermediate is rate limiting at low pH values. Assuming that k_2 (scheme 6.1) is rate limiting at pH 6.0, we can estimate the effect of Glu114 upon His162 as a general acid. The kinetic effect of the E114G DDAH mutation reflects a $\Delta\Delta G^{\ddagger}$ on k_2 of 2.8 kcal/mol towards EI formation. This value is similar to the typical range of $\Delta\Delta G$ values (3-5 kcal/mol) reported for buried salt bridges (*70*), and is consistent with the role of Glu114 stabilizing the protonated form of His162.

The E114Q mutation is also catalytically impaired but has very different characteristics when compared to the other Glu114 mutants. Sterically, an E114Q mutation is very conservative, but the amide functional group is neutral so it would not be expected to form an ion pair with H162. ESI–MS analysis of acid quenched steady–state reactions of E114Q and SMTC at pH 7.3 reveal that approximately 100% of the enzyme contains the covalent adduct, demonstrating that k_3 (Scheme 6.1) is rate limiting for this mutant enzyme. The pH rate profile for E114Q DDAH catalyzed hydrolysis of SMTC shows a severely impaired rate at acidic pH values ($\leq 5 \times 10^{-3}$ s^{-1} at pH 6), but rapidly increases with pH (Figure 6.2) to within 4–fold of the wild–type DDAH rate. In comparison, serine proteases have a conserved active site triad of Ser, His, and Asp where His and Asp function as an ion pair, although these are oriented differently than the catalytic triad in DDAH. The catalytic contribution of Asp was evaluated in trypsin by a D102N mutation, where Craik et al. noted that at neutral pH values k_{cat} was 10^4 lower than wild–type but was rescued by $^{-}$OH ion to within 10% of wild–type at pH 10

(*79*). It is interesting that E114Q is rescued in a similar manner. No such rate enhancement is seen with E114G, thus ruling out the possibility that hydroxide alone can effectively attack the covalent intermediate. It seems likely that the E114Q mutation constrains His162 to a catalytically unfavored position at neutral pH values, but that high pH values can restore His162 to a productive orientation.

To test the hypothesis that E114G and E114Q mutations constrain His162 to different degrees, metal binding studies were conducted using cobalt (II) as a spectroscopic probe. Wild-type DDAH was found to bind cobalt (II) with an apparent K_d of 80 μM (Figure 6.4 B) whereas C249S mutant DDAH was incapable of binding cobalt (II), indicating that cobalt (II) binds at the active–site. (An EXAFS study of Zinc(II)–bound *Pa* DDAH also indicates that metals bind at the active–site, with residues Cys249 and His162 as two of the ligands (*74*).) We reasoned that if E114G and E114Q constrain His162 to different extents, they should also have a different affinity for cobalt. Interestingly, the E114G mutant showed no measurable affinity for cobalt (II), and was observed to precipitate after addition of several equivalents of Co^{2+}. However, the E114Q mutant was found to bind cobalt (II) with a K_d of 12 μM, approximately 7–fold tighter than wild–type DDAH (Figure 6.5). The spectroscopic characteristics of E114Q bound cobalt (II) were similar to wild–type DDAH. A ligand to metal charge transfer (LMCT) band is observed at 340 nm with an apparent extinction coefficient of 850 $M^{-1}cm^{-1}$ indicating cobalt bound to one thiol. The weak features observed between 500 and 650 nm upon cobalt (II) binding are indicative of Laporte-forbidden cobalt (II) d–d transitions, and have an extinction coefficient of 380 $M^{-1}cm^{-1}$, consistent with a 4- or 5-coordinate cobalt (II) site. The lack of observed metal binding for E114G suggests that

His162 no longer occupies a favorable orientation for metal binding, consistent with its impaired function as a general acid for protonation of the methylamine leaving group of NMMA. On the other hand, the E114Q mutation appears to reorient His162 to a more favorable position for chelating metals, contributing a $\Delta\Delta G_{Kd}$ of ~1.1 kcal/mol toward binding cobalt (II) ($\Delta\Delta G_{K_d} = -RT\ln(K_{d(wt)}/K_{d(mut)})$). However, this repositioning is not favorable for catalysis as E114Q DDAH–catalyzed hydrolysis of NMMA showed a 1500–fold reduction in k_{cat} as compared to wild–type DDAH at pH 7.3 (Data not shown).

We propose that the function of Glu114 in the mechanism of *Pa* DDAH is to both stabilize the ionized form of His162 and constrain it to a catalytically productive orientation. Although Glu114 is not strictly essential to catalysis, it provides nearly 3 kcal/mol towards catalyzing hydrolysis of the natural substrate NMMA and the enhanced catalytic activity provided by this amino acid explains why it is highly conserved. Constraining His162 to a productive orientation appears to be especially important for protonating the methylamine leaving group of NMMA. To a lesser extent constraining His162 is also important to hydrolysis of the covalent intermediate. The negative charge of the Glu114 carboxylate is also critical to proper His162 orientation. Constraining His162 with the neutral E114Q mutation resulted in improved metal binding, but severely impaired catalysis at neutral pH values. This suggests that His162 is in a different position when binding metals as compared to when it acts as a general acid. In contrast, the unconstrained His162 in the E114G DDAH enzyme was not able to bind cobalt (II) at all.

Conclusion

The results of the work presented here (Chapters 2–6), provides evidence for the roles of the active–site residues Cys249, His162, and Glu114 in the reaction mechanism of DDAH. During these studies we have developed two new methods for continuously monitoring DDAH activity using the activated substrate SMTC (Chapters 3, 5). Information about the mechanism has also led to the identification of an active–site directed covalent inactivator motif (haloacetamidine) (Chapter 4).

We propose that the in the resting state (at physiological pH values) the active–site Cys249 residue (Scheme 6.2) is the neutral thiol, as evidenced by UV–vis difference spectroscopy and reactivity experiments (Chapter 5). The positive charge of the substrate guanidinium group depresses the pK_a of Cys249, activating it for nucleophilic attack. This was observed directly through UV–vis difference spectroscopy with positive– and neutral– ligands, and supported by a depressed pK_a seen with k_{cat} versus pH profiles. The thiolate attack on the guanidinium carbon forms a proposed tetrahedral intermediate concomitant with protonation of the methylamine leaving group. His162 acts as the general acid in protonating the leaving group as observed by pH profiles and mutational studies (Chapter 5). Glu114 plays an integral role in ionizing and orienting the general acid form of His162, as was observed from mutational, pH kinetic effect and spectroscopic experiments (Chapter 6). The proposed transient tetrahedral intermediate collapses upon loss of methylamine to form a covalent *S*–alkylthiouronium intermediate, as shown by ESI–MS and MALDI experiments (Chapter 2, 5).

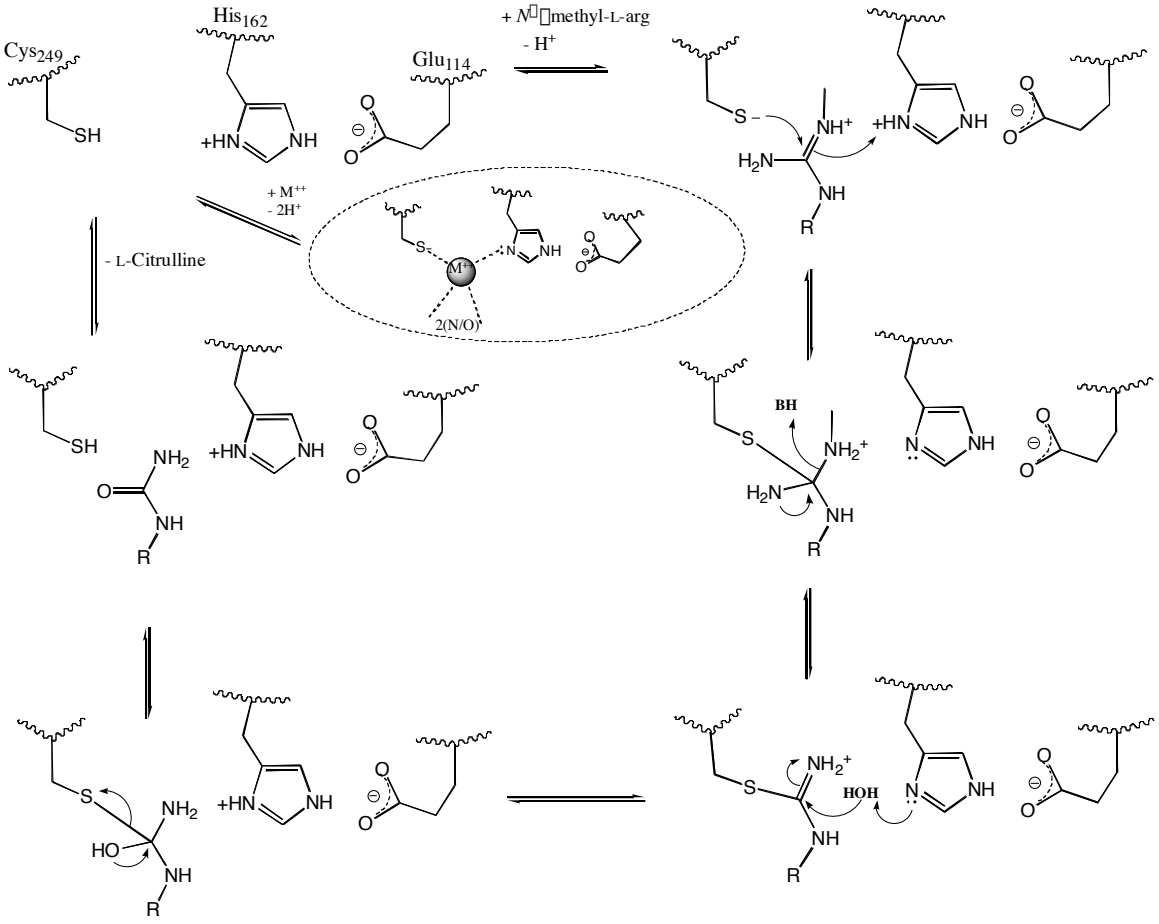

Scheme 6.2 Proposed Reaction Mechanism of *Pa* DDAH

His162 acts as a general base, deprotonating H_2O and generating a hydroxide ion for attack on the covalent adduct, as deduced from mutational and ESI–MS, studies (Chapter 5). A second proposed tetrahedral intermediate forms, which subsequently collapses to form L–citrulline and regenerate resting enzyme. Divalent metal ions can also bind at the active–site, as evidenced by mutational and spectroscopic experiments (Chapter 6). Together these experiments have outlined much of the reaction mechanism of DDAH,

and contribute to our understanding of catalytic mechanisms in the entire amidinotransferase superfamily.

Bibliography

1. Voet, D., and Voet, J. G. (1995) *Biochemistry*, 2nd ed., J. Wiley & Sons, New York.
2. Vallance, P., and Leiper, J. (2002) *Nat Rev Drug Discov 1*, 939-50.
3. Leiper, J., and Vallance, P. (1999) *Cardiovasc Res 43*, 542-8.
4. Boger, R. H., and Bode-Boger, S. M. (1997) *Vasa 26*, 180-4.
5. Boger, R. H., Bode-Boger, S. M., Szuba, A., Tsao, P. S., Chan, J. R., Tangphao, O., Blaschke, T. F., and Cooke, J. P. (1998) *Circulation 98*, 1842-7.
6. Boger, R. H. (2003) *Cardiovasc Res 59*, 824-33.
7. Martens-Lobenhoffer, J., and Bode-Boger, S. M. (2006) *Eur J Clin Pharmacol 62*, 61-68.
8. Knipp, M. (2006) *ChemBioChem 7*, 879-889.
9. Abe, T., Tohgi, H., Murata, T., Isobe, C., and Sato, C. (2001) *Neurosci Lett 312*, 177-9.
10. Kilbourn, R. G., Fonseca, G. A., Trissel, L. A., and Griffith, O. W. (2000) *Cancer J Sci Am 6 Suppl 1*, S21-30.
11. Tran, C. T., Fox, M. F., Vallance, P., and Leiper, J. M. (2000) *Genomics 68*, 101-5.
12. Dayoub, H., Achan, V., Adimoolam, S., Jacobi, J., Stuehlinger, M. C., Wang, B. Y., Tsao, P. S., Kimoto, M., Vallance, P., Patterson, A. J., and Cooke, J. P. (2003) *Circulation 108*, 3042-7.
13. Ogawa, T., Kimoto, M., Watanabe, H., and Sasaoka, K. (1987) *Arch Biochem Biophys 252*, 526-37.
14. Ogawa, T., Kimoto, M., and Sasaoka, K. (1989) *J Biol Chem 264*, 10205-9.
15. Santa Maria, J., Vallance, P., Charles, I. G., and Leiper, J. M. (1999) *Mol Microbiol 33*, 1278-9.
16. Shirai, H., Blundell, T. L., and Mizuguchi, K. (2001) *Trends Biochem Sci 26*, 465-8.
17. Murray-Rust, J., Leiper, J., McAlister, M., Phelan, J., Tilley, S., Santa Maria, J., Vallance, P., and McDonald, N. (2001) *Nat Struct Biol 8*, 679-83.
18. Frey, D., Braun, O., Briand, C., Vasak, M., and Grutter, M. G. (2006) *Structure 14*, 901-11.
19. Leiper, J., Murray-Rust, J., McDonald, N., and Vallance, P. (2002) *Proc Natl Acad Sci U S A 99*, 13527-32.
20. Knipp, M., Braun, O., Gehrig, P. M., Sack, R., and Vasak, M. (2003) *J Biol Chem 278*, 3410-6.
21. Knipp, M., Charnock, J. M., Garner, C. D., and Vasak, M. (2001) *J Biol Chem 276*, 40449-56.
22. MacAllister, R. J., Parry, H., Kimoto, M., Ogawa, T., Russell, R. J., Hodson, H., Whitley, G. S., and Vallance, P. (1996) *Br J Pharmacol 119*, 1533-40.
23. Ueda, S., Kato, S., Matsuoka, H., Kimoto, M., Okuda, S., Morimatsu, M., and Imaizumi, T. (2003) *Circ Res 92*, 226-33.
24. Lu, X., Galkin, A., Herzberg, O., and Dunaway-Mariano, D. (2004) *J Am Chem Soc 126*, 5374-5.

25. Gill, S. C., and von Hippel, P.H. (1989) *Anal Biochem 182*, 319-326.
26. Boyde, T. R., and Rahmatullah, M. (1980) *Anal Biochem 107*, 424-31.
27. Veniamin, M. P., and Vakirtzi-Lemonias, C. (1970) *Clin Chem 16*, 3-6.
28. Knipp, M., and Vasak, M. (2000) *Anal Biochem 286*, 257-64.
29. Wang, S. C., Person, M. D., Johnson, W. H., Jr., and Whitman, C. P. (2003) *Biochemistry 42*, 8762-73.
30. Person, M. D., Monks, T. J., and Lau, S. S. (2003) *Chem Res Toxicol 16*, 598-608.
31. Clauser, K. R., Baker, P., and Burlingame, A. L. (1999) *Anal Chem 71*, 2871-82.
32. Geoghegan, K. F., Dixon, H. B., Rosner, P. J., Hoth, L. R., Lanzetti, A. J., Borzilleri, K. A., Marr, E. S., Pezzullo, L. H., Martin, L. B., LeMotte, P. K., McColl, A. S., Kamath, A. V., and Stroh, J. G. (1999) *Anal Biochem 267*, 169-84.
33. Plevin, M. J., Magalhaes, B. S., Harris, R., Sankar, A., Perkins, S. J., and Driscoll, P. C. (2004) *J Mol Biol 341*, 171-84.
34. Kimoto, M., Miyatake, S., Sasagawa, T., Yamashita, H., Okita, M., Oka, T., Ogawa, T., and Tsuji, H. (1998) *Eur J Biochem 258*, 863-8.
35. Bogumil, R., Knipp, M., Fundel, S. M., and Vasak, M. (1998) *Biochemistry 37*, 4791-8.
36. Stone, E. M., and Fast, W. (2005) *Anal Biochem 343*, 335-7.
37. Biemann, K. (1990) *Methods Enzymol 193*, 886-7.
38. Humm, A., Fritsche, E., Mann, K., Gohl, M., and Huber, R. (1997) *Biochem J 322 (Pt 3)*, 771-6.
39. Narayanan, K., and Griffith, O. W. (1994) *J Med Chem 37*, 885-7.
40. Smith, D. W., and Fahrney, D. E. (1978) *Biochem Biophys Res Commun 83*, 101-6.
41. Grazi, E., and Rossi, N. (1968) *J Biol Chem 243*, 538-42.
42. Humm, A., Fritsche, E., Steinbacher, S., and Huber, R. (1997) *Embo J 16*, 3373-85.
43. Das, K., Butler, G. H., Kwiatkowski, V., Clark, A. D., Jr., Yadav, P., and Arnold, E. (2004) *Structure (Camb) 12*, 657-67.
44. Coll, M., Knof, S. H., Ohga, Y., Messerschmidt, A., Huber, R., Moellering, H., Russmann, L., and Schumacher, G. (1990) *J Mol Biol 214*, 597-610.
45. Leiper, J. M., Santa Maria, J., Chubb, A., MacAllister, R. J., Charles, I. G., Whitley, G. S., and Vallance, P. (1999) *Biochem J 343 Pt 1*, 209-14.
46. Martens-Lobenhoffer, J., and Bode-Boger, S. M. (2003) *J Chromatogr B Analyt Technol Biomed Life Sci 798*, 231-9.
47. Beal, D. D., and Bryan, G. T. (1978) *Biochem Med 19*, 374-82.
48. Jencks, W. P., and Regenstein, J. (1968) in *Handbook of Biochemistry* (Sober, H. A., Ed.) pp J-148 - J-189, CRC, Cleveland, Ohio.
49. Stone, E. M., Person, M. D., Costello, N. J., and Fast, W. (2005) *Biochemistry 44*, 7069-78.
50. Riddles, P. W., Blakeley, R. L., and Zerner, B. (1983) *Methods Enzymol 91*, 49-60.
51. Eyer, P., Worek, F., Kiderlen, D., Sinko, G., Stuglin, A., Simeon-Rudolf, V., and Reiner, E. (2003) *Anal Biochem 312*, 224-7.
52. Walmsley, T. A., Abernethy, M. H., and Fitzgerald, H. P. (1987) *Clin Chem 33*, 1928-31.

53. Zhu, J., Dhimitruka, I., and Pei, D. (2004) *Org Lett 6*, 3809-12.
54. Segel, I. H. (1975) *Enzyme Kinetics*, John Wiley and Sons, Inc., New York.
55. Segel, I. H. (1975) *Enzyme kinetics : behavior and analysis of rapid equilibrium and steady state enzyme systems*, Wiley, New York.
56. Riener, C. K., Kada, G., and Gruber, H. J. (2002) *Anal Bioanal Chem 373*, 266-76.
57. Choi, S. J., Hwang, J. M., and Kim, S. I. (2003) *J Biochem Mol Biol 36*, 417-20.
58. Dowling, R. B., Newton, R., Robichaud, A., Cole, P. J., Barnes, P. J., and Wilson, R. (1998) *Am J Respir Cell Mol Biol 19*, 950-8.
59. Stuhlinger, M. C., Tsao, P. S., Her, J. H., Kimoto, M., Balint, R. F., and Cooke, J. P. (2001) *Circulation 104*, 2569-75.
60. Knipp, M., Braun, O., and Vasak, M. (2005) *J Am Chem Soc 127*, 2372-3.
61. Rossiter, S., Smith, C. L., Malaki, M., Nandi, M., Gill, H., Leiper, J. M., Vallance, P., and Selwood, D. L. (2005) *J Med Chem 48*, 4670-8.
62. Ho, S. N., Hunt, H. D., Horton, R. M., Pullen, J. K., and Pease, L. R. (1989) *Gene 77*, 51-9.
63. Plapp, B. V. (1982) *Methods Enzymol 87*, 469-99.
64. Falick, A. M., Hines, W. M., Medzihradszky, K. F., Baldwin, M. A., and Gibson, B. W. (1993) *J. Am. Soc. Mass Sectrom 19*.
65. Kubota, K., Yoneyama-Takazawa, T., and Ichikawa, K. (2005) *Rapid Commun Mass Spectrom 19*, 683-8.
66. Stone, E. M., Schaller, T. H., Bianchi, H., Person, M. D., and Fast, W. (2005) *Biochemistry 44*, 13744-52.
67. Luo, Y., Knuckley, B., Lee, Y. H., Stallcup, M. R., and Thompson, P. R. (2006) *J Am Chem Soc 128*, 1092-3.
68. Wang, P. F., McLeish, M. J., Kneen, M. M., Lee, G., and Kenyon, G. L. (2001) *Biochemistry 40*, 11698-705.
69. Malinen, A. M., Belogurov, G. A., Salminen, M., Baykov, A. A., and Lahti, R. (2004) *J Biol Chem 279*, 26811-6.
70. Fersht, A. (1999) *Structure and Mechanism in Protein Science*, W.H. Freeman and Company, New York.
71. Polgar, L. (1974) *FEBS Lett. 38*, 187-190.
72. Cleland, W. W. (1977) *Adv. Enzymol. Relat. Areas Mol. Biol. 45*, 273-387.
73. Tolbert, B. S., Tajc, S. G., Webb, H., Snyder, J., Nielsen, J. E., Miller, B. L., and Basavappa, R. (2005) *Biochemistry 44*, 16385-91.
74. Stone, E. M., Costello, A. L., Tierney, D. L., and Fast, W. (2006) *Biochemistry 45*, 5618-5630.
75. Maret, W., and Vallee, B. L. (1993) *Methods Enzymol 226*, 52-71.
76. Alexander, R. S., Kiefer, L. L., Fierke, C. A., and Christianson, D. W. (1993) *Biochemistry 32*, 1510-8.
77. Vallee, B. L., and Galdes, A. (1984) *Adv Enzymol Relat Areas Mol Biol 56*, 283-430.
78. Kearney, P. L., Bhatia, M., Jones, N. G., Yuan, L., Glascock, M. C., Catchings, K. L., Yamada, M., and Thompson, P. R. (2005) *Biochemistry 44*, 10570-82.
79. Craik, C. S., Roczniak, S., Largman, C., and Rutter, W. J. (1987) *Science 237*, 909-13.

Vita

Everett M Stone was born in Danbury, Connecticut, on December the 13th 1971, to Robert and Jane Stone. He grew up near Seymour, Missouri, where he and his sister Genny were educated at home. He owned and operated a Farrier service from 1988 to 2002. Everett matriculated Drury University in Springfield MO, in 1998, and received the degree of Bachelor of Arts in August 2002, after which he attended the University of Austin for his graduate studies in August, 2002.

Publications

Stone EM, Costello AL, Tierney DL, Fast W. Substrate-Assisted Cysteine Deprotonation in the Mechanism of Dimethlargininase (DDAH) from Pseudomonas aeruginosa. *Biochemistry*. 2006 May 2;45(17):5618-30.

Stone EM, Schaller TH, Bianchi H, Person MD, Fast W. Inactivation of two diverse enzymes in the amidinotransferase superfamily by 2-chloroacetamidine: Dimethylargininase and peptidylarginine deiminase. *Biochemistry*. 2005 Oct 25;44(42):13744-52.

Liu D, Lepore BW, Petsko GA, Thomas PW, **Stone EM,** Fast W, Ringe D. Three-dimensional structure of the quorum-quenching N-acyl homoserine lactone hydrolase from Bacillus thuringiensis. *Proc. Natl. Acad. Sci.* USA. 2005 Aug 16;102(33):11882-7.

Stone EM, Fast W. A continuous spectrophotometric assay for dimethylarginine dimethylaminohydrolase. *Anal. Biochem.* 2005 Aug 15;343(2):335-7.

Thomas PW, **Stone EM**, Costello AL, Tierney DL, Fast W. The quorum-quenching lactonase from Bacillus thuringiensis is a metalloprotein. *Biochemistry*. 2005 May 24;44(20):7559-69.

Stone EM, Person MD, Costello NJ, Fast W. Characterization of a transient covalent adduct formed during dimethylarginine dimethylaminohydrolase catalysis. *Biochemistry*. 2005 May 10;44(18):7069-78.

Permanent address: 3509 B, Woodrow St.

Austin, TX, 78705

This dissertation was typed by Everett M Stone.